IN-SITU DETECTION OF ATRAZINE AND ITS METABOLITES CONTAMINATION IN NATURAL WATERS

A Dissertation

presented to

The Faculty of the Graduate Studies

at the University of Missouri-Columbia

In Partial Fulfillment

Of the Requirements for the Degree

Doctor of Philosophy

By

Zahra Salahshoor

Dr. Maria Fidalgo, Dissertation Supervisor

May 2022

The undersigned, appointed by the dean of the Graduate School, have examined the dissertation entitled

IN-SITU DETECTION OF ATRAZINE AND ITS METABOLITES CONTAMINATION IN NATURAL WATERS

Presented by Zahra Salahshoor

A candidate for the degree of doctor of philosophy,

And hereby certify that, in their opinion, it is worthy of acceptance.

Dr. Maria Fidalgo

Dr. Kathleen Trauth

Dr. Enos Inniss

Dr. Chung-Ho Lin

DEDICATION

In loving memory of my mother

And

To my father, with love and eternal appreciation

ACKNOWLEDGEMENTS

I would like to sincerely thank my dissertation advisor, Dr Maria Fidalgo, who gave me the great opportunity to do my PhD research along with her brilliant knowledge, enthusiast, and patience. She provided great support and mentorship in each step of my journey.

I also would like to appreciate all the members in my committee, Dr. Kathleen Trauth, Dr Chung-Ho Lin, and Dr. Enos Inniss, who have been providing their knowledge, guidance, experience, and encouragement along past years.

I would also like to express my gratitude to collaborators and friends, Dr. Mohamed Bayati, Dr. Abbas Kadhem, Dr. Ezequiel Rossi, Sally Qasim, Dr. Federico Fookes, Dr. Khanh-Van Ho, and Shu Yu Hsu for their advice and expertise.

Table of Contents

LIST OF FIGURES

LIST OF TABLES

Abstract

Water and soil contamination caused by extensive atrazine (ATZ) application in agriculture, could be a potential risk to the environment and human health. Common analytical methods are expensive and complex. A sensor for low-cost and simple detection of ATZ and its metabolites, deethylatrazine (DEA) and deisopropylatrazine (DIA), in aqueous solutions was developed by combining colloidal crystal with molecular imprinting technique. The sensor is formed by 3D interconnected macroporous structure with numerous nanocavities derived from ATZ and its metabolites imprinting in a thin polymeric film. The MIPs were fabricated with acrylic acid monomers crosslinked by ethylene glycol dimethacrylate with 4:1 molar ratio, polymerized under UV radiation initiated by azobisisobutyronitrile. The films were characterized by Fourier Transform Infrared spectroscopy (FTIR) and Scanning Electron Microscopy (SEM). The MIPs were incubated in solutions of each target at variable concentrations. Target molecules were specifically absorbed in nanocavities and caused swelling in the polymer film resulting in changes of Bragg diffraction peak wavelength. Kinetic tests showed that rebinding equilibrium was reached within 20 minutes. The sensor had a dynamic range of 0.1 to 10 ppb for quantifying target analytes in aqueous solutions with limit of detection of 0.1, 0.2, and 0.3 ppb, and limit of quantification of 0.33, 0.66, and 1 ppb for ATZ, DEA, and DIA, respectively. Cross-reactivity tests were conducted in 1 and 5 ppb solutions combining all three targets and showed absence of positive interferences effects and low probability of false positives given by individual sensors. Ionic strength effect on MIPs investigation showed up to 26% decrease and 23% increase in MIP response for NaCl and $CaCl_2$, respectively. Presence of NOM caused 28% and 35% increase in wavelength shift for

NIPs and MIPs, respectively. Rinsing NIPs before measuring the reflectance spectra resulted in less increase in wavelength shift. Natural waters samples were collected after rain events and were characterized for physicochemical properties and the content of ATZ, DEA, and DIA to be eventually used for MIPs application in them. MIPs were examined in natural waters spiked with target molecules, showing good agreement with real concentrations of targets. The resulting molecularly imprinted polymer (MIP) yields rapid and efficient detection of target molecules in aqueous solutions close to environmentally relevant concentrations.

1. Introduction

1.1. Background of the study

Atrazine is one of the most common herbicides used by farmers in the United States due to their selectivity against broadleaf weeds and annual grasses (1). Although it is beneficial for agricultural purposes, extensive use of this herbicide has caused contaminations in drinking water and soil and it can be harmful to living organisms even at low concentrations(2). Atrazine is degraded by plants, animals, and microorganisms to four main metabolites: hydroxyatrazine (HA; 6-hydroxyN-ethyl-N´-isopropyl-[1,3,5]triazine-2,4- diamine), diaminochlorotriazine (DACT; 6-chloro[1,3,5]triazine-2,4-diamine), deisopropylatrazine (DIA; 6-chloro-N-ethyl- [1,3,5]triazine-2,4-diamine), and deethylatrazine (DEA; 6-chloro-N-isopropyl- [1,3,5]triazine-2,4-diamine)(3). Since atrazine metabolites also demonstrate potential health effects, concerns have been raised over their extensive use in the United States and efficient approaches of detection and removal of these compounds (2,4).

Molecularly Imprinted Polymers (MIPs), are synthetic receptors created on a polymer film for a targeted molecule (5). They have highly specific sites in their polymeric structure which leads them to selectively adsorb target molecules in those sites (6). Fabricating molecularly imprinted polymers includes following essential steps: integrating the target in monomer solution, designing the spatial distribution of target molecules within the polymeric matrix by doing the polymerization, removing target molecules to create void spaces of complementary morphology of the target, and rebinding the target molecules similar to “key-lock” principle of enzymes mechanism (7).

MIPs have attracted attentions recently due to their improved stability, facile fabrication, great potential of capturing small molecules, reusability, and longer period of validity (8). Therefore, in this work, a photonic sensor is used for detection of atrazine and its metabolites.

Wetlands are areas where water covers the soil or is present either at or near the surface of the soil all year or for varying periods of time during the year, including during the growing season. Wetlands provide many societal benefits: food and habitat for fish and wildlife, including threatened and endangered species; water quality improvement; flood storage; shoreline erosion control; economically beneficial natural products for human use; and opportunities for recreation, education, and research (9). So, it is essential to preserve the environment of wetland against potential threats such as pesticides and herbicides runoff to wetlands from farms around them. In this proposal, a photonic MIPs has been established to detect and quantify atrazine and its metabolites primarily in aqueous solutions and eventually in natural waters, particularly in wetlands.

1.2.Research Objectives

The overall objective of this work is to develop a photonic sensor capable of detecting atrazine and its metabolites (DEA and DIA) in aqueous solutions and eventually using it as a potable sensor for in-situ detection of atrazine and its metabolites in natural waters.

In chapter two, a literature review on molecularly imprinted polymers and their features, characterization and application has been done. Also, atrazine and its metabolites, its benefits in agricultural industry and its harms at levels higher than maximum contaminant level has been discussed. Atrazine runoff to the wetlands and

jeopardizing them, resulting in the demand to preserve those ecosystems has led to covering the topics of natural waters chemical properties influence on the MIPs functionality.

In chapter three, the specific objective is to develop a sensor and calibrate it to detect and quantify atrazine and its metabolites in water. A photonic MIP has been fabricated to detect atrazine and its metabolites in aqueous solutions. It is a highly porous molecularly imprinted poly (acrylic acid) (PAA) film generated from combining noncovalent imprinting with colloidal crystal template technique capable of selectively recognizing atrazine, DEA, and DIA. Colloidal crystal deposition of silica nanoparticles obtained by self-assembly technique were used to provide a porous structure and high surface area in the film. UV-Vis spectrometer was used to detect the target molecules recognition depending on Bragg diffraction. When the target molecules rebind to nanocavities on the film, it causes swelling of the film resulting in peak wavelength change in reflectance spectra and hence, a clear optical signal will be detected. Also, the cross-reactivity of the MIPs has been studied by MIPs incubation in solutions combined of all three targets at equal concentrations.

In chapter four, the specific objective is to investigate the effect of ionic strength and natural organic matter (NOM) on the fabricated MIP efficiency. Natural waters chemical properties impact is studied on the MIP-based sensor functionality. Effect of ionic strength and NOM has been studied on photonic MIPs of atrazine. The purpose of this study is to analyze if those factors of natural waters would interfere with nonspecific and specific adsorption of atrazine on the MIP, or compounds other than the target would cause swelling or shrinkage in the polymer hydrogel. An adjusted calibration and a

methodology are also proposed to minimize the effect of natural waters chemical properties.

In Chapter five, the specific objective is to analyze the samples taken from wetlands for determining concentrations of atrazine, DEA, and DIA. Samples are taken from locations adjacent to wetlands around northeast Columbia MO area and they were analyzed using LCMS/MS. Sampling campaign took place in each season during or after rainfall. LCMS/MS analysis is done to quantify the concentration of atrazine and its metabolites (DEA and DIA) in the samples. The sampling sites are located in the vicinity of farms (mostly corn farms), so the analysis is done to investigate the amount of atrazine runoff from the fields to the nearby wetlands and also the extent of its degradation to the metabolites in each site.

In chapter six, the specific purpose is to apply the fabricated MIPs as in-situ sensors in the wetlands for detection and quantification of atrazine, DEA, and DIA. Using results of MIP-based sensors cross-reactivity and effect of ionic strength and NOM on MIPs response from previous chapters makes the sensors function predictable when used in natural waters which contain atrazine and the metabolites, simultaneously. Although, the effect of chemical properties of natural waters should not be neglected when applying the sensors in-situ.

2. Literature review and Introduction

2.1. Agrochemicals and the environment

2.1.1. Use and need of agrochemicals for food production

Modern agriculture greatly depends on pesticides, that keep weeds, herbs, and insects under control from harming agricultural products. In the United States, around 1 billion pounds of pesticides are consumed annually to the crops (10). In recent years, agrochemicals such as insecticides, herbicides, and fungicides have had many benefits for the industrial agriculture system (11). Studies showed that in case of not using such compounds in modern agriculture, the capacity of agricultural productivity would decrease by almost 10-15% (12). Using pesticides and herbicides in agriculture industry offers many advantages such as increased crop and livestock yields, improved food safety, human health, quality of life and longevity, and reduced drudgery, energy use and environmental degradation (13). However, excessive use of agrochemicals may lead to threatening biodiversity conservation, reducing soil fertility, developing a resistance of targeted species, and accumulation of nitrate in the soil (14).

2.1.2. Atrazine and its application, chemical characteristics, toxicology, and its degradation to metabolites

Among all those pesticides, atrazine has been applied as a pre- and post-emergent herbicide in the production of corn, sugarcane, sorghum, etc. since it has a high

selectivity to control broadleaf weeds and annual grasses (1). A vast range of half-life values has been reported for atrazine; from 45 days to 3-5 years, depending on the environmental conditions considered (15). Atrazine does not dissolve in water for the most part, with a solubility of only 33 mg/l at 25°C. Its degradation occurs at pH 6-8 by UV radiation as direct and indirect photolysis (15). Extensive use of atrazine for farming purposes and its relative persistence in the environment has resulted in its frequent run off agricultural fields into soil, surface, and ground water and it is detected in those media in addition to precipitation, gas phase, and even in has raised concerns about accumulation in food products. The range of concentrations detected in ground and surface water is around 100 ng/L to 30 ug/L in countries like Portuguese, France, and China (16) (12).

Despite all the benefits of atrazine in modern agriculture, its possible carcinogenic effect is controversial. It is classified as a potential endocrine disruptor chemical in mammals and aquatic life, although the United States Environmental Protection Agency (USEPA) has classified it as a "not likely human carcinogen" chemical (15). The European union has set drinking water MCL for pesticides at 0.1 μg/L and USEAP has set 3 μg/L as atrazine MCL in drinking water (15). The USEPA has reported that potential heart, lung, kidney congestion, low blood pressure, muscle spasms, weight loss, and damage to adrenal glands may occur in case of short-term exposure to atrazine higher than drinking water maximum contaminant level (MCL), to more severe diseases in case of long-term exposure (2)

Since atrazine does not absorb strongly to soil particles, it has a moderately high mobility in soils. Also, it can transfer to ground water and contaminate it because of its high mobility in soil. The most important route known for the disappearance of atrazine

from soil and aquatic environment is degradation by microorganisms naturally present in those media followed by chemical hydrolysis. Acidic and basic conditions enhance hydrolysis of atrazine, which is much slower at neutral pHs. One way of increasing hydrolysis rate is adding humic material to the environment (17,18). Four major metabolites of atrazine, hydroxyatrazine (HA; 6-hydroxyN-ethyl-N´-isopropyl-[1,3,5]triazine-2,4- diamine), diaminochlorotriazine (DACT; 6-chloro[1,3,5]triazine-2,4-diamine), deisopropylatrazine (DIA; 6-chloro-N-ethyl- [1,3,5]triazine-2,4-diamine), and deethylatrazine (DEA; 6-chloro-N-isopropyl- [1,3,5]triazine-2,4-diamine), are produced of catabolizing atrazine by plants, microbes, and animals (3).

In Figure 1, the paths of degrading atrazine to its metabolites have been demonstrated.

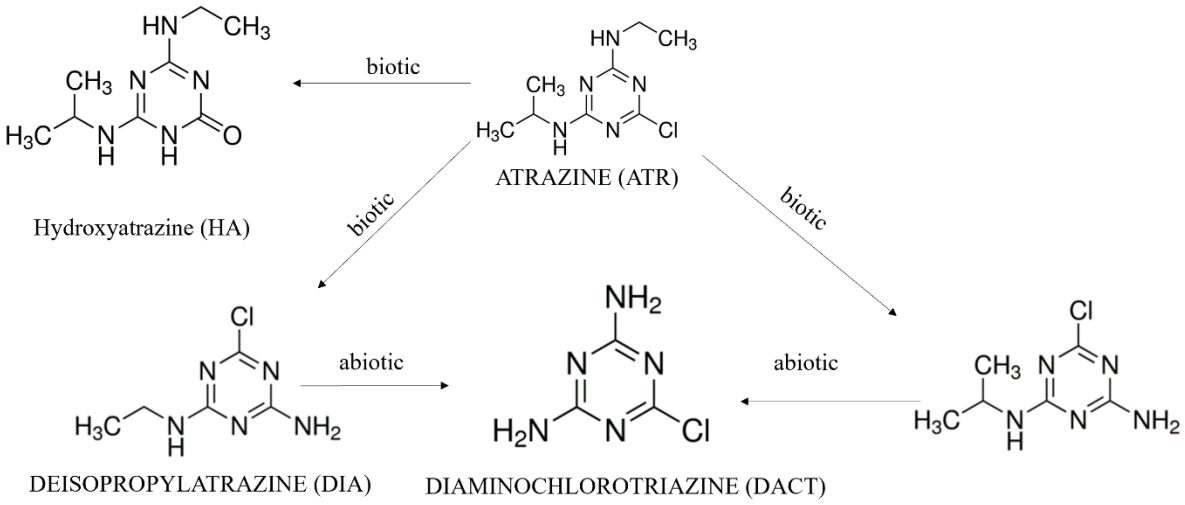

Figure 1. Atrazine degradation in the environment. Atrazine can be metabolized to HA, DIA, and DEA. DIA and DEA both are degraded to DACT.

A number of methods have been established for analyzing atrazine and its metabolites including thin-layer chromatography (TLC), gas chromatography (GC), high

performance liquid chromatography (HPLC), gas chromatography-mass spectrometry (GC/MS), liquid chromatography-mass spectrometry (LC/MS), and enzyme-linked immunosorbent assay (ELISA) (1,19). These methods are precise and specific for atrazine detection, although they are expensive, time-consuming, and need complicated equipment and expert technicians (1). The gold standard for atrazine analysis, LC-MS, has sensitivity and specificity but it is expensive, complex and time-consuming. In this method, depending on analyte limit of detection (LOD) or range of analyte concentration, the sample might need some preparation steps such as dilution in order to prevent clogs in column or Solid Phase Extraction (SPE) in order to concentrate the analyte to reach to its LOD. These sample preparation steps are both time-consuming and requires adequate training (18)(20) The ELISA method, although relatively precise, has been found to be inaccurate in many cases and have positively biased results due to interference with other organic compounds in the sample. Therefore, developing an inexpensive, rapid, facile, and applicable substitute technique for atrazine detection has been considered (1). So, developing a method which is inexpensive, rapid, and facile applicable is demanding.

2.2. Wetlands

2.2.1. Wetlands and their ecological role

Wetlands are lands that transition between terrestrial and aquatic systems where the water table is usually at or near the surface, or the land is covered by shallow water or saturated with water. A wetland's water could be groundwater flowing up from an aquifer or spring through porous media of the soil, come from a nearby lake or river, or created by strong tides of seawater that form coastal wetlands. They occur on every continent

including antarctica (21) and on high lands like mountains down to flat lands like coasts (22). There are so many types of wetlands mainly classified as swamp, marsh, fen, and bog. A swamp is a forested wetland and it's considered a transition zone between land and water. While a marsh is a type of wetland dominated by herbaceous rather than woody plants species. A marsh is a type of wetland that is accumulated by peat, i.e. deposit of dead plants materials (23). Along with bogs, a fen is a mire accumulated by peats and usually fed by mineral-rich surface water or ground water(24). Back in the days, wetlands were mostly considered as places to be avoided, because they were believed to be useless and disease-ridden. A study published in 1990 reported that most of the 221 million acres of wetlands in the lower 48 states in the late 1700s have been destroyed. Nowadays, it is proven that wetlands have some ecological functions that are accounted significant roles in society, such as fish and wildlife habitats, natural water quality improvement, flood storage, shoreline erosion protection, opportunities for recreation and aesthetic appreciation, and natural products for our use at little or no cost. Keeping the wetlands safe preserves the water quality and reduces flood damages which results in gaining the advantage of protecting humans health and safety (9,25). Wetlands are known as most diverse ecosystem, and they improve water quality and nutrient cycling, conserve the composition of atmosphere, decrease chances of flooding, treat stormwater runoff, and remove non-point source (NPS) pollution (26,27) (22).

2.2.2. Factors threatening wetlands health and safety

Different threats such as habitat loss and degradation, climate change, pollution, overharvesting and disease would jeopardize wetlands and conversion to agriculture is

among the most serious impact. Furthermore, extreme application of pesticides and fertilizers endangers wetlands ecosystems (28).

Wetlands safety are endangered due to a number of factors in rural and urban areas. In rural areas, the factors that contaminate wetlands media includes agriculture, mining, road construction, and recreational developments. In urban areas, activities jeopardizing wetlands include industrial discharge, municipal sewerage system, and urban development in general. Depending on those activities, different kinds of pollutants stress wetlands, such as sediments, pesticides and herbicides, toxic chemicals, and nutrients and organic matters (29). Agricultural activities in rural and urban areas have brought bioaccumulation and biomagnification of pesticides and herbicides in wetlands. In rural areas, due to small sizes of wetlands and quite proximity of wetlands to farming fields, pesticides entrance to wetlands in many direct and indirect routes has been facilitated to an extent that it has reached significant quantities and in some cases, has endangered the health and reproduction of wetland species (29).

Depending on the method of applying pesticides to farms, there are different ways for their transport to wetlands. They could be transported in gaseous and/or droplet form, or wind-blown when adsorbed to particulates, if the pesticide is applied aerially. In some cases, the pesticide is dissolved and transported by surface water runoff, snowmelt, or groundwater flow. The whole process of off-site transport depends on the pesticide's physicochemical properties such as water solubility, volatility and tendency to adsorb to suspended particulates (30). Fate of pesticides in wetlands depends on their residue loss process as a result of degradation (biodegradation, photolysis, hydrolysis), volatilization, adsorption to suspended particulates or sediments, and outflow in surface and ground

water. Chemical properties of the pesticide and the site features affect these processes and define the persistence of the pesticide. Previous studies show that pesticides like atrazine are among the most persistent pesticides, whereas more labile pesticides such as bromoxynil, may degrade rapidly (31). So, in order to improve each state's waters by promoting practices that minimize atrazine runoff and make it hold onto the field where it's the most beneficial for farming purposes and leaves the least environmental impact, best management practices (BMP) should be done specific to each state. These kinds of practices decrease the amount of atrazine loss after it is applied and also increase infiltration of runoffs containing atrazine before it leaves the field resulting in decrease in requires atrazine rate used for the fields and efficient crops production while preserving water quality. Some of those practices for the state of Missouri includes using atrazine in top two inches of soil for field with preplant tillage, applying atrazine in a postemerge time frame in no-till fields, integrating pest management strategies (prevention, avoidance, monitoring, and suppression), using buffers and buffer zones, keeping an eye on the weather (not applying atrazine close to a heavy rainfall), using proper mixing, loading, and disposal practices. Early preplant application of atrazine and reduced soil-applied rates should be avoided in the state of Missouri (32).

2.3. Molecularly Imprinted Polymers

Molecularly imprinted polymers are fabricated via two principles. The most common method which is also known as self-assembly approach, is using noncovalent interactions between template molecules and the functional monomers. In the other method covalent interaction is deployed between template molecule and the functional monomer, however after polymerization template molecule severs from the monomer molecule (33). In a

hybrid approach, the template molecule and functional monomer interact covalently before polymerization, but after removing the template molecule from the MIP, target molecules rebind via non-covalent forces. This method is called semi-covalent imprinting (34).

There are multiple factors that are involved in forming MIPs infrastructure including template molecules, functional monomers, cross-linker, initiator and in some cases porogenic and extraction solvent. The template molecules interact with specific functional groups of the functional monomers and this results in creating binding sites imprinted in the polymer structure. The cross-linker holds the functional monomers in the polymer matrix and gives it a rigid structure to fix the binding sites and contribute in the MIP-template selectivity. Initiator breeds free radicals to initiate the polymerization in presence of monomer, template and crosslinker. To bring all the elements together in polymerization, porogenic solvent is utilized, while the extraction solvent is utilized to elute the template molecules from the polymer and leave void binding sites in the matrix (35).

There will be tremendous amount of binding sites created by template molecules and functional monomers. Functional groups pre-organization type and also size and shape specificity of binding effect on molecular recognition characteristics. The selectivity of the MIPs relies on factors including the level of interaction between template molecules and imprinted groups along with shape and rigidity of template molecules.

According to molecular cluster theory, the nanocavities are complementary in shape and size to the template molecule as in key-lock mechanism. MIPs fabricated with crystal nuclei have better adsorption capabilities and the template-template interactions are more

prone to occur in the cavities of the MIPs with the formed molecular clusters of chiral imprinted molecules (36).

The chemical equilibrium in polymerization solution is related by the following equation:

$$[MTM] = K^2[T][M^2] \quad \text{Equation 1.1}$$

where K is the association constant; T is the concentration of the template molecule; M is the concentration of functional monomer; and MTM is the concentration of the desired template monomer complex.

If the association of two functional monomers and one template molecule is assumed to be independent and identical, the following equation is derived:

$$N = N_S + N_{NS} = P(K^2.[L].[MTM] + K.[L].([M_0 - 2[MTM]])) \quad \text{Equation 1.2}$$

Where N, N_S, and N_{NS} are total, specific, and nonspecific binding, respectively; L is the free ligand concentration; and P is a polymer concentration factor (related to concentrations of template molecules and the polymer).

The thermodynamics of molecular imprinting reactions can be explained by thermodynamics theory and following equation:

$$\Delta G = \Delta G_{(trans+rot)} + \Delta G_{(rotors)} + \Delta G_H + \Sigma \Delta G_i + \Delta H_{conform} + \Delta G_{vdw} \quad \text{Equation 1.3}$$

Where ΔG is the change in Gibbs free energy for the formation of monomer-template complex; $\Delta G_{(trans+rot)}$ is the change in Gibbs free energy for both translational and rotational; $\Delta G_{(rotors)}$ is the change in Gibbs free energy caused by restricted rotational motion of template molecule; ΔG_H is the change in Gibbs free energy of the whole group

participating in the reaction; $\Delta H_{conform}$ is the strain energy in the complex in relation with the introduction of unfavorable bond lengths, bond angles, dihedral angles, and so on; and ΔG_{vdw} is the change in Gibbs free energy by van der Waals forces.

In some cases, some of the above terms can be negligible and the equation would be briefed as:

$$\Delta G = \Delta G_{(trans+rot)} + \Delta G_{(rotors)} + \Sigma \Delta G_i + \Delta G_{vdw} \qquad \text{Equation 1.4}$$

2.3.1. Colloidal crystals and inverse opals

An ordered array of colloidal particles into a fine deposition analogous to a standard crystal is called a colloidal crystal. Diffraction and interferences of light in those ordered arrays provides the astounding optical property of the colloidal crystals (37). A periodic modulated constant is possessed by highly ordered crystalline structure of photonic crystal in the range of visible light wavelengths (380-750 nm). Electromagnetic waves spread due to Bragg reflections on lattice planes of materials can impact these periods (38). Recently, the combination of colloidal crystal and molecular imprinting to create polymers with 3D, highly ordered, microporous structures and specific binding sites for a fast method to detect organic compounds such as bisphenol A (39), atrazine (1), and 2,4-dinitrotoluene (40) has been implemented. This combination provides a high surface to volume ratios in the structure leading to a more efficient mass transport in submicrometer-sized pores and enhanced surface reactions which all results in high sensitivity and specificity of the polymers. Implementing this highly ordered porous structure in a hydrogel enables the polymer to swell or shrink in case of target recognition or environmental stimuli resulting in optical properties changes (41). This technique

benefits sensor applications in numerous ways including elevated specific surface areas, more interaction sites, promoted mass transport, better access to active sites through the interconnected microporous system, and high specificity to analytes (42,43).

Inverse opals are three dimentionally ordered microporous materials formed through the infiltration of nanospheres with dielectric properties with a material precursor and then, removal of the nanospheres either by chemical etching (SiO_2) or calcination method (38). Inverse opal films of MIPs have been reported using the colloidal crystal template method to detect bisphenol A and pH sensing, and controlling the thickness of inverse opal hydrogel by Langmuir-Blodgett technique. Since the structure is a uniformly ordered porous structure, the reflection peaks recorded by spectrophotometer can be attributed to interferences of light reflections on dense (111) planes (39). Bragg equation, as defined below, relates the peak wavelength of the porous hydrogel, λ_{max}, to the structure of porous film:

$$\lambda_{max} = 1.633\left(\frac{d}{m}\right)\left(\frac{D}{D_0}\right)\sqrt{(n_a^2 - \sin\Theta^2)} \qquad \text{Equation 1.5}$$

where *d* is the sphere diameter of the silica particle, *m* is the order of Bragg diffraction, (D/D_0) is the degree of gel swelling (*D* and D_0 are the diameters of the gel in the equilibrium state at a certain condition and in the reference state, respectively), n_a is the average refractive index of the porous gel at a certain condition, and Θ is the angle of incidence.

The hydrogel polymers that can swell or shrink in response to various stimuli such as pH, temperature, organic compounds, ionic strength, etc. have highly ordered

structures that translates the stimuli to a change in peak wavelength and visual structural color (44).

2.3.2. Optical features of photonic MIPs

The optical features of the MIPs are associated with nanoparticles that are used as templates to create macroporous structure and are made of materials with refractive index, transparency, photoluminescence, and photonic crystal characteristics. Optimized synthesis methods of nanoparticles play an important role in the particles size distribution which subsequently affects morphology, crystallinity, and composition of them (45). Nanoparticles have been implemented in sensors for various environmental contaminations detection. Au nanoparticles were used in fabrication of optical sensors via Surface-enhanced Raman Scattering (SERS) for detection of bisphenol A in surface and potable water. In this method SERS signal was enhanced as a result of target molecule specific binding to MIPs core-shell on Au nanoparticles surface and yielded a fast and efficient mechanism for bisphenol A detection in water (46). Another report of applying nanoparticles in optical sensors represents for fabrication of a chitosan/graphene oxide-magnetite MIP (Cs/GM-MIP) that has combined CdTe quantum dots@luminol nanoparticles to detect chrysoidine which is an industrial dye used for paper, fiber, and leather. In this method, the adsorption affinity of Cs/GM on MIPs is made by an increase in chrysoidine concentration and resulted in high sensitivity of the sensor (47).

2.3.3. MIPs characterization

MIPs can be imaged by Scanning Electron Microscopy (SEM). SEM scans a focused electron beam over a surface to create an image. The electrons interact with the atoms at the surface of the object to produce different types of signals such as back-

scattered, secondary electrons, X-rays, etc. The detector gets these signals and gives information about the samples surface structures and chemical composition. Since most MIPs are not conductive, they are coated with a thin layer of conductive material such as gold, platinum, or carbon using a sputter coater. SEM is used to image the macroporous surface and inner structure of the MIPs (48).

Fourier Transform Infrared Spectroscopy (FTIR) is used for identifying chemical bonds of present functional groups in a sample via infrared spectrum. The information regarding the functional groups and covalent bonding of the polymer is extracted from FTIR spectra. Comparing the polymer and functional monomer FTIR spectra differences as an indication of polymerization and interaction of template with polymer is implemented to characterize the MIPs (8).

Polymers have different morphologies as shown in Figure 2. Their morphology plays an important role in their imprinting performance; i.e. more binding sites would be

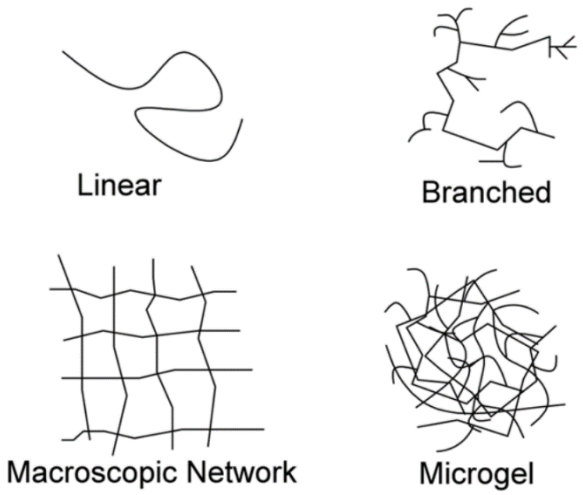

Figure 2. Imprinting effects of MIPs are affected by their morphologies including linear, branched, macroscopic network, and microgel (30).

accessible when they have larger surface area. SEM can also be used to obtain these kinds of information.

In order to assess specific surface area of the material more precisely, Braunauer-Emmett-Teller (BET) is used for analysis. BET is the fundamental theory of measuring specific surface area of a material and is based on physical adsorption of gas molecules on a solid surface. BET measurement and mathematical models yield the specific surface area (m^2/g), specific pore volume (ml/g), average pore diameter, and pore size distribution (35).

The intermolecular interactions between template molecule and functional monomer is measured by UV-Vis spectroscopy and H NMR (49). UV-Vis spectrometer can be used to measure absorbance or reflectance spectra using light in visible and near UV and infrared range. It is extensively used in analytical chemistry for quantification of different materials. Using a UV spectrometer, the change of absorbance (ΔA) of solutions

with different concentrations of functional monomer that are titrated by template molecule and equilibrated, would be measured at a specific wavelength and dissociation constant for polymerization and interaction and amount of unreacted template would be calculated from the results of absorbance change (50,51).

Physical and chemical properties including structure, dynamics, reaction state, and chemical environment of atoms or molecules can be determined by Nuclear Magnetic Resonance (NMR). NMR identifies functional groups with high resolution. However, it is not a cost-effective approach and requires a very large liquid helium-cooled super-conducting magnet (52).

To assess binding capacity and selectivity of MIPs, batch rebinding is used as demonstrated in Figure 3. (53).

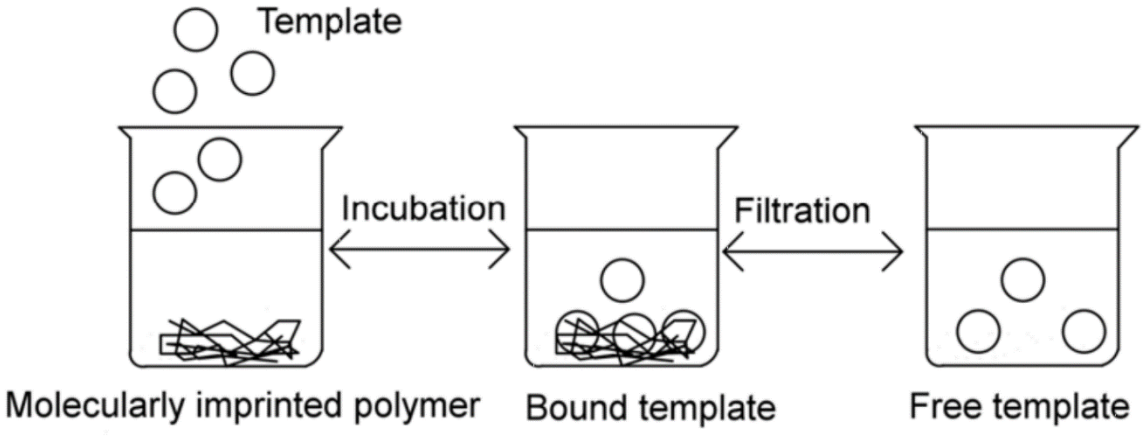

Figure 3. Batch rebinding method used to evaluate binding capacity and selectivity of MIPs (49).

Assumingly, after serial incubation, equilibrium is reached between template molecule and the MIP. The rection is defined as:

$R_{free} + L_{free} \rightleftarrows RL$ Equation 1.6

And at equilibrium:

$\frac{[R_{free}][L_{free}]}{[RL]} = \frac{C(N_t - B)}{B} = \frac{K_{-1}}{K_1} = K_d$ Equation 1.7

Where $R_{free} = N_t - B$, N_t is the amount of existing active centers per unit of volume in the MIP, k_1 stands for adsorption constant, k_{-1} stands for desorption constant, and k_d stands for the equilibrium desorption constant. The equation can be simplified to:

$\frac{B}{N_t} = \frac{C}{K_d + C}$ Equation 1.8

Hence, the amount of template bound per gram of imprinted polymer can be calculated (53).

2.3.4. MIPs as environmental sensors

Chromatographic techniques used for pesticides analysis need laborious sample pretreatment and preparation. MIP-based sensors have facile application and cost-effective development procedure, improved shelf-life, and the possibility of mass production with minimized differences in performance batch-to-batch (54). This is the reason they have been considered a suitable candidate to be used as sensors. The key-lock mechanism of MIPs has been a favorable feature to consider them as substitutes for the biological counterparts and produce matrices in more research fields. Combining sensors with molecular imprinting feature has extended the potential for more interdisciplinary research areas. The main parameters to evaluate the efficiency of sensors include

recognition, selectivity, specificity, limit of detection, and more in general, the quality and soundness of its results (55).

A functioning MIP-based sensor is formed of two major parts of recognition site and signal transducer (56). The recognition process is affected by three main parameters including the number of functional groups that have a role in the interaction, functional groups proper settlement around the binding site, and the physiques of the binding site and the recognition process has a crucial role in sensing performance (57). The physiques (i.e. shape and size) of the binding site mostly provides the specificity of the sensor, albeit it can be improved when the template involves with one or more proper functional monomers (8).

Conformational change in the polymer is induced by stimuli such as template interactions or change in the pH and it is a key factor that translates the presence of such stimuli by shrinking or swelling of the hydrogel. This conformational change effect has led to developing photonic polymer or pH-responsive MIP-based sensors (8,58).

2.3.5. Physicochemical properties of natural waters effects on MIPs response

Detection and quantification of various contaminants can be achieved using MIP-based sensors. Different transducing mechanisms have been utilized to translate the sensor recognition capability to a sensible signal including optical, chemical, or electrical properties variations. High sensitivity and simplicity of optical technics application has led to their extensive utilization in studying MIPs binding efficiency, recognition capacity, and selectivity (59). Parameters like linearity, limit of detection, response time, robustness, sensitivity, selectivity, reproducibility, accuracy, and lifetime can also be

characterized for sensing properties (60). However, the impact of physicochemical characteristics of natural waters (i.e. ionic strength, natural organic matter) on sensing performance of photonic MIPs needs to be investigated more.

Since synthesis of MIPs is approached as creating a SPE media, there has been more researches focused on the steps of conditioning, washing, and eluting of the process rather than the mechanism of detecting and sensing the target and hence, the mechanisms of those interferences have not yet fully studied. Capability of predicting and analyzing these interferences would make it possible to use MIPs as in-situ sensors in natural waters.

Sensing performance of the MIPs can be compromised by sample properties that is highly probable in natural waters such as ionic strength and presence of natural organic matter and those effects have not been fully studied. It is reported that MIPs can be induced by changes in temperature (61), pH (58), and ionic strength (62). It is reported that increasing ionic strength from 1 to 100 mM has decreased quenching of fluorescent-based MIPs by 30% and also basic environments increases quenching of MIPs due to higher swelling ratio of the MIP, while rinsing MIP will neutralize that effect (63). Other parameter that potentially can compromise performance of the MIPs, is interferences in detection of target and in this work, interferences are compounds that are capable of obstructing the bonding sites available in polymer film and blocking the target molecules access to those sites resulting in pore blockage, steric repulsion or electrostatic interactions at or near the surface of the film. This happens due to the interfering compound nonspecific adsorption onto the film and decreases the sensing capacity of the MIPs. Some of possible interferences that might occur in natural waters are due to

presence of dissolved salts and organic matters, inorganic colloidal particles, and microorganisms.

MIPs have been reported to be used as sorbent for solid phase extraction in natural waters (64,65). Different parameters in water chemistry matrix impact on the use of MIPs in natural water has not been thoroughly investigated (66,67). It is reported that atrazine was used as the template molecule and then the MIP extracted atrazine, simazine, ametryn, and propazine from natural water samples (68). In another study, for detection of tetrabromobisphenol A (TBBPA), diphenolic acid (DPA) and bisphenol A (BPA) were used as template molecules. It is reported that TBBPA capture in tap, river, and lake water was in range of 85% to 97% with detection limit of 2 ng/ml (69). Monitoring atrazine in both contaminated and uncontaminated natural waters was done by conductometric transducer based sensor and it yielded detection limit of 1 ppb, although the technique required laboratory instruments which impeded in-situ application of the sensor (70).

Photonic MIPs are suitable for in-situ applications since they are supported on a polymethylmethacrylate (PMMA) slide and they provide facile measurement. The concentration of contaminants in the environment are fairly low, given the complex chemical composition of natural waters, detecting them could be a challenging task in natural waters because of probable interferences of sample chemical compounds and preventing the sensor to perform efficiently.

3. Detection of Atrazine and its metabolites by photonic molecularly imprinted polymers in aqueous solutions

3.1. Introduction

Atrazine is one of the most common herbicides used by farmers in the United States due to their selectivity against broadleaf weeds and annual grasses (1). Although it is beneficial for agricultural purposes, extensive use of this herbicide has caused contaminations in drinking water and soil and it can be harmful to living organisms even at really low concentrations (19). According to the United States Environmental Protection Agency (USEPA), short time exposure to atrazine above the drinking water maximum contaminant level (MCL) of 3 μg/L may lead to lung, heart, and kidney

diseases, low blood pressure, muscle spasms, weight loss, and damage to adrenal glands (2), while long-time exposure might cause much more severe diseases.

Atrazine is degraded by plants, animals, and microorganisms to different metabolites. While some byproducts of the degradation are hydrophobic and have low water solubility, three main metabolites are of interest in aqueous solutions (Figure 4): diaminochlorotriazine (DACT; 6-chloro[1,3,5]triazine-2,4-diamine), deisopropylatrazine (DIA; 6-chloro-N-ethyl- [1,3,5]triazine-2,4-diamine), and deethylatrazine (DEA; 6-chloro-N-isopropyl- [1,3,5]triazine-2,4-diamine) (3). DEA, DIA, and DACT have lower soil adsorption coefficient (K_d) and organic carbon-water partition coefficient (K_{oc}) than other metabolites of atrazine (71). These coefficients are criteria for mobility of a substance in soil and higher values are indicative of substance adherence to soil particles and low solubility in water. These water-soluble atrazine metabolites demonstrate relatively long aerobic aquatic half-life. Due to their potential health effects, concerns have been raised over the extensive use of atrazine in the United States and efficient

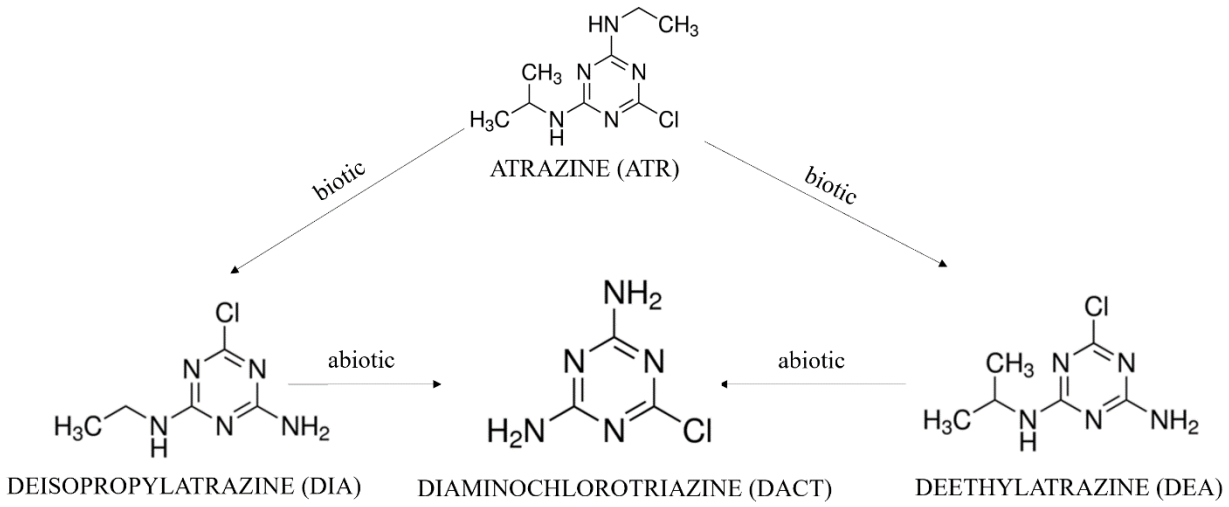

Figure 4. Structure of Atrazine metabolites. Atrazine can be metabolized to DIA, and DEA via biotic degradation routes. DIA and DEA both are degraded to DACT via abiotic degradation routes.

approaches of detection and removal of these compounds (3,4). Hence, monitoring levels of atrazine and related compounds in the environment is of high importance.

Methods currently used for the analysis of atrazine include gas chromatography (GC), gas chromatography-mass spectrophotometry (GC/MS), high pressure liquid chromatography (HPLC), liquid chromatography mass spectrophotometry (LC/MS) and enzyme-linked immunosorbent assay (ELISA) (1). These methods are precise and specific for atrazine detection, but they are expensive, time-consuming, and need complicated equipment and expert technicians. The gold standard for atrazine analysis, LC-MS, might require some preparation steps on sample, such as dilution to prevent clogs in the chromatography column or Solid Phase Extraction (SPE) to concentrate the analyte to above the Limit of Detection (LOD). These sample preparation steps are both time-consuming and require adequate facilities and trained operators (18)(20). The ELISA method, although relatively precise, has been found to be labor intensive and have positively biased results due to interference with other organic compounds in the sample

(72). Therefore, there is a need for a rapid, facile, and applicable substitute technique for atrazine analysis (1).

Molecularly Imprinted Polymers (MIPs) are a promising alternative to current methods for the detection and quantification of atrazine and its metabolites. MIPs are polymerized and crosslinked in presence of a "target" molecule that is afterwards eluted, leaving empty spaces in the polymeric matrix that are complementary in size, shape and chemical compatible with the target and act as specific binding sites for the molecule (53). In this sense, MIPs' mechanism of target rebinding is similar to biomolecular recognition as in enzyme and substrate molecule act like key-lock mechanism (73). The fabrication of molecularly imprinted polymers includes the following essential steps: integration of the target in monomer and crosslinker solution, design of the spatial distribution of target molecules within the polymeric matrix by means of the polymerization reaction, and the removal of the target molecules in order to create void spaces of complementary morphology of the target molecules (7).

MIPs have been studied broadly for analytical chemistry applications and as sensors in environmental, chemical, and biomedical fields and have demonstrated several advantages over their biological counterparts such as improved stability, facile fabrication, great potential of capturing small molecules, reusability, and longer period of validity. However, there are still considerable challenges that prevent large scale application and achieving this method's fullest capabilities (74,75). MIPs have been reported for detection and quantification of several pollutants such as 2,4-dinitrotoluene, 2-butoxyethanol (40,76), testosterone (77), triclosan (78), and atrazine (1). Atrazine and its metabolites residues in agro-products and a watershed soil were extracted using MIPs

and dual-template MIPs were proposed as SPE media for pre-concentration before analysis by LCMS/MS (79,80) of beef liver extracts, grape juice, herbal medicine, and water samples(81). Recoveries ranged from 60% - 95%; lower recoveries reported for more complex matrices. ATZ MIPs were used for pre-concentration of purified and unpurified beef liver extracts for LC analysis and reported 89% and 61% recoveries from purified and unpurified extracts, respectively (82). Xu et al. reported 92% to 107% recovery of ATZ MIPs for adsorbing triazine herbicides from Radix Paeoniae Alba (PRA), a traditional Chinese herbal medicine(83). ATZ MIPs have been reported using methacrylic acid (MAA) as the functional monomer, but acrylic Acid-based MIPs showed more sensitivity at the same concentration of ATZ in comparison with MAA-based MIPs(1,84). Double water compatible MIPs (DWC-MIPs), which have a water-compatible core and hydrophilic polymer brush, were used as SPE sorbent for extracting triazines from water samples and reported recoveries ranging from 69% to 95% for four triazines (ATZ, ametrine, simetryn, propazine)(85).

In spite of extensive previous studies on ATZ MIPs, there is a gap in using those MIPs as sensors for detection and monitoring ATZ and its metabolites in aqueous solutions. When applied to sensor development, MIPs are combined with a mechanism (electrochemical, chemical, fluorescent or optical) that allows for the assessment of the amount of rebinding after exposure to a sample (86,87). In particular, MIPs can be fabricated in an optically active structure, which results in a label free sensor and avoids response to non-specific binding, one of the main limitations of MIPs (88). Colloidal crystals are ordered, long-range arrays of monodispersed colloidal particles, presenting a crystalline organization (89). Using colloidal-crystal templating within the MIP to create

3D-ordered interconnected macroporous structure results in useful optical properties (Bragg diffraction) and bright structural color, enabling them to change optical properties of the material as a result of swelling or shrinkage in aqueous solution (1); this mechanism fulfills the detection purpose of the sensor by transducing the recognition to some sensible signal.

The objective of this work is to develop and test an array of MIP sensors for atrazine and its water-soluble metabolites in aqueous environmental samples, as they are the ones that are expected to be present and detected in water bodies. A complete assessment of the effect of ATZ use in natural waters should include its soluble metabolites, as they will prolong the impacts of pesticide runoff after degradation of the parent compound occurs. The MIPs were fabricated in an inverse opal-like structure for a label-free colorimetric detection of the targets. Kinetics and equilibrium tests were conducted in laboratory made solutions. Moreover, we studied the cross-reactivity of each MIP to other analytes since their combined presence in natural waters is highly probable.

3.2. Material and methods

The following chemicals were purchased from Sigma-Aldrich (St. Louis, MO, US) and used without any purification: acrylic acid (AA) (99%), ethylene glycol dimethacrylate (EGDMA) (98%), 2,2'-azobisisobutyronitrile (AIBN) (98%), hydrofluoric acid (HF) (48%), ethanol (99.5%, 200 proof), acetic acid (96%), DEA (100%), DIA (100%), and ATZ (100%) used for LCMS/MS standard. ATZ (>97%) was purchased from Santa Cruz Biotechnology (Dallas, TX, US) and used for MIP fabrication

and preparation of test solutions. Commercial silica particles (300 nm diameter) were supplied by Pinfire Gems and Colloids (Frankfurt, Germany). Glass microslides (3”×1”×0.04”) were purchased from FisherBrand (Pittsburgh, PA, USA) and cut in 0.04”×1/3”×3” pieces before use. Poly (methyl methacrylate) (PMMA) plastic slides of dimensions 0.04”×1/3”×3” were obtained from ePlastics (San Diego, CA, USA).

3.2.1. Fabrication of MIPs and non-imprinted polymers (NIPs)

The steps for the fabrication of MIPs is illustrated in Figure 5. First, 142.5 mg SiO_2 particles were added to 75 ml ethanol and the suspension was stirred and sonicated alternatively for 24 hours to obtain a well-dispersed 0.1% volume fraction suspension. Glass slides were vertically inserted in the SiO_2 particle suspension and kept at 50ºC for 24 hours. As ethanol evaporated, the silica particles self-assembled on the glass slides forming organized structures of 10 to 12 layers of particles. In the preparation of the polymerization solution, the target molecule was added to 1 ml ethanol and 0.8 ml AA as monomer to have a 1:80 molar ratio target to monomer. Then, 0.55 ml EGDMA (1:4 molar ration of EGDMA:AA) was added as crosslinker and the solution was left overnight to produce the noncovalent complexation via hydrogen bonds among hydroxyl group and oxygen atom of AA and nitrogen atoms and hydrogen atoms of amino groups in atrazine and its metabolites. Finally, 6 mg AIBN was added as initiator. In the next step, a PMMA slide was placed on each side of a glass slide where the colloidal crystals were formed, and the three were firmly held together while immersing one end in the polymerization solution. The solution infiltrated the interspaces of the colloidal crystal structure by capillary forces and filled its void spaces. In order to complete the

polymerization, the slides were irradiated with UV light (power = 36kW, wavelength= 365 nm) for 3 hours. Ice packs were placed under the samples to keep temperature below the glass transition temperature (T_g) for the polymer of 50°C (40). The assembly was placed at -18°C for 30 minutes to aid in the separation from the glass slide. The porous films remained attached to the PMMA slides and were immersed in 5% HF overnight to etch the silica particles remaining in the polymer, leaving large cavities within the film.

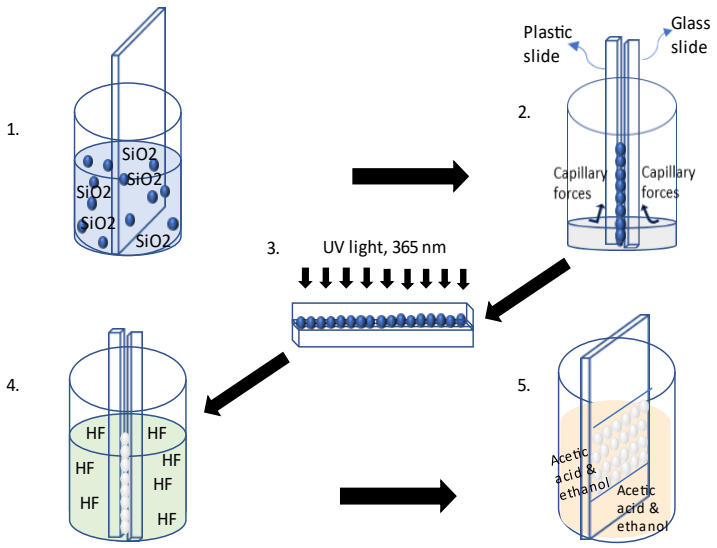

Figure 5. Schematic of MIPs fabrication steps: 1) self-assembled colloidal crystal formation; 2) infiltration of pre-polymerization solution; 3) polymerization; 4) SiO2 particle removal using HF; 5) target molecule elution using acetic acid and ethanol.

An acetic acid in ethanol solution (volume ratio 1:9) removed the target molecules from the MIPs. Three 15 minute-cycles of washing were conducted, under gently stirring to facilitate the elution of the target molecules from the polymeric matrix. Non imprinted polymers (NIPs) were also fabricated as controls, following the same general procedure but in the absence of a target.

3.2.2. Characterization

SiO_2 particles, colloidal crystals and polymeric films were imaged by scanning electron microscopy in a FEI Quanta 600 FEG (ThermoFisher Scientific, Hillsboro, OR, USA) Environmental Scanning Electron Microscope (ESEM) to investigate particle size, thickness and inner morphology of the structures. The glass slide was copper taped to the stub and coated with a conductive layer of platinum (1.5-3 nm) with an Emitech K575x sputter coater (Quorum Technologies Ltd., Ashford, Kent, UK).

Fourier Transformed Infrared Spectroscopy (FTIR) spectra was collected in a Cary 660 spectrometer (Agilent Technologies, Santa Clara, CA, USA) in the wavelength range of 4000-400 cm^{-1}. Both MIP (before and after elution of target molecules) and NIP films were characterized by FTIR to identify the functional groups present on the films.

3.2.3. Analytical measurement of concentration

Stock solutions of atrazine and its metabolites (100 ppm) were prepared in methanol and used for serial dilution in DI water.

Concentration of atrazine and its metabolites in all solutions tested were determined by Liquid Chromatography-Mass Spectrometry (LCMS/MS), in a Waters Alliance 2695 High Performance Liquid Chromatography (HPLC) system coupled with Waters Acquity TQ triple quadrupole mass spectrometer (MS/MS). The analytes were separated by a Phenomenex (Torrance, CA) Kinetex C18 (100mm x 4.6 mm; 2.6 µm particle size) reverse-phase column. The mobile phase consisted of 10 mM ammonium acetate and 0.1% formic acid in water (A) and 100% acetonitrile (B). The gradient conditions were 0 – 0.5

min, 2% B; 0.5-7 min, 2- 80% B; 7.0 -9.0 min, 80-98% B; 9.0 – 10.0 min, 2% B; 10.0 – 15.0 min, 2% B at a flow rate of 0.5 mL/min. The ion source in the MS/MS system was electrospray ionization (EI) operated in the positive ion mode with capillary voltage of 1.5 kV. The ionization sources were programmed at 150°C and the desolvation temperature was programmed at 450°C. The MS/MS system was in the multi-reaction monitoring (MRM) mode with the optimized collision energy. The ionization energy, MRM transition ions (precursor and product ions; **Table 3.1**), capillary and cone voltage, desolvation gas flow and collision energy were optimized by Waters IntelliStart™ optimization software package. The retention time, calibration equations, and limits of the detection for the analyses of ATR, DEA, and DIA are summarized in **Table 3.1**.

Table 3.1. Precursor and product ions selected for the analysis of ATR, desethylatrazine (DEA) and deisopropylatrazine (DIA) by HPLC-MS/MS (LOD = limit of detection)

Compound	RT (min)	Molecular ions (m/z)	Product ions (m/z)	Polarity	Linear equation	Correlation coefficient (R square)	Collision Energy	Cone voltage (V)	LOD (ug/L)
ATR	9.471	215.86	173.89	ES+	y=58890x	0.9986	Tune	30	0.06
DEA	7.632	187.86	145.78	ES+	y=10336x	0.9957	Tune	30	1.45
DIA	6.829	173.82	131.76	ES+	y=3321x	0.9973	Tune	30	5.72

Preconcentration by solid phase extraction (SPE) was conducted for samples which the concentration of analyte was below the LC-MS/MS LOD. Samples were filtered through a 0.2 µm Whatman Anotop syringe membrane filter (Sigma-Aldrich, St. Louis, MO, USA) and a 50 mL of aliquot was spiked with 500 µl of the internal standard terbuthylazine (TRB, 1 ppm), to achieve a final concentration of 10 µg/L of TRB (Sigma-Aldrich, St. Louis, MO, US). Oasis HLB solid-phase extraction cartridges (500 mg;

Waters, Milford, MA) were conditioned with 8 mL of methanol, followed by washing with 8 mL of DI water twice. Following the condition and washing process, the samples (50 mL) were passed through the cartridges at a flow rate of 5 mL/min and the cartridges were washed with 8 mL of DI water and the sorbent dried under vacuum in a SPE manifold system for 5 min. The analytes were subsequently eluted with 7 mL of methanol at 2 mL/min. The eluates were then concentrated under a stream of nitrogen in a temperature bath at 27 ^{o}C until dryness. The resulting extracts were resuspended with 1 mL of water: methanol (10:90, v/v), and filtered through a 0.2 μm PTFE Acrodisc syringe membrane filter (Waters, Milford, MA).

3.2.4. Measurement of optical response

The constructive interference of light as it is reflected from the porous structure of the polymer creates peaks at variable wavelengths that depend on the incident wavelength and the distance between pore layers in the film structure, which in turn is modified by the rebinding of the target molecules. The peak wavelength of the Bragg diffraction spectrum is given by:

$$\lambda_{max} = \mathbf{1.633}\left(\frac{d}{m}\right)\left(\frac{D}{D_0}\right)\sqrt{(n_a^2 - \sin\Theta^2)} \qquad (1)$$

where d is the sphere diameter of the silica particle, m is the order of Bragg diffraction, (D/D_0) is the degree of gel swelling (D and D_0 are the diameters of the gel in the equilibrium state at a certain condition and in the reference state, respectively), n_a is the average refractive index of the porous gel at a certain condition, and Θ is the angle of incidence.

Reflection spectra were collected using a UV-Visible spectrophotometer (Cary 60, Varian, Palo Alto, CA, USA) with a Harrick Scientific's Specular Reflection Accessory (ERA-30G) at a fixed angle of 30º, in wavelength range of 200-800 nm and double-beam mode.

In order to determine the rebinding kinetics, MIP films were incubated in 5ppb solutions of the corresponding target. The reflectance spectra were collected at predetermined time intervals until no significant change in peak wavelength was observed. After each interval, the MIP was removed from the test solution, patted dry softly with a paper tissue before reflectance spectrum measurement and promptly immersed back in the test solution for next time interval. A gently mixing was provided by a shaker at 90 rpm while the films were in the test solution.

In the equilibrium incubation experiments, MIPs were tested in a series of solutions of ATZ, DEA and DIA at concentrations ranging from 0.1 ppb to 10 ppb, starting with the most diluted one. MIPs were first equilibrated in DI water as a blank, taken out of the solution, patted dry softly and examined in UV-Vis spectrophotometer for their initial reflectance peak wavelength. Then, the MIPs were incubated in the test solutions in order of increasing concentrations following the same procedure to record their response and generate the calibration curve. In the case of test solutions of unknown concentration, a new MIP was used each time, equilibrated in DI water first and followed by incubation in the test solution. The concentration of the test solutions was validated by LCMS/MS. The details of validation method are provided in Supplementary Materials.

Cross-reactivity of the MIPs was examined by incubation tests of ATZ, DEA, and DIA MIPs in solutions with all three targets at the same concentrations, either 1 ppb or 5

ppb. Each MIP was first equilibrated in DI water as a blank, patted dry softly and their initial reflectance spectra were recorded. Finally, they were incubated in the combined test solution and their peak wavelength shift was determined. These experiments were repeated 3 times using 3 newly fabricated MIPs of each target.

3.3. Results

3.3.1. Characterization

SEM. The concentration of the SiO_2 particle suspension used for the colloidal crystal formation directly affects its thickness, and therefore the thickness of the polymeric film and the performance of the MIP sensor. If the film is too thin, there will not be enough light reflections in the pore layers to produce a strong constructive interference and the intensity of the peak of the reflection spectra will be low. On the other hand, if the film is too thick, despite of larger total surface area, diffusion to the cavities in the lower layers would take longer and the time until equilibrium during incubation would make the sensor impractical due to its slow response. Particle suspensions with volume fractions of 0.1%, 0.15% and 0.3% were used to grow colloidal crystals and the number of layers in the resulting deposits were determined by ESEM. Jiang et al. showed that the number of layers of colloidal crystals obtained by vertical self-can be estimated by (90):

$$k = \frac{\beta L \varphi}{0.605\, d(1-\varphi)} \quad (1)$$

where k is the number of layers, L is the meniscus height, β is the ratio between the velocity of a particle in solution and the fluid velocity and is taken to be 1, d is the

particle diameter, and φ is the particle volume fraction in solution. Given L = 3500 μm (90), φ = 0.001, and d = 300 nm, k would equal 19. According to equation 2, the colloidal crystal thickness obtained from 0.1%, 0.15% and 0.3% were expected to be 19, 29 and 58 layers of particles, respectively. However, SEM images showed that 0.1%, 0.15%, and 0.3% particle volume fractions yielded 12, 19, and 35 layers, respectively (Figure 6). The reason of this difference in number of layers from the equation and images may be due to the fact that meniscus height (L), which depends on the surface tension of ethanol and its contact angle on glass surface, cannot be exactly measured (90).

In this work, L was assumed to be at upper limit, which is meniscus height of ethanol on glass surface in absence of colloids and caused the difference in calculated number of layers with the actual number of layers from the SEM images. In this work, 0.1% volume fraction was selected since it is expected that the number of layers would be approximately 12. Preliminary work showed that less than 10 layers decreases the intensity of the peaks in reflectance spectra and over 20 layers creates slow response of the MIP. After choosing 0.1% as volume fraction, silica particles were deposited on glass slides to achieve colloidal crystals. Figures 6a and 6b shows top view and cross section of colloidal crystals using 0.1% volume fraction.

After polymerization and etching silica particles by HF, the porous structure in the MIP film was generated. Figure 7a shows porous structure of MIP film surface after etching silica particles and Figure 7b shows MIP film internal pore structure. This morphology will create a large number of readily available binding sites in the film, that would facilitate the access to target molecules.

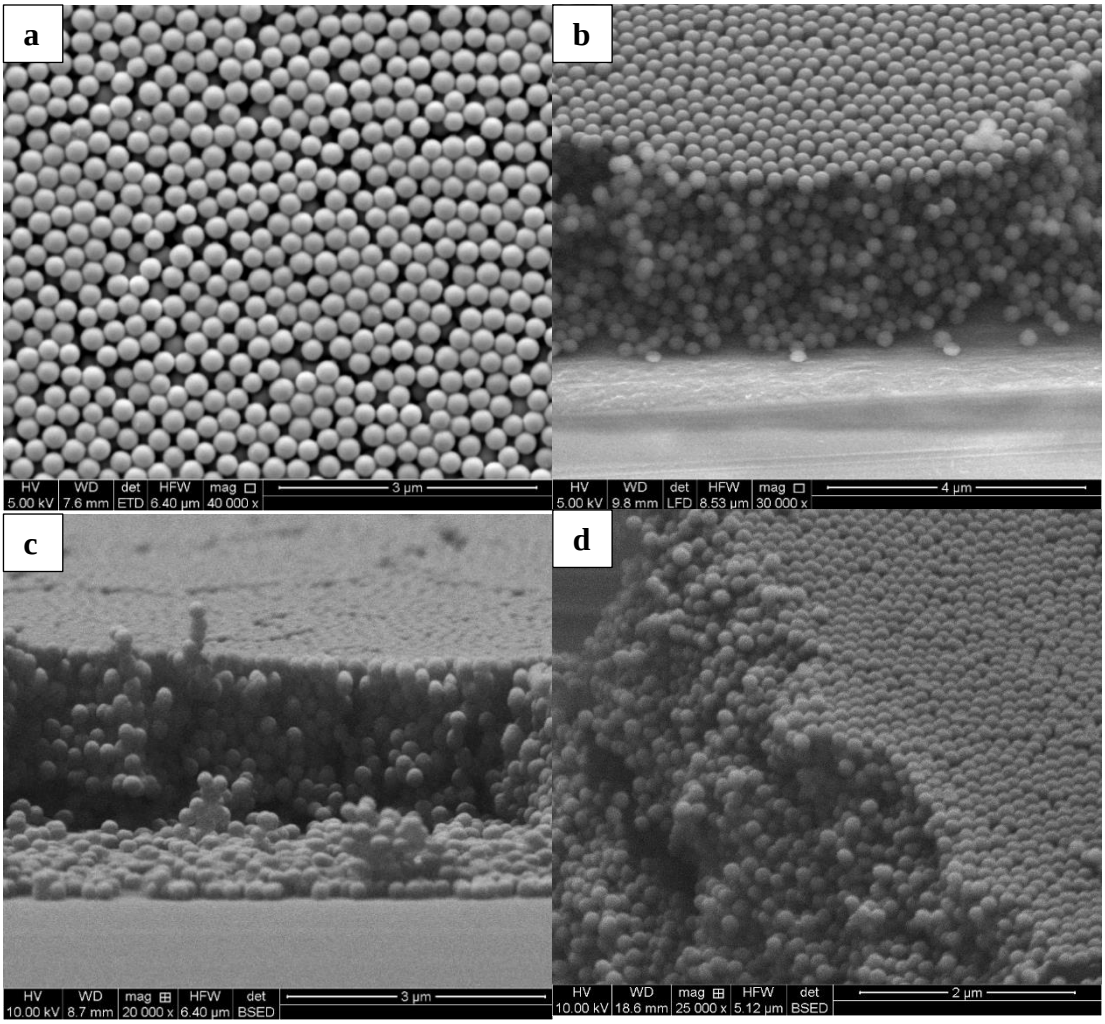

Figure 6. SEM images of SiO2 colloidal crystals on glass slides; a) top view, 0.1% volume fraction, b) side view, 0.1% volume fraction, c) side view, 0.15% volume fraction, d) side view, 0.3% volume fraction.

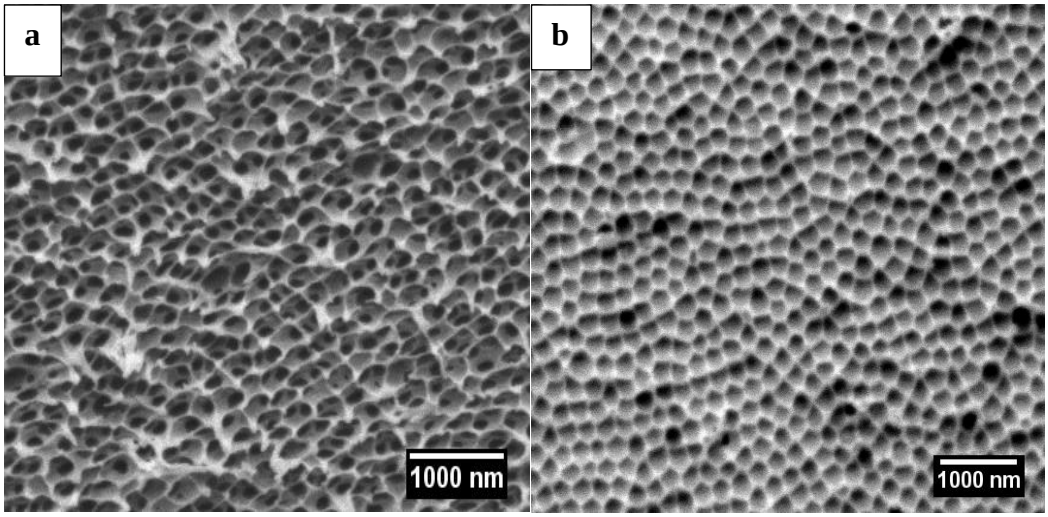

Figure 7. SEM images of polymeric film porous structure supported on PMMA slides a) MIP film, top view, b) MIP film internal structure

FTIR. *Chemical functional groups of the polymer and their interactions with target molecules were analyzed by FTIR. Figures 8, 9, and 10 show the FTIR spectra for NIP and MIPs before and after target removal for ATZ, DIA and DEA, respectively. Some different bands and intensities can be identified for NIP and MIPs after target removal with MIPs before target removal. The higher absorbance peaks for NIP and MIPs after target removal is due to functional groups involved in the non-covalent bonding with the target molecule that become free to interact with the incident light, and result in increased adsorption* (91)*. The peaks around 3000 and 1760 cm^{-1} are clearly observed for NIP and MIP after target removal and correspond to OH bonding in carboxylic acid group. However, those peaks are not noticeable in MIPs before target removal, due to the interaction between carboxylic group and target molecule in the polymer since the carboxylic group acts as both acceptor and donor of hydrogen bond interacting with hydrogen atoms of amino group and nitrogen atoms of triazine cycles.*

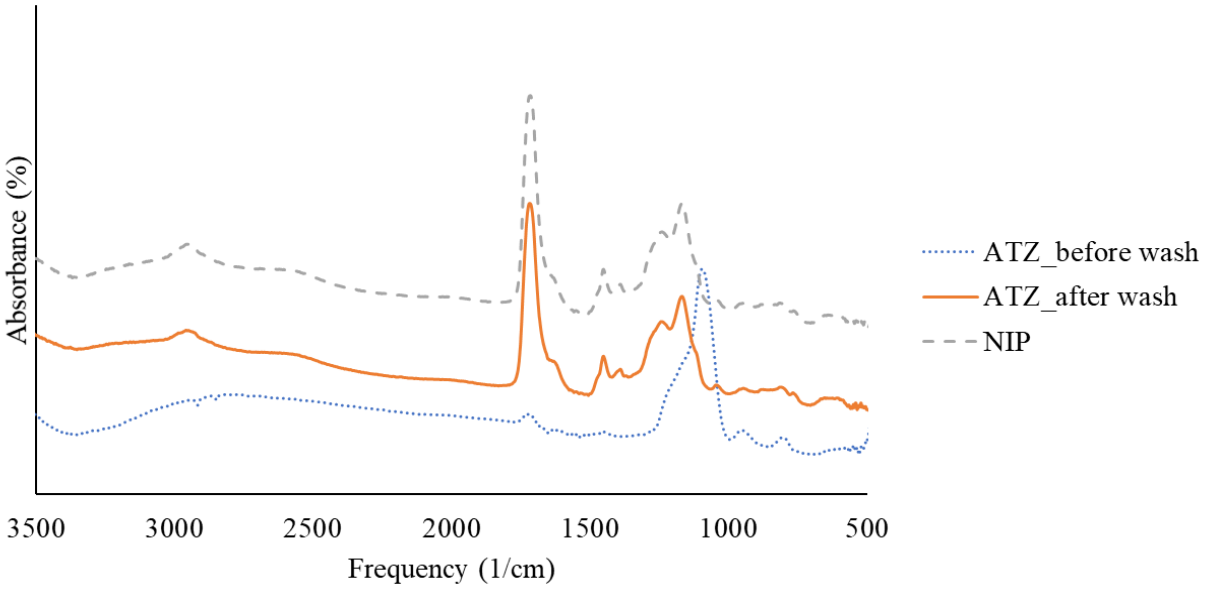

Figure 9. FTIR spectra for NIP and ATZ MIP before and after wash.

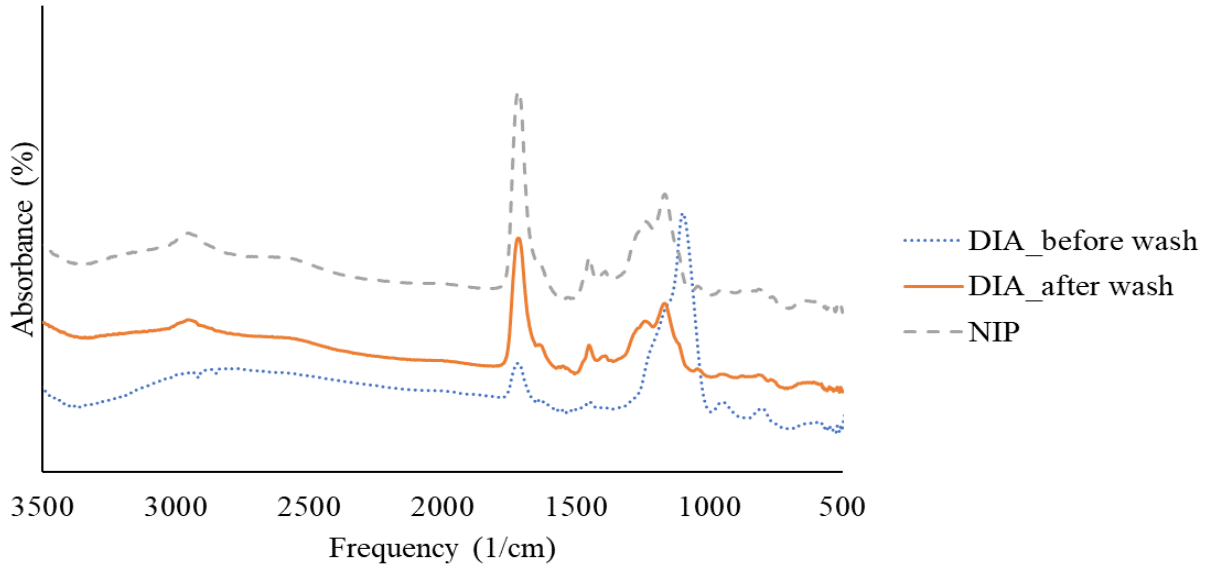

Figure 8. FTIR spectra for NIP and DIA MIP before and after wash.

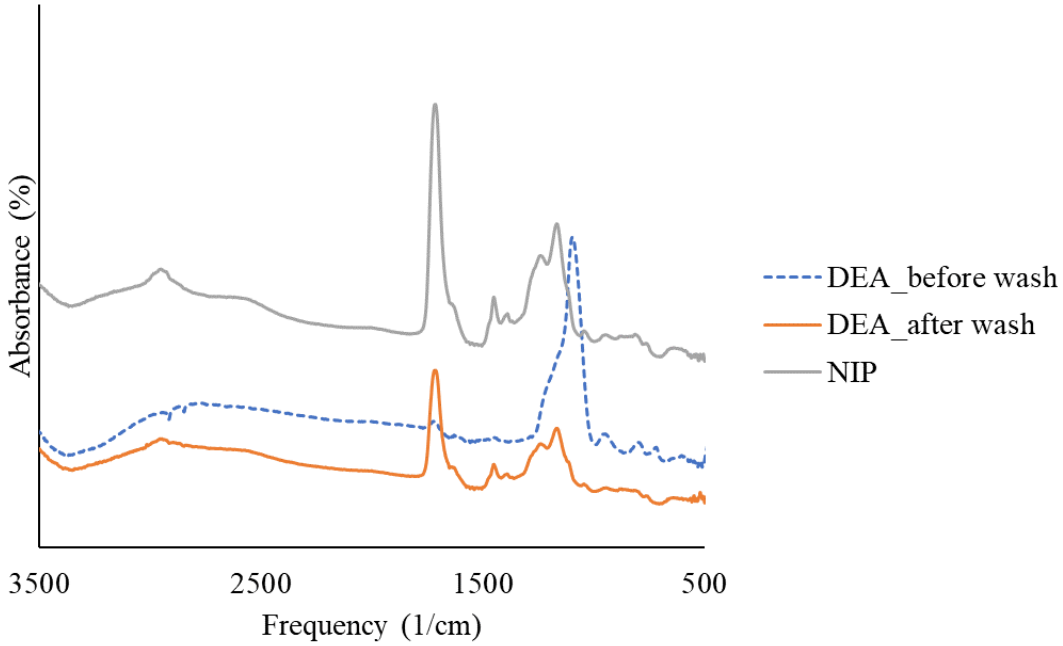

Figure 10. FTIR spectra for NIP and DEA MIP before and after wash.

3.3.2. Sensor Kinetics

The rebinding kinetics tests were conducted with ATZ MIPs and confirmed with DEA MIPs. Same trend for both compounds was observed (Figure 11). Under sample stagnant conditions, the peak wavelength changed fast in the first 16 minutes, approximately 87% of the maximum peak wavelength shift, and only 9.5% of the shift occurred after 20 minutes, on an average. In an effort to speed up response by minimizing the role of molecular diffusion as the mass transfer mechanism during incubation,

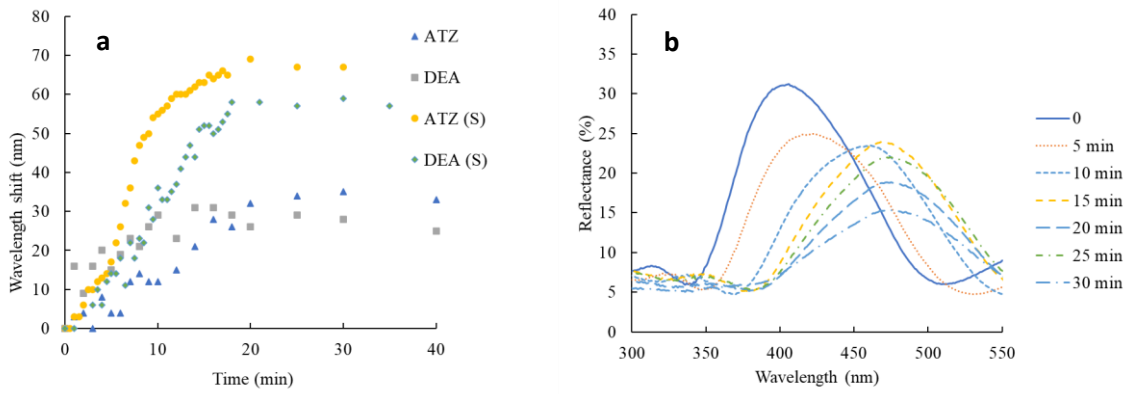

Figure 11. Kinetics test for MIPs in 5 ppb solutions of the corresponding target compound. a) Wavelength shift as a function of incubation time in the target solution (S represents Stirred for mixing conditions.) b) Reflectance spectra for ATZ MIP kinetics test incubated in a 5-ppb solution (STIRRED).

experiments were repeated applying a gentle shaking to cause a flow around and in the pore volume of the MIPs. The target solutions were placed in the shaker at 90 rpm. Interestingly, the mixing did affect slightly the time to equilibrium, but produced a much larger shift of the peak wavelength, over 90% more for both ATZ and DEA MIPs. In mixing conditions, both MIPs had 88% of their maximum shift in 16 minutes and after 20 minutes, on average 1.5% of the shift occurred. Applying a gentle mixing provides convective transport in addition to diffusive transport of the target molecules around the

MIP and overcomes the molecular diffusion barrier. This effect facilitated target molecules movement through the macroporous structure of the film (Figure 11) to the binding sites, and consequently increased peak wavelength shift. It was therefore determined that the optimum required time for MIPs incubation would be 20 minutes and all further tests were conducted under the gently mixing conditions.

3.3.3. Equilibrium incubation experiments

The effects of equilibrium rebinding of ATZ, DEA, and DIA MIPs on their optical response were examined by immersing each MIP in a series of solutions with different concentrations of the target compound in DI water for 20 minutes using a shaker at 90 rpm, following the results in the kinetics tests. Figures 12a, 13a, and 14a show the average shifts of MIPs in response to different

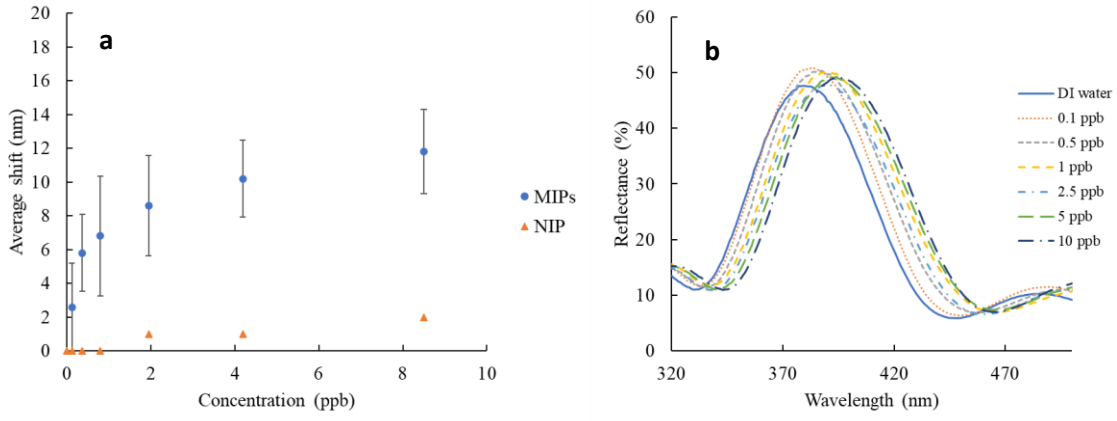

Figure 12. ATZ MIPs and NIP response to incubation in a series of solutions with different ATZ concentrations. a) wavelength shift; b) reflectance spectra of one representative MIP in response to test solutions.

concentrations of the validated solutions and Figures 12b, 13b and 14b show the reflectance spectra of the MIPs vs. the nominal concentration of the solutions. Reflectance spectra of the MIPs were modified by the adsorption of target molecules in binding spaces and consequent swelling of hydrogel. An increase in the concentration of the incubating solution produced a shift in peak reflectance to higher wavelengths. When a MIP is used for incubation tests, all the binding sites in the polymer matrix are

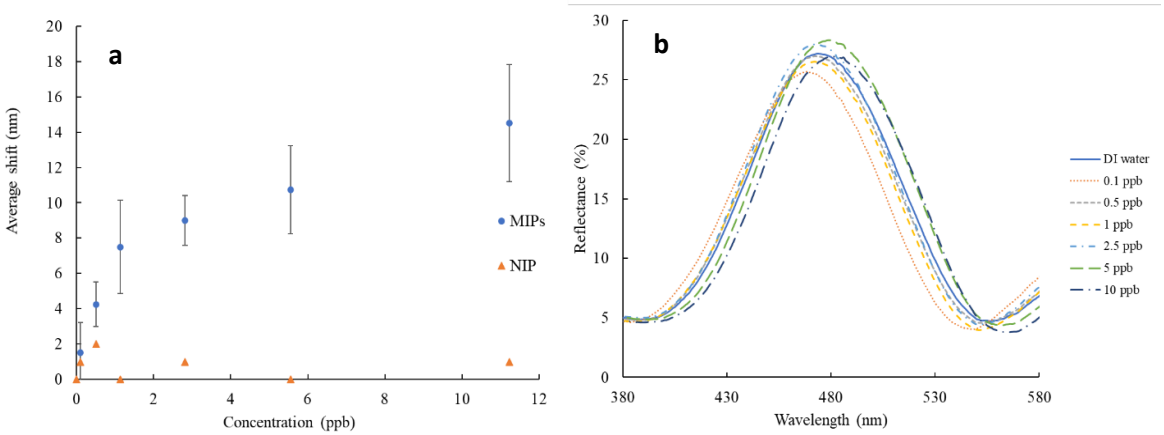

Figure 13. DIA MIPs and NIP response to incubation in a series of solutions with different DIA concentrations. a) wavelength shift; b) reflectance spectra of one representative MIP in response to test solutions.

available. So, there are more potential sites for target molecules to bind to them which results in more binding and as a result, the changes in Bragg diffraction. Consequently, distinct changes in peak wavelength shift were observed at the beginning and as more binding sites are expected to be occupied, a higher percentage of occupied sites can possibly exert a resistance and availability and access to void binding sites would be more

limited. In other words, the first few molecules occupying empty sites may affect the most swelling of the polymer film and milder changes are observed in peak wavelength shift as more sites are occupied. The shape of the response curves reflected these effects.

All three MIPS showed linear responses at the beginning of incubation, but the response curves started to flatten and adopted a logarithmic trend as more binding sites were occupied. Then, the MIPs showed low sensitivity of response for large variation of input at higher concentrations, while they are useful for lower concentrations where their responses have a linear trend.

Each test solution concentration was measured with 5 different MIPs; the average values are reported and the error bars show the standard deviation of those measurements. The variability in the observed average shift was large, which impedes precise measurements of concentration with single calibration curve for the sensor. The response of each MIP in terms of rebinding and swelling, strongly depends on process of fabricating the MIPs that includes different steps from silica particles deposition to precursor infiltration and polymerization. Colloidal crystal growth that creates the macroporous structure within the film to facilitate the movement of target molecules through the hydrogel and since there are some minor variabilities during that process

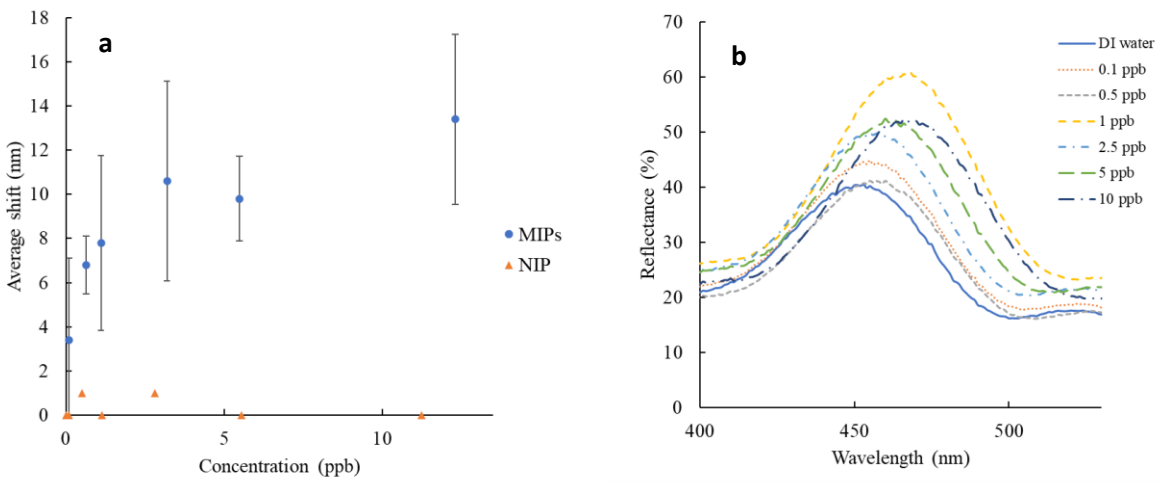

Figure 14. DEA MIPs and NIP response to incubation in a series of solutions with different DEA concentrations. a) wavelength shift; b) reflectance spectra of one representative MIP in response to test solutions.

such as changes in temperature, humidity and vibrations, there might be slight differences in the structure of polymer film and consequently differences in MIPs responses. Given this variability, the sensor would not provide a measurement of the analyte concentration as precise as the gold standard (LC_MS), but they would constitute a useful screening tool for pesticide monitoring in the field. It is important to note that although the overlap of the error bars might look considerable, meaningful environmentally relevant information can be derived from these measurements.

The experiments were repeated with a NIP film as control. There was a slight shift in reflectance peak wavelength for the NIP. The highest peak wavelength shift observed was 2 nm that is negligible in comparison with the MIPs peak wavelength shift (Figures 12a-14a). The small shift in the NIP can be attributed to nonspecific adsorption on the surface of hydrogel or carryover a small part of the standard solution by the NIP film and UV light absorption.

The average response curves obtained for each compound can be used as calibration curves for the sensor and used to determine the concentration of the target in unknown solutions. Before measuring an unknown solution, dry, unused MIP films should first be equilibrated in clean water to “zero” the sensor and to determine the initial peak wavelength. After a 20-minute immersion in the test solution, the new peak position can be determined to calculate the resulting wavelength shift. The limit of detection (LOD) and limit of quantification (LOQ) were calculated from the linear part of the calibration curves. LOD and LOQ were determined to be 0.1, 0.2, and 0.3 ppb and 0.33, 0.66, and 1 ppb for ATZ, DIA, and DEA respectively. The dynamic range of

measurement was 0.12-8.5 ppb, 0.1-11.2 ppb, and 0.1-12.3 ppb for ATZ, DIA and DEA respectively.

3.3.4. Cross-reactivity experiments

Cross-reactivity of the MIPs was examined by incubation tests (20 minutes on shaker at 90 rpm) of ATZ, DEA, and DIA MIPs in solutions containing the three targets in equal concentrations: 1 ppb and 5 ppb. Each MIP was first equilibrated in DI water as a blank; after patting dry softly and getting their initial reflectance spectra, they were incubated in the combined target solutions, and their peak wavelength shift was recorded.

Figure 15 shows the average response of the MIPs in those solutions; at least 3 MIPs were tested for each target in each experiment. Among the MIPs, ATZ MIPS had larger average peak wavelength shift than the metabolites when tested in the combined solutions. DEA and DIA MIPs were in average less responsive in the combined solutions than when incubated in their specific target solutions, which hints to the absence of positive interference effects and the low probability of false positives given by individual sensors. The results suggest the specificity of each MIP to its target, since no response was observed to other molecules present in the test solution. Since the binding sites in the MIPs are complementary to the target molecule in size and shape, only the molecules imprinted on the polymer film are expected to occupy those sites.

Comparing these results with MIPs responses in solutions of a single corresponding target compound at 1 and 5 ppb showed that while the response of ATZ MIP seems to

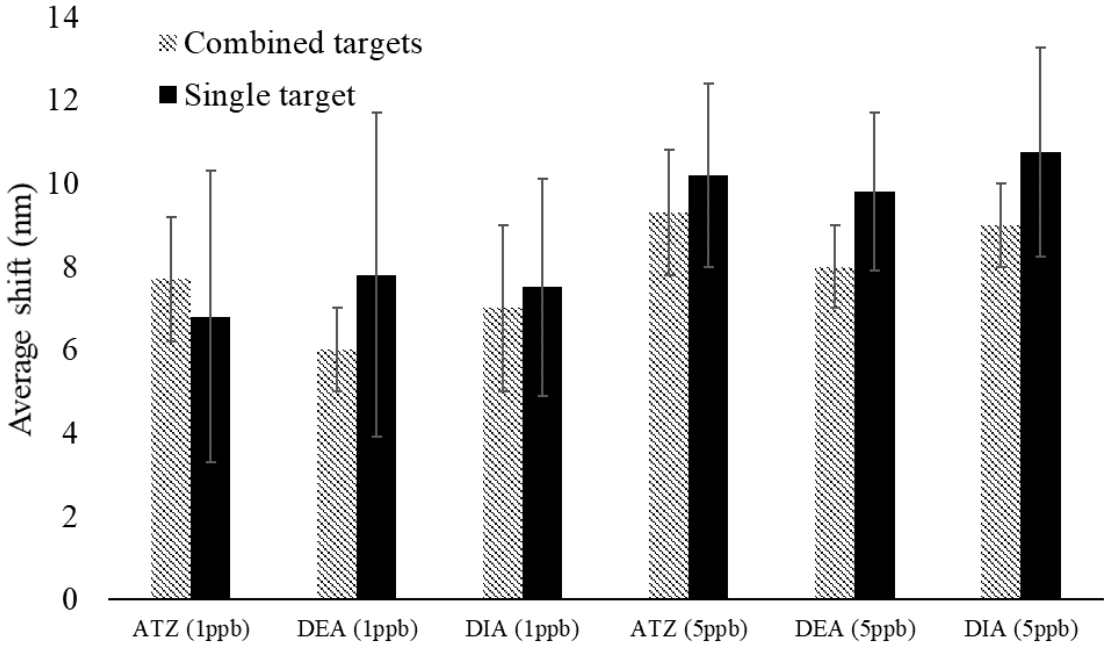

Figure 15. Average wavelength shift for ATZ, DEA and DIA MIPs in test solutions of 1 ppb and 5 ppb of each target (combined solutions) and comparing them to average peak wavelength shifts produced by 1 ppb and 5 ppb solution of each target compound when present in single solutions.

increase slightly when in the combined 1 ppb solutions, all responses are lower than expected for the actual concentrations at 5 ppb. Moreover, DIA and DEA solutions resulted in lower peak wavelength shifts even at the lower concentration. These observations can be related to their chemical structure. Chemicals other than the target compound for each MIP can potentially bind into the imprinted cavities, if they have comparable molecular size and functional groups in common, and as a result interfere in the accurate determination of the target. Atrazine is the largest molecule of the three targets considered and has some functional groups in common with the metabolites (Figure 4). Thus, DEA and DIA are able to bind into the ATZ specific sites, even if the

"fit" is not exact and the interaction is not as strong as expected with the original target. However, the additional methyl and/or ethyl groups in the parent compound (ATZ) seem to hinder its binding to the metabolites specific MIP, and even block the adsorption of DIA and DEA to some of those sites, resulting in lower adsorption and consequent peak wavelength shift. At the 5 ppb, the highest concentration considered, the hindrance in adsorption is more noticeable and even affects the ATZ MIP, which suggest that increasing the number of molecules present in the solution may produce a secondary effect in the diffusion of the target from the bulk of the solution to the binding sites.

3.4.Conclusion

Photonic molecularly imprinted polymer films supported on PMMA slides were fabricated by combining MIP technology with colloidal crystals to create inverse opal structures for the detection of dissolved pesticides in natural waters. The sensors showed response when incubated in laboratory made solutions of each target individually down to 0.1-0.3 ppb range and was able to quantify their concentrations up to 10 ppb, which lies within the environmentally relevant range.

Stable readings were obtained after 20 minutes equilibration. Interference between targets when all three compounds were present in solution proved to be low, resulting in a slight underestimation of DEA and DIA and a minimal increase in the average response to ATZ, probably due to steric hinderance of ATZ adsorption on the metabolites specific sites. The high sensitivity of technology to the structural changes of the polymeric film coupled with a multi-step fabrication process conducted in a lab bench by an operator resulted in variations in responses between different sensors and uncertainty in the quantification at low concentrations. However, the fabricated sensor constitutes a useful

tool for screening pesticide presence in water in-situ, and a simpler and faster technique than currently available analytical methods.

4. Effect of Ionic Strength and Natural Organic Matter on Atrazine Photonic MIP-based Sensor

4.1. Introduction

Molecularly Imprinted Polymers (MIP) with optical features were fabricated and used to detect and quantify atrazine and its metabolites in aqueous solutions. There are different ways of transducing detection of target by MIPs into some sort of signal and among them, optical recognition was developed in this sensor by combining molecular imprinting with colloidal crystal templating. MIPs characteristics such as binding efficiency, recognition capacity and selectivity have been thoroughly investigated by optical features since they have high selectivity and are facile in application (59). Other parameters such as limit of detection, sensitivity, selectivity, reproducibility, accuracy, robustness, response time, and lifetime that establish sensing properties of MIPs, can also be characterized (60). Since synthesis of MIPs is approached as creating a SPE media, there has been more research focused on the steps of conditioning, washing, and eluting of the process rather than the mechanism of detecting and sensing the target and hence, the mechanisms of those interferences have not yet fully studied. Capability of predicting and analyzing these interferences would make it possible to use MIPs as in-situ sensors in natural waters.

Sensing performance of the MIPs can be compromised by sample properties that is highly probable in natural waters such as ionic strength and presence of natural organic

matter and those effects have not been fully studied. It is reported that MIPs can be induced by changes in temperature (61), pH (58), and ionic strength (62). It is reported that increasing ionic strength from 1 to 100 mM has decreased quenching of fluorescent-based MIPs by 30% and also basic environments increases quenching of MIPs due to higher swelling ratio of the MIP, while rinsing MIP will neutralize that effect (63). Other parameter that potentially can compromise performance of the MIPs, is interferences in detection of target and in this work, interferences are compounds that are capable of obstructing the bonding sites available in polymer film and blocking the target molecules access to those sites resulting in pore blockage, steric repulsion or electrostatic interactions at or near the surface of the film. This happens due to the interfering compound nonspecific adsorption onto the film and decreases the sensing capacity of the MIPs. Some of possible interferences that might occur in natural waters are due to presence of dissolved salts and organic matters, inorganic colloidal particles, and microorganisms.

MIPs have been reported to be used as sorbent for solid phase extraction in natural waters (64,65). Different parameters in water chemistry matrix impact on the use of MIPs in natural water has not been thoroughly investigated (66,67). It is reported that atrazine was used as the template molecule and then the MIP extracted atrazine, simazine, ametryn, and propazine from natural water samples (68). In another study, for detection of tetrabromobisphenol A (TBBPA), diphenolic acid (DPA) and bisphenol A (BPA) were used as template molecules. It is reported that TBBPA capture in tap, river, and lake water was in range of 85% to 97% with detection limit of 2 ng/ml (69). Monitoring atrazine in both contaminated and uncontaminated natural waters was done by

conductometric transducer based sensor and it yielded detection limit of 1 ppb, although the technique required laboratory instruments which impeded in-situ application of the sensor (70).

Photonic MIPs are suitable for in-situ applications since they are supported on a polymethylmethacrylate (PMMA) slide and they provide facile measurement. The concentration of contaminants in the environment are fairly low, given the complex chemical composition of natural waters, detecting them could be a challenging task in natural waters because of probable interferences of sample chemical compounds and preventing the sensor to perform efficiently.

In previous work, a photonic MIP sensor was developed for detection of atrazine and two of its metabolites, desethylatrazine (DEA) and desisopropylatrazine (DIA), in aqueous samples and quantifying them in a range of 0.1 ppb to 10 ppb. Molecular imprinting was combined with colloidal crystal to synthesize a thin polymer film with macroporous structure which facilitates the accessibility to numerous binding sites within the films.

The objective of this study is to investigate the effects of ionic strength and dissolved organic matter on atrazine rebinding and sensor efficiency, in general. The effect of ionic strength and Natural Organic Matter (NOM) was investigated on the performance of photonic MIPs to detect atrazine in natural waters as those parameters can interfere with specific and nonspecific adsorption of atrazine as well as impacting the hydrogel itself and consequently cause under/overestimation of target. As reported in previous work (Chapter 2: Detection of Atrazine and its metabolites by photonic molecularly imprinted polymers in aqueous solutions), photonic MIP can be successfully applied for detection

and quantification of atrazine and its metabolites in aqueous samples and by studying water chemical matrix influence on the sensor performance, it could potentially be used in-situ for detection and quantification purposes.

4.2. Materials and Methods

The following chemicals were purchased from Sigma-Aldrich (St. Louis, MO, US) and used without any purification: acrylic acid (AA) (99%), ethylene glycol dimethacrylate (EGDMA) (98%), 2,2'-azobisisobutyronitrile (AIBN) (98%), hydrofluoric acid (HF) (48%), ethanol (99.5%, 200 proof), acetic acid (96%). Atrazine was purchased from Santa Cruz Biotechnology (Dallas, TX, US). Commercial silica particles (300 nm diameter) were supplied by Pinfire Gems and Colloids (Frankfurt, Germany). Suwannee River Natural Organic Matter (SRNOM) was purchased from International Humic Substances Society (St. Paul, MN, USA). Ionic strength of solutions was adjusted by NaCl (reagent grade, Acros Organics) and $CaCl_2$ (reagent grade, J. T. Baker).

4.2.1. Fabrication of MIPs and Non-Imprinted Polymers (NIPs):

The schematic of steps for fabrication of MIPs is illustrated in Figure 16 The first step was the preparation of silica particles deposition on glass substrate to create a colloidal crystal. In the fabrication of the colloidal crystals, ethanol was added to commercial silica particles (Pinfire Gems and Colloids, Frankfurt, Germany) to achieve a solution of 0.1% volume fraction. For that purpose, 142.5 mg silica particles were added

to 75 ml ethanol and the suspension was stirred and sonicated alternatively for 24 hours to obtain a well-dispersed suspension. Microscope glass slides, 0.04”×1/3”×3” dimensions, were vertically positioned inside the beakers with silica particle suspension and the deposition conducted in an oven for 24 hours at 50ºC. As ethanol evaporated, the silica particles self-assembled on the glass slides forming organized structures of 10 to 12 layers of particles.

The method used for atrazine-imprinted polymer is noncovalent, self-assembly approach. Hence, the target (atrazine), functional monomer (acrylic acid), and crosslinker (EGDMA) form pre-polymerization bonds using hydrogen bonds and electrostatic bonds when they are mixed before starting the polymerization process. In order to have a more specific noncovalent interactions between the nanocavities and target molecules, it is necessary to optimize the complexation of the target molecule and functional monomer. Many research groups have used methacrylic acid (MAA) and acrylic acid (AA) as functional monomer for atrazine and they have reported that using AA as functional monomer results in higher sensitivity at the same atrazine concentration than using MAA as functional monomer (1). Based on these studies, AA was used as functional monomer and EGDMA as crosslinker for the atrazine and its metabolites complexation at a molar ratio of 0.05:4:1 (target: monomer: crosslinker) to form the nanocavities in 3D porous matrices. The noncovalent complexation takes place via hydrogen bonds among hydroxyl group and oxygen atom of acrylic acid and nitrogen atoms and hydrogen atoms of amino groups in atrazine and its metabolites structure.

In the preparation of the polymerization solution, 31.47 mg of atrazine was added to 1 ml ethanol and then 0.8 ml acrylic acid as monomer was added to have a 1:80 molar

ratio of atrazine to monomer. Then, 0.55 ml EGDMA (1:4 molar ration of EGMA to AA) was added as crosslinker and the solution was left overnight to have a good complexation. Finally, 6 mg AIBN was added as initiator.

After being mixed and left to interact overnight, the mixture was infiltrated through the interspaces of the colloidal crystal structure by capillary forces and filled its void spaces. In this step, a poly(methyl methacrylate) (PMMA) plastic slide (ePlastics, San Diego, CA, USA) was placed on each side of a glass slide and the three were firmly held together while immersing one end in the polymerization solution.

To conduct the polymerization reaction, the slides were irradiated with UV light (power = 36kW, wavelength= 365 nm) for 3 hours. Ice packs were placed under the samples to avoid damage due to overheating. The temperature was maintained below the glass transition temperature (T_g) for the polymer of 50°C (40). The bonding of monomer and crosslinker reaction is exothermic and in addition, the UV light adds heat between the slides. So, to prevent damaging the hydrogel, the slides were placed in a freezer at -18°C for 30 minutes to separate them easily. The films remained attached to the PMMA slides.

The separated PMMA slides were immersed in 5% HF overnight to etch the silica particles remaining in the polymer, leaving large cavities within the film. Removing silica spheres followed by removing target molecules from the polymer hydrogel introduces a 3D interconnected porous arrays with nanocavities that could potentially have

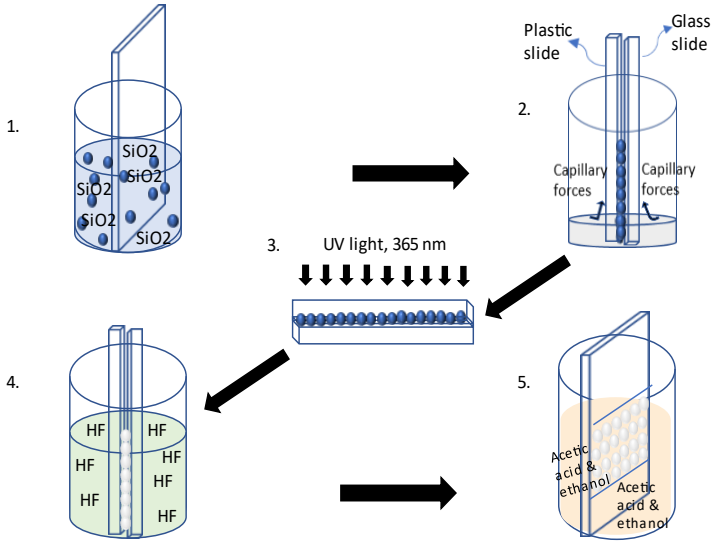

Figure 16. Schematic of MIPs fabrication steps 1. Self-assembly technique to create colloidal crystal. The glass slide is placed vertically in a beaker containing silica nanoparticles. 2. Infiltration: polymerization precursor is infiltrated between glass and plastic slide due to capillary forces. 3. Placing glass and plastic sandwich before UV light for polymerization to take place. 4. Creating porosity in polymer film by etching silica nanoparticles using 5% Hydrofluoric acid solution in DI water. 5. Removing target molecules from polymer film structure by immersing it in a solution of acetic acid and ethanol (1:9).

noncovalent interactions with target molecules.

In order to remove atrazine molecules from MIPs, the films were washed with acetic acid and ethanol solution with a volume ratio of 1:9. Three cycles of washing were conducted; each one with a duration of 15 minutes and stirring to enhance turbulence and facilitate the transport of the atrazine molecules from the polymeric matrix to the bulk of

the solvent. Non imprinted polymers (NIPs) were also fabricated as controls, with the same polymeric solution composition but in the absence of a target.

4.2.2. Characterization

Silica particles deposition were imaged by electron microscopy in a FEI Quanta 600 FEG (ThermoFisher Scientific, Hillsboro, OR, USA) Environmental Scanning Electron Microscopy (ESEM) to investigate size, morphology and number of layers of silica particles deposition. The glass slide was copper taped to the stub and coated with a conductive layer of platinum (1.5-3 nm) with an Emitech K575x sputter coater (Quorum Technologies Ltd., Ashford, Kent, UK).

Fourier Transformed Infrared Spectroscopy (FTIR) spectra will be collected in a Cary660 spectrometer (Agilent Technologies, Santa Clara, CA, USA) in the wavelength range of 4000-400 cm^{-1}. Both MIP (before and after elution of target molecules) and NIP films will be characterized by FTIR to identify the functional groups present on the films.

4.2.3. Analytical measurement of concentrations:

Stock solution of atrazine were first prepared in methanol at 100 ppm concentration, given its high solubility in this solvent. Using serial dilution, 10 ppm and 1 ppm solutions in methanol were prepared; this last one was used as stock solution for serial dilution in DI water.

The stock solution used in dilution and preparation of standard solutions for the sensor testing and calibration were analyzed by Liquid Chromatography-Mass Spectrometry (LCMS/MS). The concentration of atrazine (ATR) was determined by a Waters Alliance 2695 High Performance Liquid Chromatography (HPLC) system coupled with Waters

Acquity TQ triple quadrupole mass spectrometer (MS/MS). The analyte was separated by a Phenomenex (Torrance, CA) Kinetex C18 (100mm x 4.6 mm; 2.6 µm particle size) reverse-phase column. The mobile phase consisted of 10 mM ammonium acetate and 0.1% formic acid in water (A) and 100% acetonitrile (B). The gradient conditions were 0 – 0.5 min, 2% B; 0.5-7 min, 2- 80% B; 7.0 -9.0 min, 80-98% B; 9.0 – 10.0 min, 2% B; 10.0 – 15.0 min, 2% B at a flow rate of 0.5 mL/min. The ion source in the MS/MS system was electrospray ionization (EI) operated in the positive ion mode with capillary voltage of 1.5 kV. The ionization sources were programmed at 150°C and the desolvation temperature was programmed at 450°C. The MS/MS system was in the multi-reaction monitoring (MRM) mode with the optimized collision energy. The ionization energy, MRM transition ions (precursor and product ions; **Table 4.1**), capillary and cone voltage, desolvation gas flow and collision energy were optimized by Waters IntelliStart™ optimization software package. The retention time, calibration equations, and limits of the detection for the analysis of ATR are summarized in **Table 4.1**.

Table 4.1. Precursor and product ions selected for the analysis of ATR by HPLC-MS/MS (LOD = limit of detection)

Compound	RT (min)	Molecular ions (m/z)	Product ions (m/z)	Polarity	Linear equation	Correlation coefficient (R square)	Collision Energy	Cone voltage (V)	LOD (ug/L)
ATR	9.471	215.86	173.89	ES+	y=58890x	0.9986	Tune	30	0.06

4.2.4. Measurement of optical properties

In this work, silica deposition is utilized to form 3D porous structure within polymer hydrogel to convert the recognition to a readable optical signal using Bragg diffraction. The Bragg equation is defined as:

$$\lambda_{max} = 1.633\left(\frac{d}{m}\right)\left(\frac{D}{D_0}\right)\sqrt{(n_a^2 - \sin\Theta^2)} \quad (1)$$

where *d* is the sphere diameter of the silica particle, *m* is the order of Bragg diffraction, (D/D_0) is the degree of gel swelling (D and D_0 are the diameters of the gel in the equilibrium state at a certain condition and in the reference state, respectively), n_a is the average refractive index of the porous gel at a certain condition, and Θ is the angle of incidence. Based on this equation, if the rebinding of target molecules causes any swelling or shrinkage in the hydrogel film, it is detected by optical signals.

In this work, a UV-Visible spectrophotometer (Cary 60, Varian, Palo Alto, CA, USA) is used with a Harrick Scientific's Specular Reflection Accessory (ERA-30G) at a fixed angle of 30º in wavelength range of 200-800 nm and double-beam mode to measure the reflectance of the MIP films.

The stock solution used for dilution and preparing series of solutions with different concentrations for equilibration experiments of the MIPs was validated for its exact concentration by LCMS/MS. Also, mixing was provided by a shaker during equilibrium tests to overcome the limiting impact of molecules diffusion. Based on previous measurements of kinetics tests, 20 minutes was considered as equilibrium time length for MIPs incubation in these solutions.

To examine the sensing properties and response of the MIPs, a series of solutions were prepared with different concentrations of atrazine using serial dilution. MIPs were tested in solutions with concentrations ranging from 0.1 ppb to 10 ppb (0.1 0.5, 1, 2.5, 5, and 10 ppb). Then, response of MIPs in each solution with different concentration was examined, starting with the most diluted one. All those responses were recorded to

generate a calibration curve for quantifying concentrations of the targets in unknown solutions. First, they were immersed in DI water as a blank test till equilibrium was reached. Then, the MIPs were taken out of the solution, pat dried softly and were examined in UV-Vis spectrophotometer for their original reflectance, moving forward to incubating in solutions in order of increasing concentrations with the same procedure to record their response and generate the calibration curve.

For studying impact of ionic strength on MIPs response, after preparing solutions with different concentration of atrazine, a measured amount of each salt (NaCl and $CaCl_2$) was added to solutions to yield 1mM, 10mM, and 100 mM ionic strength of each.

Due to plants degradation and animals or anthropogenic pollutions, organic materials are present in natural waters. Natural Organic Matter (NOM) can be capable of adsorbing to the sensor surface, resulting in error in sensor response. In order to examine this effect, MIPs and NIP responses were measured in solutions with different concentrations of atrazine mixed with 1 ppm NOM. For control experiments, the results were compared with MIPs responses in absence of NOM. Studying effect of NOM on MIPs and NIPs responses, experiments were performed in a mixture of different concentrations of atrazine with 1 ppm NOM in the background.

4.3. Results

4.3.1. Characterization

Silica particles colloidal crystals were imaged by ESEM to investigate the morphology and crystalline format of the silica deposition. The monodispersed silica particles yield

macroporous structure within the MIP film. The MIP film surface and cross-section (after silica particles were etched) were also imaged by ESEM to investigate the internal porous structure of the MIP film. The ESEM images of both silica deposition and MIP film were shown in Chapter 3.

Chemical functional groups of the polymer and their interactions with target molecules were analyzed by FTIR and the results were reported in Chapter 3. The FTIR spectra showed some differences in bands and intensities of MIPs before target removal with NIPs and MIPs after target removal.

4.3.2. Effect of ionic strength with different salts

MIPs equilibrium experiments were performed with atrazine solutions with different levels of background ionic strength (1, 10, and 100 mM), given by NaCl or $CaCl_2$ to study the effect of ionic strength and presence of salts on MIPs response.

To investigate the impact of salts on MIPs in absence of atrazine, the MIPs were immersed in blanks with different ionized strengths (i.e. 1, 10, and 100 mM) for 20 minutes. Figure 17 demonstrates the average peak wavelength shift for those MIPs. NaCl decreases the swelling in the hydrogel and shrinkage of polymer film causes lower peak wavelengths, although it is minor. $CaCl_2$, on the other hand, increases the peak

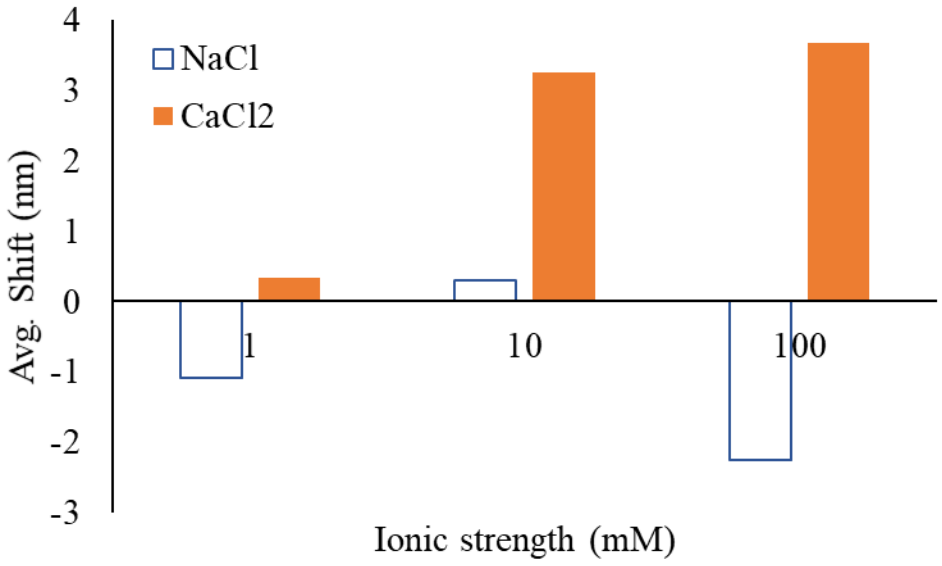

Figure 17. Effect of salts (NaCl and CaCl2) at different ionized strengths on MIPs in absence of atrazine.

wavelength of the polymer film and it means that it increases swelling ratio of the hydrogel.

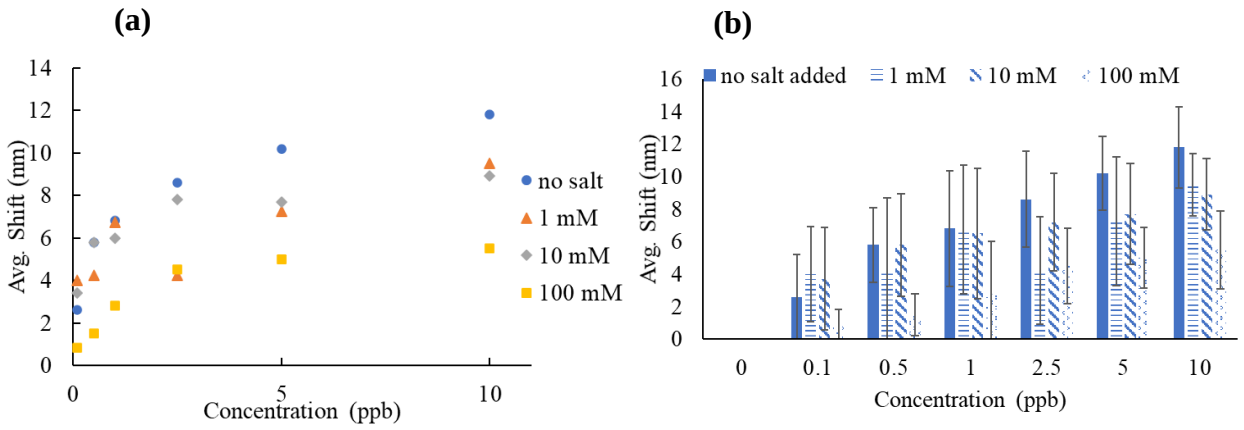

Figure 18. a) Comparison of MIPs calibration curve in DI water with MIPs responses in presence of NaCl at 1, 10, and 100 mM levels of ionized strength. b) MIPs responses in absence and presence of NaCl at different concentration levels and ionic strengths

In presence of NaCl, there was a decrease in peak wavelength shift. As the ionic strength increased from 1 mM to 100 mM, atrazine binding to the MIPs decreased by 26%. Figure 18 shows the calibration curve for atrazine in DI water and differences in MIPs response in presence of NaCl at different levels.

It was reported that binding capacities of targets to MIPs is affected by cations following the Hofmeister series (92). These experiments were done at near neutral *p*H and due to carboxylic acid's pK_a of approximately 5, most of carboxylic groups in the polymer matrix were deprotonated. A higher concentration of NaCl resulted in higher charge densities at the surface of hydrogel, which suppressed the thickness of electric double layer and caused less electrostatic repulsion and swelling of hydrogel compared to the conditions in DI water (63). So, a shrunken hydrogel had less swelling and lower peak wavelength, resulting in underestimation of target in presence of NaCl and the range of underestimation expanded in solutions with greater ionized strength. In Figure 18b,

error bars for atrazine in DI water and in different ionic strengths have been included and based on the range of the intrinsic error of the MIPs in absence of NaCl, the calibration curve can still be used for solutions at 1 and 10 mM ionized strong of NaCl. At higher ionic strengths, the calibration curve obtained had very large error bars and would not be considered accurate for measuring purposes.

In presence of $CaCl_2$, a quite opposite result was observed. Increasing ionic strength from 1 mM to 100 mM using $CaCl_2$, increased the peak wavelength shift by 23%. As shown in figure 19, the average wavelength shift decreased at 1 mM ionized strength. However, increasing ionic strength, which corresponds to an increase in $CaCl_2$ concentration, augmented the average peak wavelength shift. Greater average shift is a result of higher swelling ratio and it is reported that poly(acrylic acid) (PAA) is capable

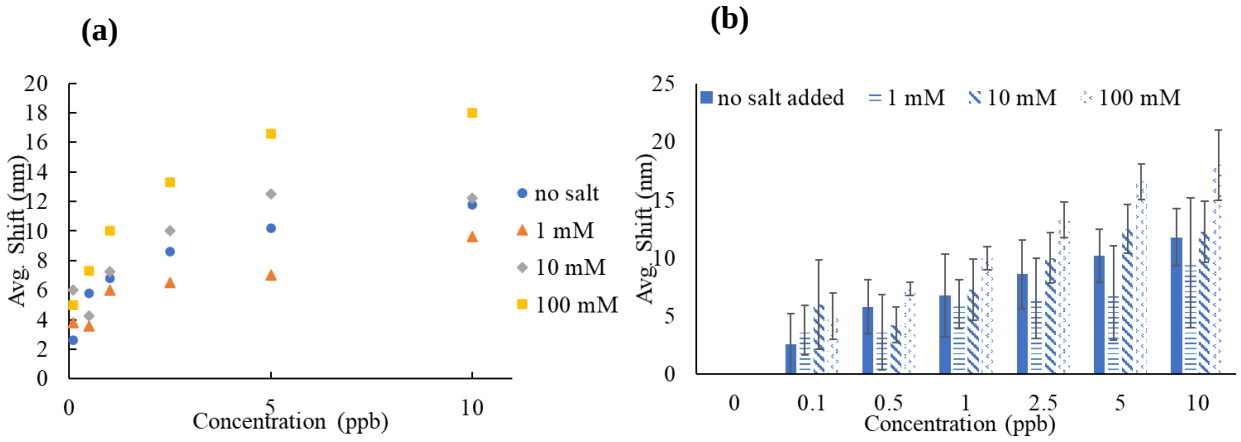

Figure 19. a) Comparison of MIPs calibration curve in DI water with MIPs responses in presence of CaCl2 at 1, 10, and 100 mM levels of ionized strength. b) MIPs responses in absence and presence of CaCl2 at different concentration levels and ionic strengths.

of high calcium ion binding power (93) and calcium ion binds to the carboxylate groups of PAA from neighboring polymer segments (94) due to calcium ion chelating property

and hence forming complexations with PAA. The incident of complexation resulted in swelling of the hydrogel and consequently, higher peak wavelengths occurred.

In the case of $CaCl_2$, similar to NaCl, the calibration is appropriate to be used for measuring atrazine in solutions with 1 and 10 mM ionized strong since the intrinsic error of the MIPs covers the differentiation of response in those solutions although it does not go as far as responses in 100 mM ionic strong solutions and cannot yield accurate results for those measurements. Also, results from incubating MIPs in solutions with different ionic strength and absence of atrazine demonstrated that increasing concentration of $CaCl_2$ causes swelling of the hydrogel and yields larger peak wavelengths in reflectance spectra which is in accordance with results from incubation of MIPs in presence of both ionic strength and atrazine.

4.3.3. Effect of NOM

In order to investigate the interference of NOM in MIP response to the target, MIPs were incubated in solutions with different concentrations of atrazine and 1 ppm of NOM in the background. For control experiment, a NIP was also incubated in the same solutions and the results were compared to the incubation experiments without any NOM. The peak wavelength shift increased in presence of NOM compared to the DI water atrazine solution is shown in Figure 20. There was a greater peak wavelength shift for NIP incubated in presence of NOM than the one in DI water. This effect may be explained due to the absorbance of light by NOM, as some solution may be carried with the porous film. So, in another attempt, the NIP was carefully rinsed with DI water after taking it out from the solution, to remove as much excess sample as possible from the surface and the internal porosity of the film. The rinsing decreased the wavelength shift

to some extent, which clarifies that some NOM molecules clung to the film, absorbed light and caused the changes in peak wavelength observed in reflectance spectra. Same incident happens while incubating MIPs and measuring their reflectance and causes the

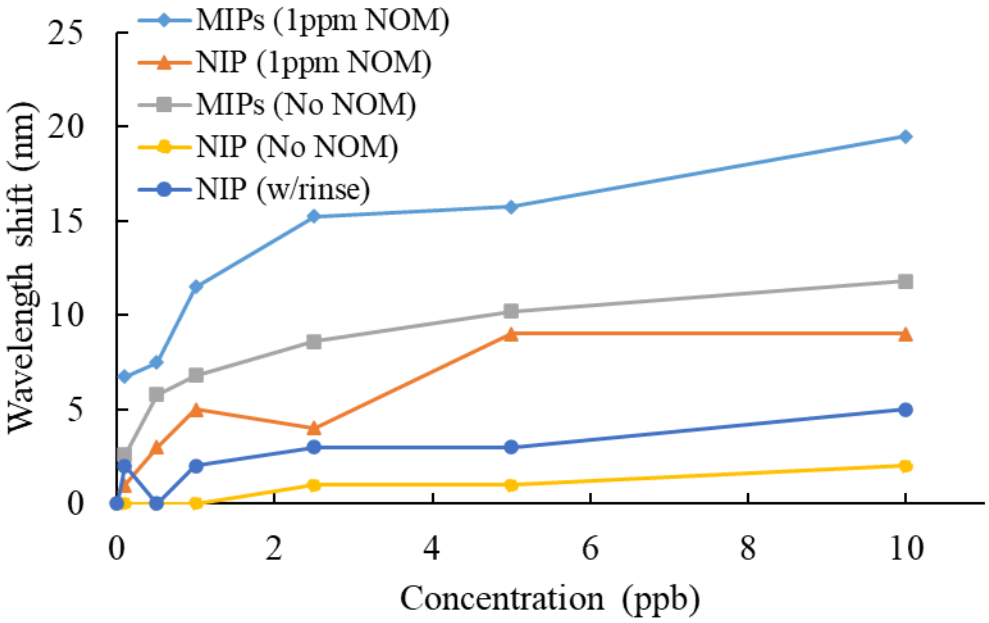

Figure 20. MIPs and NIPs response to atrazine in presence and absence of NOM.

deformation in the reflectance spectra.

So, presence of 1 ppm NOM in the solutions caused 28% increase in peak wavelength shift of the NIPs and 35% increase in the peak wavelength shift for the MIPs. This difference in the amount of shift change for MIPS and NIPs is because of the rinsing step that was just done for the NIPs. This amount of increase in the overestimation is covered by the intrinsic error of the MIPs and they can be used in natural waters with NOM around 1 ppm concentration.

4.4. Conclusion

The effect of ionic strength and NOM on photonic molecularly imprinted polymers response was investigated. Those parameters could be potential interferences to MIPs performance in terms of target rebinding and/or under/overestimation of analyte in an unknown solution. In presence of NaCl, MIPs presented lower responses by 26% that resulted in target underestimation, and it could be a result of film conformational change due to lower swelling. In presence of $CaCl_2$, as the ionic strength increased, MIPs showed higher responses by 23% resulting in overestimation of the target and it occurred due to calcium ion forming complexes with PAA. In presence of NOM, the responses measured by MIPs and NIP were higher than responses recorded in absence of them and this augment in response of NIP were in accordance with those of MIPs and is attributed to NOM molecules absorbing light and changing the reflectance spectra.

5. Occurrence of atrazine in natural waters in northeast Columbia, Missouri.

5.1. Introduction

Wetlands are lands that transition between terrestrial and aquatic systems where the water table is usually at or near the surface, or the land is covered by shallow water or saturated with water. A wetland's water could be groundwater flowing up from an aquifer or spring through porous media of the soil, come from a nearby lake or river, or created by strong tides of seawater that form coastal wetlands. They occur on every continent including Antarctica (21) and on high lands like mountains down to flat lands like coasts (22). There are many types of wetlands and they are mainly classified as swamp, marsh, fen, and bog. A swamp is a forested wetland and it is considered a transition zone between land and water, while a marsh is a type of wetland dominated by herbaceous rather than woody plants species and it is accumulated by peat, i.e. deposit of dead plants materials (23). Along with bogs, fens are mires accumulated by peats and usually fed by mineral-rich surface water or ground water (24).

Wetlands are known as the most diverse ecosystems; they improve water quality and nutrient cycling, conserve the composition of atmosphere, and decrease chances of flooding (22). Different threats, such as habitat loss and degradation, climate change, pollution, overharvesting and disease, jeopardize wetlands but conversion to agriculture is among the most serious impact. Furthermore, excessive application of pesticides and fertilizers endangers wetlands ecosystems (28).

Using pesticides and herbicides in agriculture industry offers many advantages such as increased crop and livestock yields, improved food safety, human health, quality of life and longevity, and reduced drudgery, energy use and environmental degradation (13). Atrazine is a herbicide of triazine class and it is used the most commonly in the United States by farmers against broadleaf weeds and annual grasses (1). However, its large-scale application may potentially contaminate the water and soil to the level above the established drinking water maximum contaminant level (MCL) by the United Sates Environmental Protection Agency (USEPA) of 3 ppb (15). Exposure to atrazine at concentrations higher than MCL may cause lung, heart, and kidney diseases, low blood pressure, muscle spasms, weight loss, and damage to adrenal glands (2).

Practices that minimize atrazine runoff and make it hold onto the field, where it's the most beneficial for farming purposes and leaves the least environmental impact, have been promoted at the state level. Best management practices (BMPs) should be developed specific to each state, with the objective of decreasing the amount of atrazine loss after application and increasing infiltration of atrazine in the field that results in lower atrazine use and more efficient crop production while preserving water quality. BMPs for the state of Missouri include using atrazine in the top two inches of soil for

field with preplant tillage, applying atrazine in a post-emerge time frame in no-till fields, integrating pest management strategies (prevention, avoidance, monitoring, and suppression), using buffers and buffer zones, avoiding application right before rain events, using proper mixing, loading, and disposal practices. Early preplant application of atrazine and reduced soil-applied rates are not recommended in the state of Missouri (32).

Atrazine is metabolized in the environment to different compounds by plants, animals, and microorganisms through biotic and abiotic pathways. Some of those metabolites as well as atrazine itself, are probably found dissolved in water and transfer through aquatic flows due to their hydrophilicity, while others are precipitated or clung to the soil particles and vegetation. The water soluble metabolites have also raised concerns due to their potential health effects as a result of their extensive use (3,4) and they are the

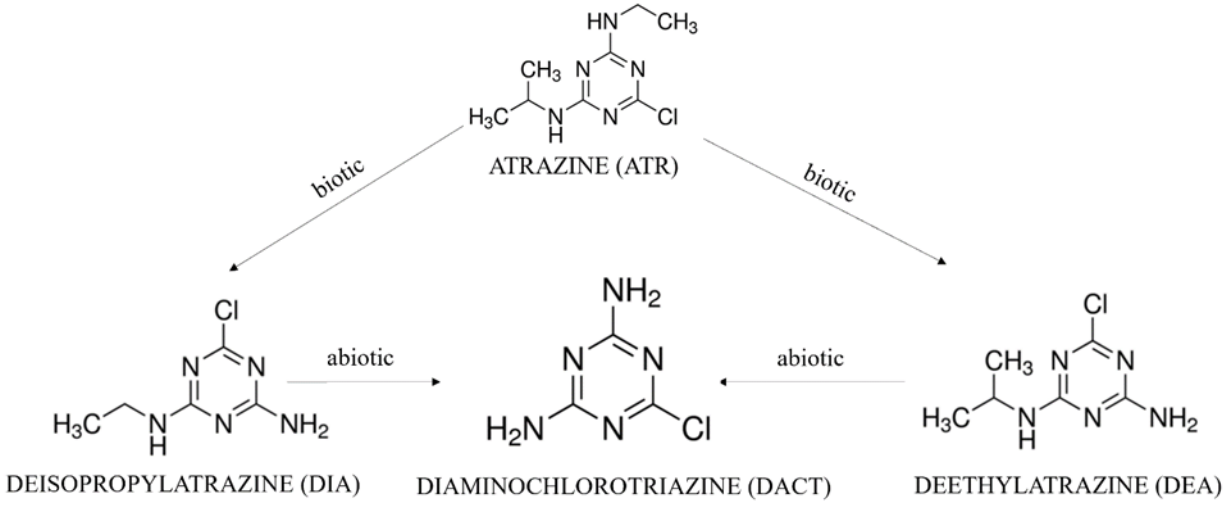

Figure 21. Structure of atrazine and its hydrophilic metabolites, DIA, HA, and DEA.

focus of this work. The metabolites of interest have been depicted in Figure 21: deisopropylatrazine (DIA; 6-chloro-N-ethyl- [1,3,5]triazine-2,4-diamine), and deethylatrazine (DEA; 6-chloro-N-isopropyl- [1,3,5]triazine-2,4-diamine).

In addition to chemical and physical properties of the pesticides, abiotic and biotic characteristics of the receiving wetland affect the pesticide distribution in the environment since ATZ is degraded to DEA and DIA metabolites via biotic procedures and those two metabolites degrade to DACT through abiotic procedures (30).

Due to use of atrazine in Missouri farms and its potential impact to natural environment, the monitoring of pesticide in wetlands in rural areas and their water quality is desirable, in order to recognize the extent of contamination and preserve wetland ecology and water health. In this work, sampling campaigns were proposed to investigate the levels of atrazine and its metabolites during preplant and cultivation seasons after rainfalls. Seven sampling sites in Centralia, Missouri were selected. Water samples were collected after precipitation events during the year and analyzed for concentrations of ATZ, DEA, and DIA. The data was used to compare the levels of atrazine and its metabolites present and their dependence on season, amount of precipitation and location. Samples were also analyzed for content of organic matter by measuring Total Organic Carbon (TOC) and their ionic strength by measuring conductivity.

5.2. Materials and Methods

There were 7 different sampling locations northeast of Columbia, Missouri within less than 3 miles from each other that are indicated in Figure 22: Two mile prairie school Rd 1 and 2 (T1 and T2), Judy school Rd (T3), Glendale Rd 1 (G1), Glendale Rd 2 (G2),

Maupin Rd (M), and Liddel Ln (L). The sites are located at the side of the roads between farms and were chosen due to the potential for pesticide containing runoffs due to their vicinity to the farms, their topographic status, and accessibility.

During spring, summer, and fall sampling was conducted twice after precipitation events. An additional sampling took place at the end of the winter, before the application of atrazine by farmers. In spring, summer, and fall the samples were collected in order to analyze the effect of atrazine application and the amount detected in the runoffs in each period.

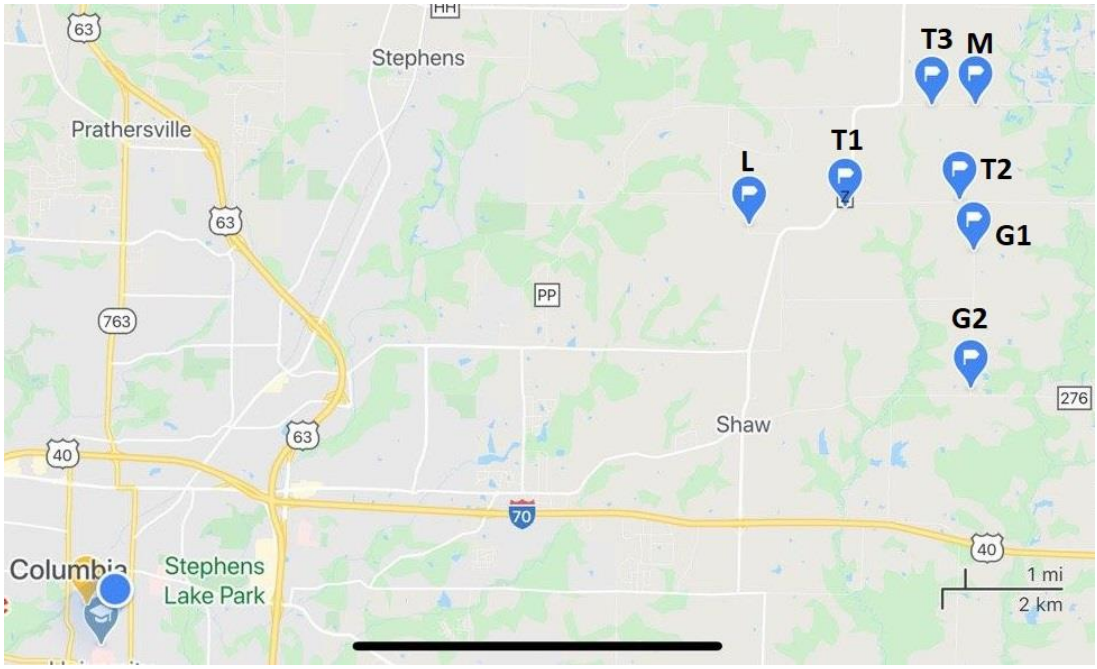

Figure 22. Location of the wetlands targeted for sampling and their routes. The sampling locations are flagged on the map.

A 10-liter polyethylene bucket was used to collect at least 1 liter of water. Immediately after sampling, pH and temperature were measured using a portable Oakton pHTester 30 (Vernon Hills, Il, USA). In some cases, due to insufficient amount of rainfall or low humidity of soil, there was not enough water to obtain the minimum volume and

then, the site was skipped for that occasion. Afterwards, water samples were transferred into 1000 ml propylene bottles (Waltham, MA, USA), labeled and capped for storage in the lab at -18°C until analysis. Photos were taken from each site to have a record of general conditions of the wetland such as vegetation, amount of water in each site, etc. Weather data from Accuweather website were also saved and are shown in Table 5.1 to relate results from rain events and analysis of samples.

Table 5.1. Sampling dates and seasons and amount of precipitation on those days.

Date	Season	Amount of Precipitation(inch)
March 12, 2020	Winter	0.5
March 19, 2020	Spring	0.92
June 10, 2020	Spring	2.75
August 11, 2020	Summer	1
October 23, 2020	Fall	0.09
March 14, 2021	Winter	0.08
April 24, 2021	Spring	0.06

The concentrations of atrazine (ATR), DEA and DIA were determined by a Waters Alliance 2695 High Performance Liquid Chromatography (HPLC) system coupled with Waters Acquity TQ triple quadrupole mass spectrometer (MS/MS). The analytes were separated by a Phenomenex (Torrance, CA) Kinetex C18 (100mm x 4.6 mm; 2.6 µm particle size) reverse-phase column. The mobile phase consisted of 10 mM ammonium

acetate and 0.1% formic acid in water (A) and 100% acetonitrile (B). The gradient conditions were 0 – 0.5 min, 2% B; 0.5-7 min, 2- 80% B; 7.0 -9.0 min, 80-98% B; 9.0 – 10.0 min, 2% B; 10.0 – 15.0 min, 2% B at a flow rate of 0.5 mL/min. The ion source in the MS/MS system was electrospray ionization (EI) operated in the positive ion mode with capillary voltage of 1.5 kV. The ionization sources were programmed at 150°C and the desolvation temperature was programmed at 450°C. The MS/MS system was in the multi-reaction monitoring (MRM) mode with the optimized collision energy. The ionization energy, MRM transition ions (precursor and product ions; **Table 5.1**), capillary and cone voltage, desolvation gas flow and collision energy were optimized by Waters IntelliStart™ optimization software package. The retention time, calibration equations, and limits of the detection for the analyses of ATR, DEA, and DIA are summarized in **Table 5.2.**

Table 5.2. Precursor and product ions selected for the analysis of ATR, desethylatrazine (DEA) and deisopropylatrazine (DIA) by HPLC-MS/MS (LOD = limit of detection)

Compound	RT (min)	Molecular ions (m/z)	Product ions (m/z)	Polarity	Linear equation	Correlation coefficient (R square)	Collision Energy	Cone voltage (V)	LOD (ug/L)
ATR	9.471	215.86	173.89	ES+	y=58890x	0.9986	Tune	30	0.06
DEA	7.632	187.86	145.78	ES+	y=10336x	0.9957	Tune	30	1.45
DIA	6.829	173.82	131.76	ES+	y=3321x	0.9973	Tune	30	5.72

The concentration of atrazine and its metabolites in some samples were below LC-MS/MS limit of detection and preconcentration by solid phase extraction (SPE) was required. For that purpose, atrazine (ATR), deethylatrazine (DEA), deisopropylatrazine (DIA), hydroxyatrazine (HA) and the internal standard terbuthylazine (TRB) in the water samples were extracted and concentrated by SPE process. The water samples were filtered through a 0.2 μm Whatman Anotop syringe membrane filter (Sigma-Aldrich, St.

Louis, MO, USA) and 50 mL of filtered samples were spiked with 500 µl of the internal standard terbuthylazine (TRB, 1 ppm), to achieve a final concentration of 10 µg/L of TRB. Before the extraction, the Oasis HLB solid-phase extraction cartridges (500 mg; Waters, Milford, MA) were conditioned with 8 mL of methanol, followed by additions of 8 mL of DI water to wash the cartridges twice. Following the condition and washing process, the samples (50 mL) were passed through the cartridges at a flow rate of 5 mL/min. After the samples were loaded, the cartridges were washed with 8 mL of DI water and sorbents were dried under vacuum in a SPE manifold system for 5 min. The analytes were subsequently eluted with 7 mL of methanol at 2 mL/min. The eluates were then concentrated under a stream of nitrogen in a temperature bath at 27^{o}C until dryness. The resulting extracts were resuspended with 1 mL of water: methanol (10:90, v/v), and then filtered through a 0.2 µm PTFE Acrodisc syringe membrane filter.

Samples were analyzed for conductivity by a portable Fisher Scientific Traceable dual-display bench digital conductivity meter and TOC was measured using a Shimadzu TOC-VCPN analyzer.

5.3. Results and discussion

Table 5.2. shows the physicochemical characteristics of the samples taken from the sites in different seasons. pH and temperature were measured on site and TOC and conductivity were measured in the lab. Temperature of the samples changed with season and were in the same range for each date. pH of the samples were in the range of drinking water (6.5 to 8.5) and never got too acidic or basic. The organic matter content and conductivity of the samples were measured, since they will affect MIP-sensor readings, to be conducted next (Chapter 4: Effect of ionic strength and NOM on atrazine photonic

MIP-based sensor). The conductivity of the samples changed from 33 to 197 μmhos/cm, depending on the amount of salts present in each sample. Also, because of differences in geotechnical status of different sites and amount of rain precipitated on each day, some of them were deep waters and some were very shallow. In the samples from shallow sites, the salts were more concentrated in the stream and conductivity increased in the sample. Samples' TOC ranged from 0 to 10.93 ppm. Amount of oxygen and level of sedentariness would affect the organic matter content in addition to population of microorganisms available in each site. Those factors have led to the different levels of TOC observed in the samples.

Table 5.3. Physicochemical characteristics of samples collected after rain in different seasons. pH and temperature were measured on-site, TOC and conductivity were measured in the lab.

Sample site	TOC (ppm)	Conductivity (μmhos/cm)	pH	Temperature (°C)
March 12th,2020				
T1	3.155	92.2	7.25	10.2
T2	~0	173.8	7.79	11.1
T3	2.121	91	7.3	11
G1	4.287	144.9	7.45	11
G2	2.052	94.8	7.45	11.1
M	3.572	120.5	7.32	11.15
L				
March 19th, 2020				
T1	2.026	42.9	7.49	17
T2	4.265	59.2	7.61	18.2
T3	4.104	33	7.21	17.7
G1	1.617	46.8	7.3	17.9
G2	2.548	61.5	7.58	17.7
M	4.437	40.8	7.01	18.7
L	~0	74.1	7.22	18.7
June 10th, 2020				
T1	9.957	52.4	7.92	21.5
T2	8.592	96.5	7.52	21.2
T3	8.501	63.7	7.31	21.1
G1	4.216	108.5	7.4	21.4

G2	10.80	85.7	7.36	22
M	7.280	99	6.93	21.8
L	2.016	134.1	7.35	23.4
August 11th, 2020				
T1	3.036	48.2	7.97	26.8
T2	7.196	116.1	7.57	27.4
T3	3.270	57.1	7.39	28.5
G1	10.93	116.5	7.4	30
G2	7.304	95.2	7.63	31.6
M	2.212	63.5	7.13	29.7
L	2.422	132.5	7.04	30.4
October 23rd, 2020				
T1	~0	171	8.13	9.8
T2				
T3	~0	177.4	7.53	9.7
G1				
G2	5.618	105.8	7.34	10.8
M	7.002	111	7.79	10.6
L				
March 14th, 2021				
T1	1.684	109	8.14	13
T2	1.589	166.5	7.9	11.4
T3	3.493	169.6	7.52	8.7
G1	3.534	149.2	7.61	8.3
G2	2.782	104.3	7.47	7.9
M	2.479	197	7.65	7.7
L	0.6182	167.4	7.32	7.2
April 24th, 2021				
T1	0.05	97.7	7.93	20.2
T2	6.193	113.8	7.64	21.9
T3	0.32	101	7.59	20.9
G1	8.03	84.5	7.65	20.6
G2	1.041	90	7.48	19.8
M	~0	108.6	7.77	18.6
L	3.153	124.4	7.45	19.6

Figure 23. demonstrates LCMS/MS analysis results of samples taken on different days from wetlands shown on Figure 22. Concentrations of atrazine and its metabolites are generally higher in samples taken on June 10th, 2020 and those compounds have been detected also in samples taken on March 12th and 19th 2020, before start of spring. The

reason of this difference in levels of analytes right before start of spring and at the end of spring is that farmers apply part of atrazine to the crops at the end of winter and most of it in the spring. Consequently, higher levels of ATR and metabolites were present in samples taken at the end of spring than in samples taken at the start of spring. Concentrations were even higher for samples taken in the summer, because in this time period ATZ was gradually washed off the farms with each rain event and emerged in surface water. Additionally, ATZ molecules were degraded to the metabolites by the summer.

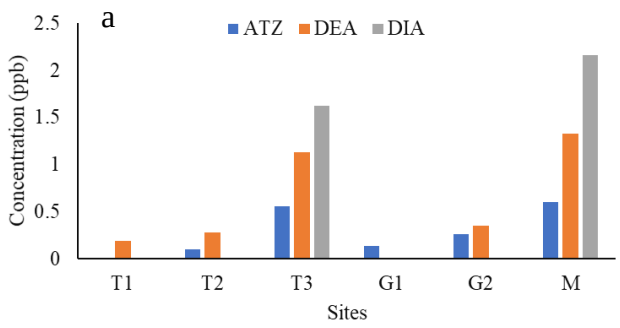
a
ATZ
DEA
DIA
Concentration (ppb)
2.5
2
1.5
1
0.5
0
T1
T2
T3
G1
G2
M
Sites

b

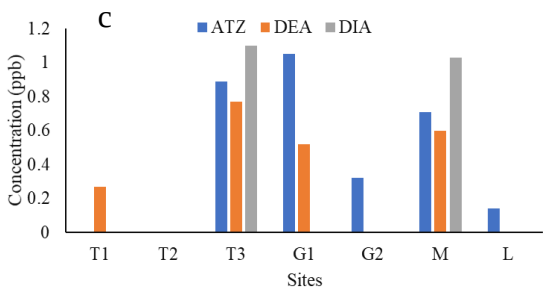
c
ATZ
DEA
DIA
Concentration (ppb)
1.2
1
0.8
0.6
0.4
0.2
0
T1
T2
T3
G1
G2
M
L
Sites

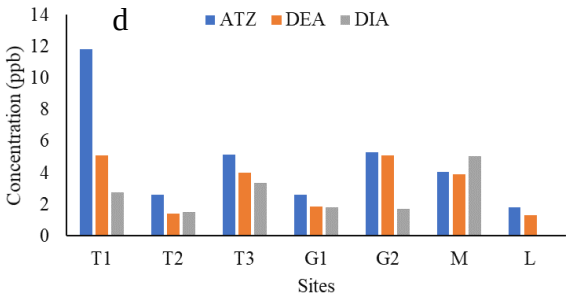
d
ATZ
DEA
DIA
Concentration (ppb)
14
12
10
8
6
4
2
0
T1
T2
T3
G1
G2
M
L
Sites

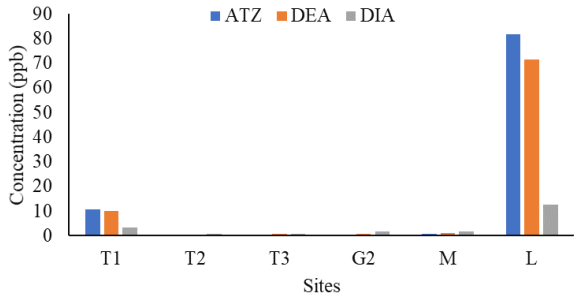
ATZ
DEA
DIA
Concentration (ppb)
90
80
70
60
50
40
30
20
10
0
T1
T2
T3
G2
M
L
Sites

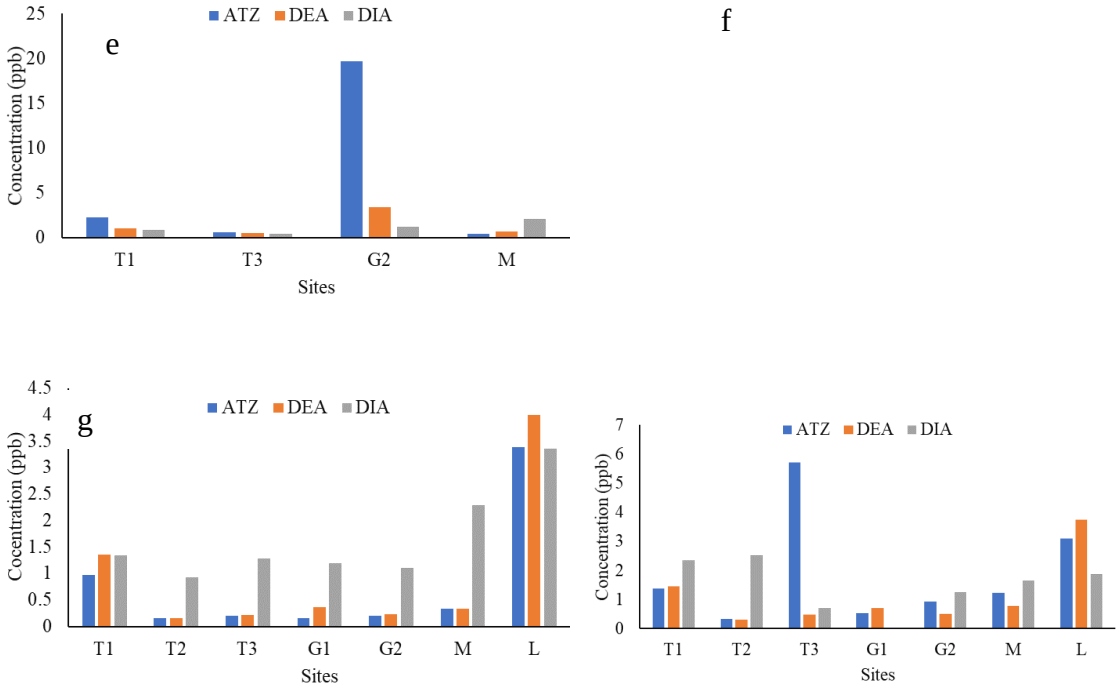

Figure 23. ATR, DEA, and DIA levels in 7 sites near Columbia, MO area, per sampling date: a) Mar. 12, 2020, b) Mar. 19, 2020, c) Jun. 10, 2020, d) Aug. 11th, 2020, e) Oct. 23rd, 2020, f) Mar. 14th, 2021, g) Apr. 24th, 2021.

Analysis data showed that on an average, sites T3, M, and T1 have the highest concentrations of ATR and its metabolites of all locations, and sites T2 and G1 are amongst those with the lowest analytes content. This could be due to number of reasons, including the sites distance from the point of atrazine application and circulation of runoffs after precipitation events.

Data also showed that for most cases ATZ had been degraded to DEA more than DIA and the extent of its degradation to different metabolites in each site was not the same, probably due to different vegetations and micro-organisms population distribution in each site. Photos of 2 different wetlands for the same sampling date (Figure 24) show

Figure 24. Diverse vegetation of two different sampling sites on the same day (June 10th, 2020) might be a reason of differences in ATR degradation.

the difference in vegetation of these sites, and a diverse population of species and microorganisms in each site can be expected.

5.4. Conclusion

Sampling campaigns were conducted to collect natural waters from rural areas in Centralia, Missouri following precipitation events in different seasons and the samples were characterized for physicochemical properties such as pH, temperature, conductivity, and TOC and levels of ATZ and its metabolites, DEA and DIA by LCMS/MS. Comparing the results for different seasons suggested that due to ATZ application timeline by farmers, higher concentrations of ATZ and its metabolites are expected at the end of spring and in the summer. Also, differences of the levels of ATZ and its metabolites in seven sites on the same day proposes that site vicinity to ATZ applying

point, geotechnical features of each site, and their position in the path of rainfall runoffs along with depth and sedentariness of water bodies are designating factors in the level of those analytes, conductivity, and TOC. ATZ degradation had different outcomes in terms of level of degradation to each metabolite and it might be a result of different vegetation and species and microorganism population in each site. Among physicochemical characteristics, pH was constantly in drinking water range (6.5-8.5), temperature changes with different seasons, and TOC and conductivity were variable depending on different factors such as amount of precipitation, DO level, and microorganism population in each site. The concentration of pesticide and metabolites observed was variable in different seasons, except for post-application seasons there was mostly low levels within dynamic range of the MIPs fabricated in previous chapters. These samples characterized for different parameters then could be used for in-situ analytes measurement using the MIP-based sensor fabricated in previous chapters.

6. Photonic Molecularly Imprinted Polymers Application in Natural Waters

6.1. Introduction

Molecular imprinting is an easy and fast method for developing tailor-made polymers, also known as Molecularly Imprinted Polymers (MIPs). For that purpose, template molecules in presence of a suitable solvent are mixed with a functional monomer to create covalent (95) or noncovalent interactions (96) in the pre-polymerization solution and then cross-linked into a 3D polymeric matrix. The template is then eluted from the polymer and leaves nanocavities complementary in shape and size to the target molecules (7). MIPs desirable features such as high selectivity and affinity, simple preparation, and mechanical and chemical stability makes them appropriate for numerous applications (97) including sensors (40,77), sorbents in solid phase extraction (98), chromatography (99), membranes (100), and drug delivery (101) targeting different template molecules.

The type of interactions between template molecule and functional monomer in the pre-polymerization solution rules the binding site formations in the MIPs ranging them from noncovalent to covalent complexes and yields heterogeneous and homogeneous imprinting during the process. Covalent complexes give homogeneous and consequently the most selective binding sites while noncovalent complexes give weaker intermolecular interactions, i.e. hydrogen binding and electrostatic interactions (97) which compromises their selectivity and makes the MIPs more prone to cross-reactivity. However, this feature

should not be contemplated as negative all the time since their advantageous applications in simultaneous recognition of compounds with similar structures have been reported (102–104). Covalent imprinting is also the least flexible and not the best candidate for aqueous media application (97).

Atrazine is an herbicide of triazine class that is extensively used by farmers for greater productivity per hectare (1). Living organisms of the environment (plants, animals, microorganisms) metabolize atrazine to different forms with similar structures but different hydrophilicities. The metabolites with highest probability of dissolution in natural waters are depicted in Figure 25. In our recent work, a photonic MIP has been developed for detection and quantification of atrazine and two of its metabolites, desisoprpylatrazine (DIA) and desethylatrazine (DEA), in aqueous solutions. In attempt to apply those MIPs in natural waters, the effect of ionic strength and Natural Organic Matter (NOM) on those MIPs have been studied. Also, samples from multiple wetlands were taken and then analyzed using LCMS/MS. It is reported that in a propazine MIP, molecular size control the rebinding mechanism and even slight differences in structure of the molecule, makes considerable change in cross-reactivity to the point that turns a heterogeneous MIP act closely similar to a homogeneous one (103).

With MIPs for detection and quantification of atrazine, DEA, and DIA, there is the need for a better understanding of how each MIP responses to the other compound since they have similar shape and size in molecular dimension. For that purpose, we proposed a series of experiments to study the cross-reactivity of each MIP to all three compounds and to investigate the MIPs function in case of their application in natural waters which most probably have more than just one of those compounds at the same time.

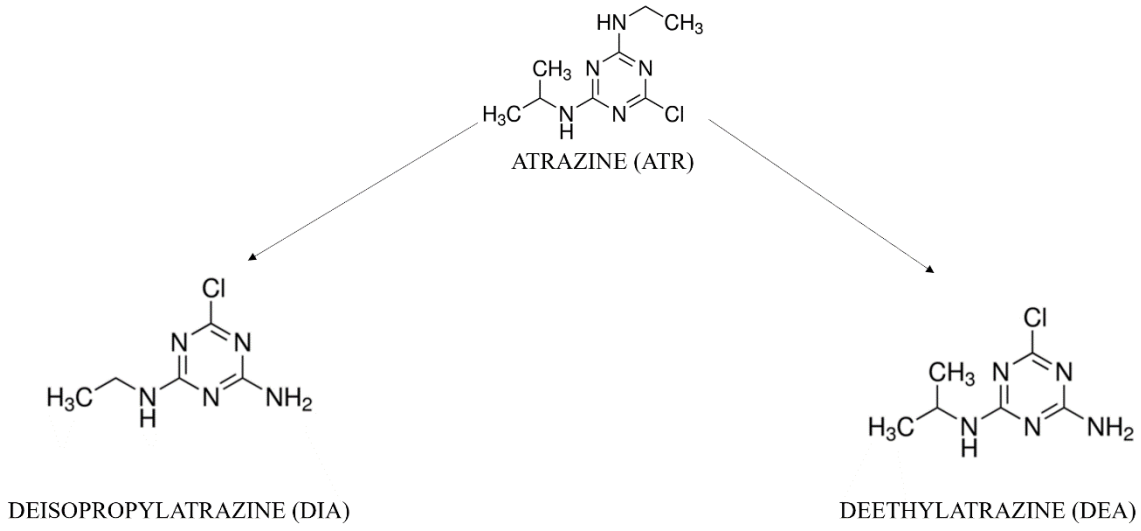

Figure 25. Atrazine is degraded to its metabolites by living organisms to DEA and DIA that are dissolved in water.

In this work, MIPs cross-reactivity to atrazine and metabolites, DIA and DEA, was studied in standard solutions and the results were compared with those of recent works. Also, the MIPs were used in natural waters taken from wetlands and the results from MIPs response were compared with those from LCMS/MS analysis.

6.2. Materials and methods

The following chemicals were purchased from Sigma-Aldrich (St. Louis, MO, US) and used without any purification: acrylic acid (AA) (99%), ethylene glycol dimethacrylate (EGDMA) (98%), 2,2'-azobisisobutyronitrile (AIBN) (98%), hydrofluoric acid (HF) (48%), ethanol (99.5%, 200 proof), acetic acid (96%), and DEA (100%), DIA (100%), and DACT (100%). Atrazine (>97%) was purchased from Santa Cruz Biotechnology (Dallas, TX, US). Silica particles (300 nm diameter) were supplied by Pinfire Gems and Colloids (Frankfurt, Germany). Glass microslides (3"×1"×0.04") were purchased from FisherBrand (Pittsburgh, PA, USA) and cut in 0.04"×1/3"×3"

pieces before use. Poly (methyl methacrylate) (PMMA) plastic slides of dimensions 0.04”×1/3”×3” were obtained from ePlastics (San Diego, CA, USA).

6.2.1. Fabrication of MIPs

The schematic of steps for fabrication of MIPs is illustrated in Figure 26. The first step was the preparation of silica particles deposition on glass substrate to create a colloidal crystal. In the fabrication of the colloidal crystals, ethanol was added to commercially available silica particles to achieve a solution of 0.1% volume fraction. For that purpose, 142.5 mg silica particles were added to 75 ml ethanol and the suspension was stirred and sonicated alternatively for 24 hours to obtain a well-dispersed suspension. Microscope glass slides, 0.04”×1/3”×3” dimensions, were vertically positioned inside the beakers with silica particle suspension and the deposition conducted in an oven for 24 hours at 50ºC. As ethanol evaporated, the silica particles self-assembled on the glass slides forming organized structures of 10 to 12 layers of particles.

The method used for atrazine-imprinted polymer is noncovalent, self-assembly approach. Hence, the target (atrazine and metabolites), functional monomer (acrylic acid), and crosslinker (EGDMA) form pre-polymerization bonds using hydrogen bonds and electrostatic bonds when they are mixed before starting the polymerization process. In order to have a more specific noncovalent interactions between the nanocavities and target molecules, it is necessary to optimize the complexation of the target molecule and functional monomer. Many research groups have used methacrylic acid (MAA) and acrylic acid (AA) as functional monomer for atrazine and they have reported that using AA as functional monomer results in higher sensitivity at the same atrazine concentration than using MAA as functional monomer (1). Based on these studies, AA was used as

functional monomer and EGDMA as crosslinker for the atrazine and its metabolites complexation at a molar ratio of 0.05:4:1 (target: monomer: crosslinker) to form the nanocavities in 3D porous matrices. The noncovalent complexation takes place via hydrogen bonds among hydroxyl group and oxygen atom of acrylic acid and nitrogen atoms and hydrogen atoms of amino groups in atrazine and its metabolites structure.

In the preparation of the polymerization solution, 31.47 mg of atrazine was added to 1 ml ethanol and then 0.8 ml acrylic acid as monomer was added to have a 1:80 molar ratio of atrazine to monomer. Then, 0.55 ml EGDMA (1:4 molar ration of EGMA to AA) was added as crosslinker and the solution was left overnight to have a good complexation. Finally, 6 mg AIBN was added as initiator.

After being mixed and left to interact overnight, the mixture was infiltrated through the interspaces of the colloidal crystal structure by capillary forces and filled its void spaces. In this step, a PMMA slide was placed on each side of a glass slide and the three were firmly held together while immersing one end in the polymerization solution.

To conduct the polymerization reaction, the slides were irradiated with UV light (power = 36kW, wavelength= 365 nm) for 3 hours. Ice packs were placed under the samples to avoid damage due to overheating. The temperature was maintained below the glass transition temperature (T_g) for the polymer of 50°C (40). The bonding of monomer and crosslinker reaction is exothermic and in addition, the UV light adds heat between the slides. So, to prevent damaging the hydrogel, the slides were placed in a freezer at -18°C for 30 minutes to separate them easily. The films remained attached to the PMMA slides.

The separated PMMA slides were immersed in 5% HF overnight to etch the silica particles remaining in the polymer, leaving large cavities within the film. Removing silica spheres followed by removing target molecules from the polymer hydrogel introduces a 3D interconnected porous arrays with nanocavities that could potentially have noncovalent interactions with target molecules.

In order to remove atrazine molecules from MIPs, the films were washed with acetic acid and ethanol solution with a volume ratio of 1:9. Three cycles of washing were conducted; each one with a duration of 15 minutes and stirring to enhance turbulence and facilitate the transport of the atrazine molecules from the polymeric matrix to the bulk of the solvent.

The same general procedure was used to fabricate metabolites MIPs and the target to functional monomer molar ratio was kept constant for all imprinted films.

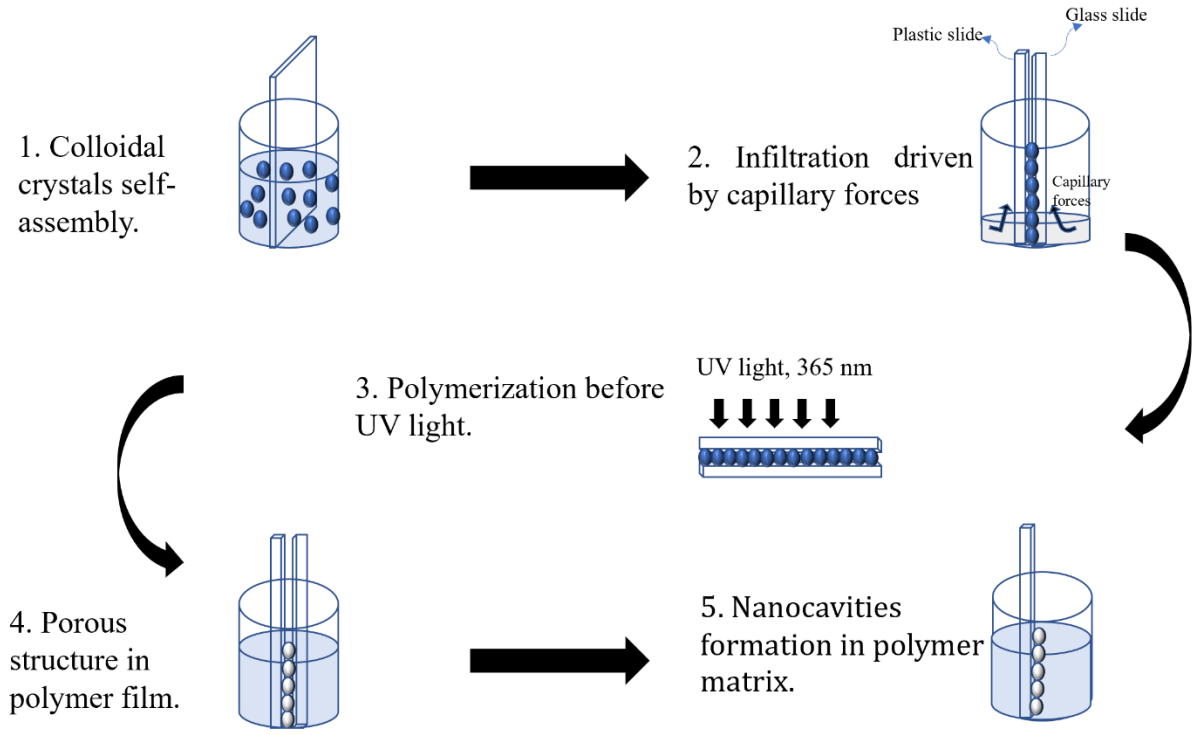

Figure 26. Schematic of MIPs fabrication steps 1. Self-assembly technique to create colloidal crystal. The glass slide is placed vertically in a beaker containing silica nanoparticles. 2. Infiltration: polymerization precursor is infiltrated between glass and plastic slide due to capillary forces. 3. Placing glass and plastic sandwich before UV light for polymerization to take place. 4. Creating porosity in polymer film by etching silica nanoparticles using 5% Hydrofluoric acid solution in DI water. 5. Removing target molecules from polymer film structure by immersing it in a solution of acetic acid and ethanol (1:9).

6.2.2. Characterization

Silica particles deposition were imaged by electron microscopy in a FEI Quanta 600 FEG (ThermoFisher Scientific, Hillsboro, OR, USA) Environmental Scanning Electron Microscopy (ESEM) to investigate size, morphology and number of layers of silica particles deposition. The glass slide was copper taped to the stub and coated with a

conductive layer of platinum (1.5-3 nm) with an Emitech K575x sputter coater (Quorum Technologies Ltd., Ashford, Kent, UK).

Fourier Transformed Infrared Spectroscopy (FTIR) spectra was collected in a Cary660 spectrometer (Agilent Technologies, Santa Clara, CA, USA) in the wavelength range of 4000-400 cm^{-1}. Both MIP (before and after elution of target molecules) and NIP films were characterized by FTIR to identify the functional groups present on the films.

6.2.3. Analytical measurement of concentrations

Stock solutions of atrazine and its metabolites were first prepared in methanol at 100 ppm concentration, given their high solubility in this solvent. Using serial dilution, 10 ppm and 1 ppm solutions in methanol were prepared; this last one was used as stock solution for serial dilution in DI water.

All solutions used in the sensor testing and calibration were analyzed by Liquid Chromatography-Mass Spectrometry (LCMS/MS). The concentrations of atrazine (ATR), DEA and DIA were determined by a Waters Alliance 2695 High Performance Liquid Chromatography (HPLC) system coupled with Waters Acquity TQ triple quadrupole mass spectrometer (MS/MS). The analytes were separated by a Phenomenex (Torrance, CA) Kinetex C18 (100mm x 4.6 mm; 2.6 µm particle size) reverse-phase column. The mobile phase consisted of 10 mM ammonium acetate and 0.1% formic acid in water (A) and 100% acetonitrile (B). The gradient conditions were 0 – 0.5 min, 2% B; 0.5-7 min, 2- 80% B; 7.0 -9.0 min, 80-98% B; 9.0 – 10.0 min, 2% B; 10.0 – 15.0 min, 2% B at a flow rate of 0.5 mL/min. The ion source in the MS/MS system was electrospray ionization (EI) operated in the positive ion mode with capillary voltage of 1.5 kV. The ionization sources were programmed at 150°C and the desolvation temperature was programmed at 450°C. The

MS/MS system was in the multi-reaction monitoring (MRM) mode with the optimized collision energy. The ionization energy, MRM transition ions (precursor and product ions; **Table 1**), capillary and cone voltage, desolvation gas flow and collision energy were optimized by Waters IntelliStart™ optimization software package. The retention time, calibration equations, and limits of the detection for the analyses of ATR, DEA, and DIA are summarized in **Table 1**.

Table 6.1. Precursor and product ions selected for the analysis of ATR, desethylatrazine (DEA) and deisopropylatrazine (DIA) by HPLC-MS/MS (LOD = limit of detection)

Compound	RT (min)	Molecular ions (m/z)	Product ions (m/z)	Polarity	Linear equation	Correlation coefficient (R square)	Collision Energy	Cone voltage (V)	LOD (ug/L)
ATR	9.471	215.86	173.89	ES+	y=58890x	0.9986	Tune	30	0.06
DEA	7.632	187.86	145.78	ES+	y=10336x	0.9957	Tune	30	1.45
DIA	6.829	173.82	131.76	ES+	y=3321x	0.9973	Tune	30	5.72

Since in some samples the concentration of atrazine and its metabolites were below the LC-MS/MS LOD, those solutions were preconcentrated by solid phase extraction (SPE). For that purpose, atrazine (ATR), deethylatrazine (DEA), deisopropylatrazine (DIA), hydroxyatrazine (HA) and the internal standard terbuthylazine (TRB) in the water samples were extracted and concentrated by SPE process. The water samples were filtered through a 0.2 µm Whatman Anotop syringe membrane filter (Sigma-Aldrich, St. Louis, MO, USA) and 50 mL of filtered samples were spiked with 500 µl of the internal standard terbuthylazine (TRB, 1 ppm), to achieve a final concentration of 10 µg/L of TRB. Before the extraction, the Oasis HLB solid-phase extraction cartridges (500 mg; Waters, Milford, MA) were conditioned with 8 mL

of methanol, followed by additions of 8 mL of DI water to wash the cartridges twice. Following the condition and washing process, the samples (50 mL) were passed through the cartridges at a flow rate of 5 mL/min. After the samples were loaded, the cartridges were washed with 8 mL of DI water and sorbents were dried under vacuum in a SPE manifold system for 5 min. The analytes were subsequently eluted with 7 mL of methanol at 2 mL/min. The eluates were then concentrated under a stream of nitrogen in a temperature bath at 27 ^{o}C until dryness. The resulting extracts were resuspended with 1 mL of water: methanol (10:90, v/v), and then filtered through a 0.2 μm PTFE Acrodisc syringe membrane filter.

6.2.4. Measurement of optical properties

Silica particle deposits were utilized to form 3D porous structure within polymer hydrogel to convert the recognition to a readable optical signal by Bragg diffraction. The Bragg equation is defined as:

$$\lambda_{max} = 1.633\left(\frac{d}{m}\right)\left(\frac{D}{D_0}\right)\sqrt{(n_a^2 - \sin\Theta^2)} \quad (1)$$

where d is the sphere diameter of the silica particle, m is the order of Bragg diffraction, (D/D_0) is the degree of gel swelling (D and D_0 are the diameters of the gel in the equilibrium state at a certain condition and in the reference state, respectively), n_a is the average refractive index of the porous gel at a certain condition, and Θ is the angle of incidence. Based on this equation, if the rebinding of target molecules causes any swelling or shrinkage in the hydrogel film, it is detected by optical signals, in particular a shift in the wavelength of the peak of the Bragg diffraction spectrum.

A UV-Visible spectrophotometer (Cary 60, Varian, Palo Alto, CA, USA) was used with a Harrick Scientific's Specular Reflection Accessory (ERA-30G) at a fixed angle of 30º in wavelength range of 200-800 nm and double-beam mode to measure the reflectance of the MIP films.

The samples collected and characterized in Chapter 5 were used to measure levels of ATZ, DEA, and DIA with the MIP-sensor. The samples that were stored frozen at -80°C, were left at room temperature overnight to defrost and reach room temperature before incubation. MIPs were incubated in each sample for 20 minutes to reach equilibrium and gentle mixing was provided by a shaker at 90 rpm. For each sample, 3 different new MIPs of each target were incubated. The peak wavelength shift was recorder by UV-Vis spectrophotometer and correlating concentration was calculated using the calibration curves generated in Chapter 3. Samples with analyte content higher than MIPs dynamic range were diluted and dilution factor was added in final concentration.

6.3. Results

6.3.1. Characterization

Silica particles colloidal crystals were imaged by ESEM to investigate the morphology and crystalline format of the silica deposition. The monodispersed silica particles yield macroporous structure within the MIP film. The MIP film surface and cross-section (after silica particles were etched) were also imaged by ESEM to investigate the internal porous structure of the MIP film. The ESEM images of both silica deposition and MIP film were shown in Chapter 3.

Chemical functional groups of the polymer and their interactions with target molecules were analyzed by FTIR and the results were reported in Chapter 3. The FTIR spectra showed some differences in bands and intensities of MIPs before target removal with NIPs and MIPs after target removal.

6.3.2. MIPs response in natural waters

Figures 27 to 33 demonstrate the average of MIPs responses along with their errors compared to real concentrations of analytes validated by LCMS/MS for 7 different days. LODs of the MIP-sensors were measured in Chapter 3 and they were determined to be 0.1, 0.2, and 0.3 ppb for ATZ, DEA, and DIA MIPs, respectively. Therefore, in the following diagrams, any MIP measurement lower than LOD is represented in black, representing a “non-detect”.

The effect of ionic strength on the sensor reading was studied in Chapter 4, resulting in up to 26% decrease of MIP response in presence of NaCl and up to 23% increase of MIP response in presence of $CaCl_2$. Depending on the ion being monovalent or divalent, MIP response could increase or decrease. For most cases studied in this work, the samples with highest conductivity, i.e. ionic strength, such as T2 of March 12th, 2020 (Figure 27) and T2, T3, and M of March 14th, 2021 (Figure 32), had MIP response higher than real concentration of the analytes that might be due to high content of divalent ions in those samples since they increase the conductivity and studies has shown that PAA has high affinity for divalent ions chelation (105). In most cases for M and L sites, the MIP response is lower than real concentration of the targets which might suggest higher content of monovalent ions in those sites.

The effect of NOM was also investigated in Chapter 4, using Suwannee River Natural Organic Matter (SRNOM) at 1 ppm concentration. It was observed that presence of NOM would increase MIP response, but this effect could be minimized by thoroughly rinsing the MIP before measuring its reflectance spectra to wash off clung NOM molecules from the surface of the MIP. In the samples studied in this work, TOC varies from 0 - 11 ppm. As demonstrated in the diagrams below, in most cases and even for the sites with highest content of TOC, the MIP response is relatively close or even lower than real concentration of the analytes which could be due to the rinsing step that helps with avoiding false increase in MIP response or the effect of monovalent ion that causes decrease in swelling ratio and hence, decrease in MIP response. Also, cross-reactivity studies showed that in higher concentration (5 ppb) the MIP response would be lower than in a single-compound solution and this might be one other reason of this observation.

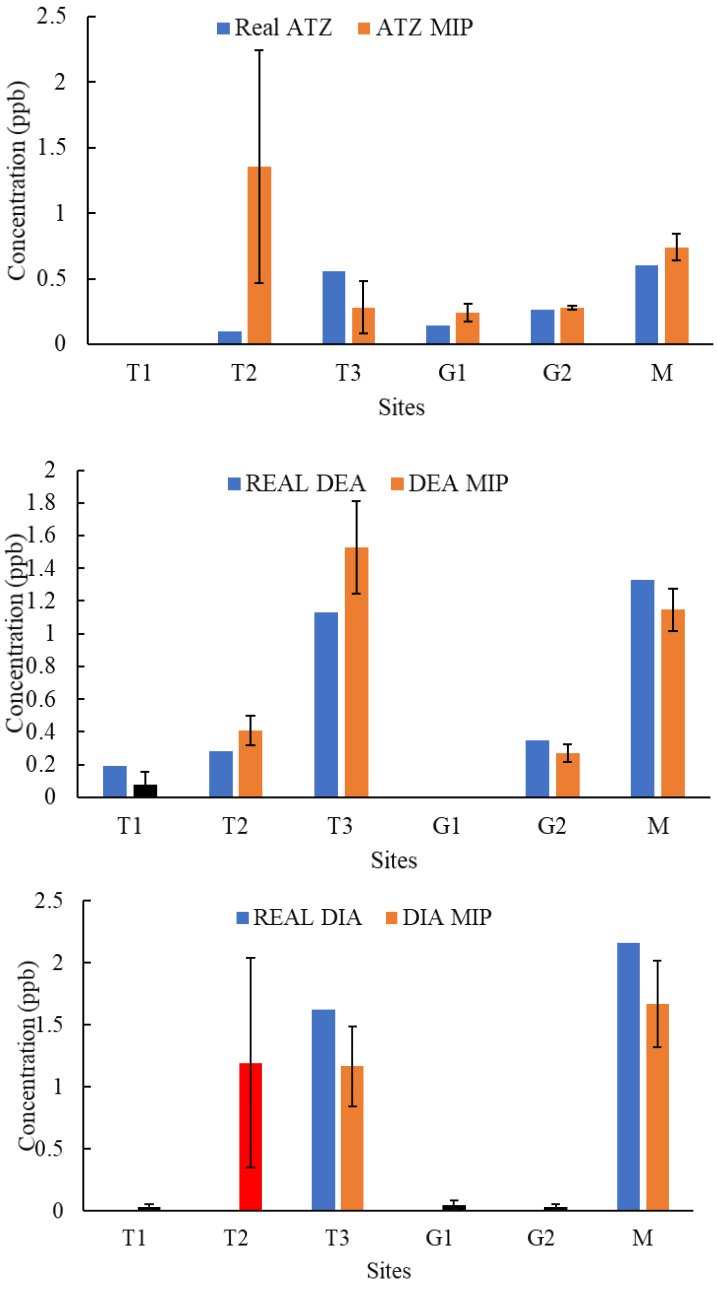

Figure 27. Average response of MIPs to ATZ, DEA, and DIA compared to real concentrations validated by LCMS/MS for samples of March 12th, 2020.

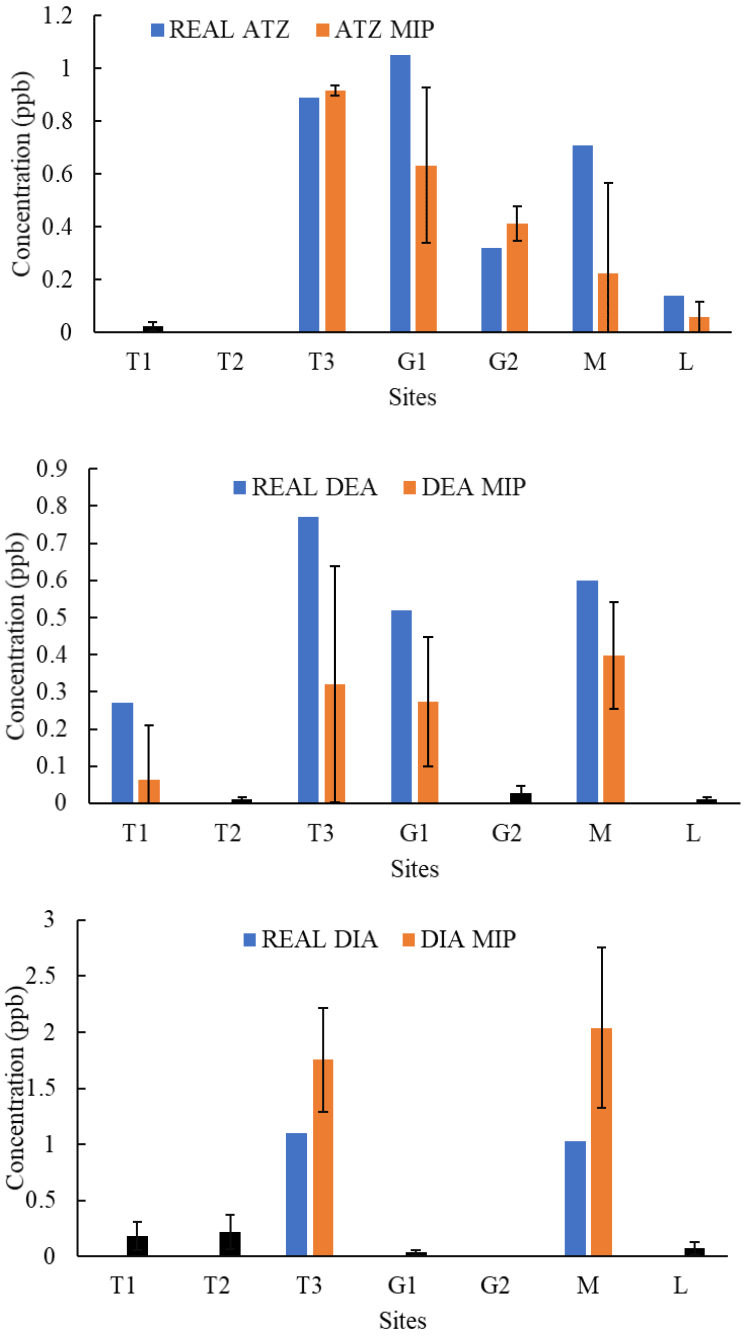

Figure 28. Average response of MIPs to ATZ, DEA, and DIA compared to real concentrations validated by LCMS/MS for samples of March 19th, 2020.

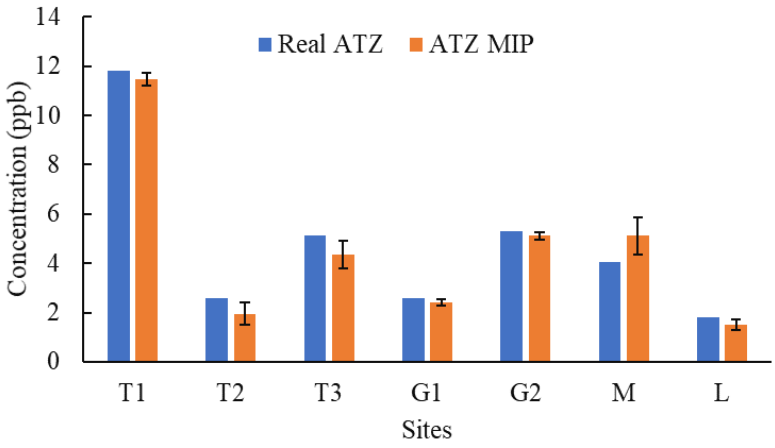

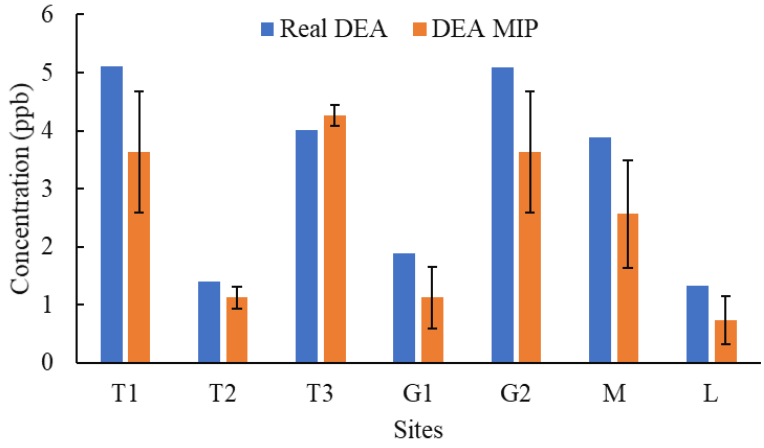

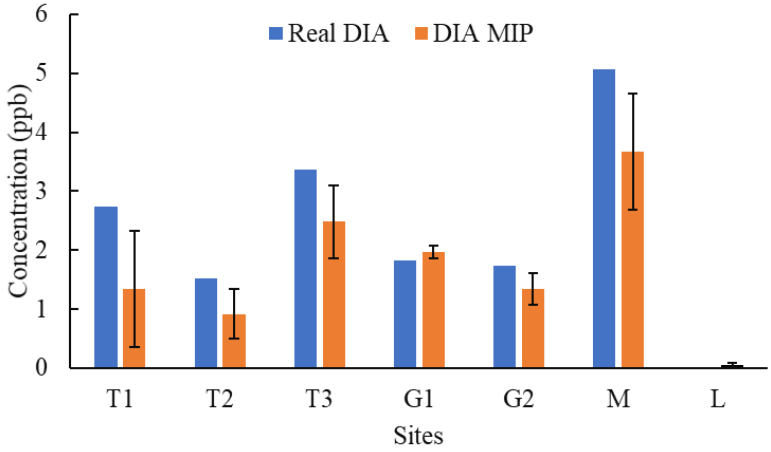

Figure 29. Average response of MIPs to ATZ, DEA, and DIA compared to real concentrations validated by LCMS/MS for samples of June 10th, 2020.

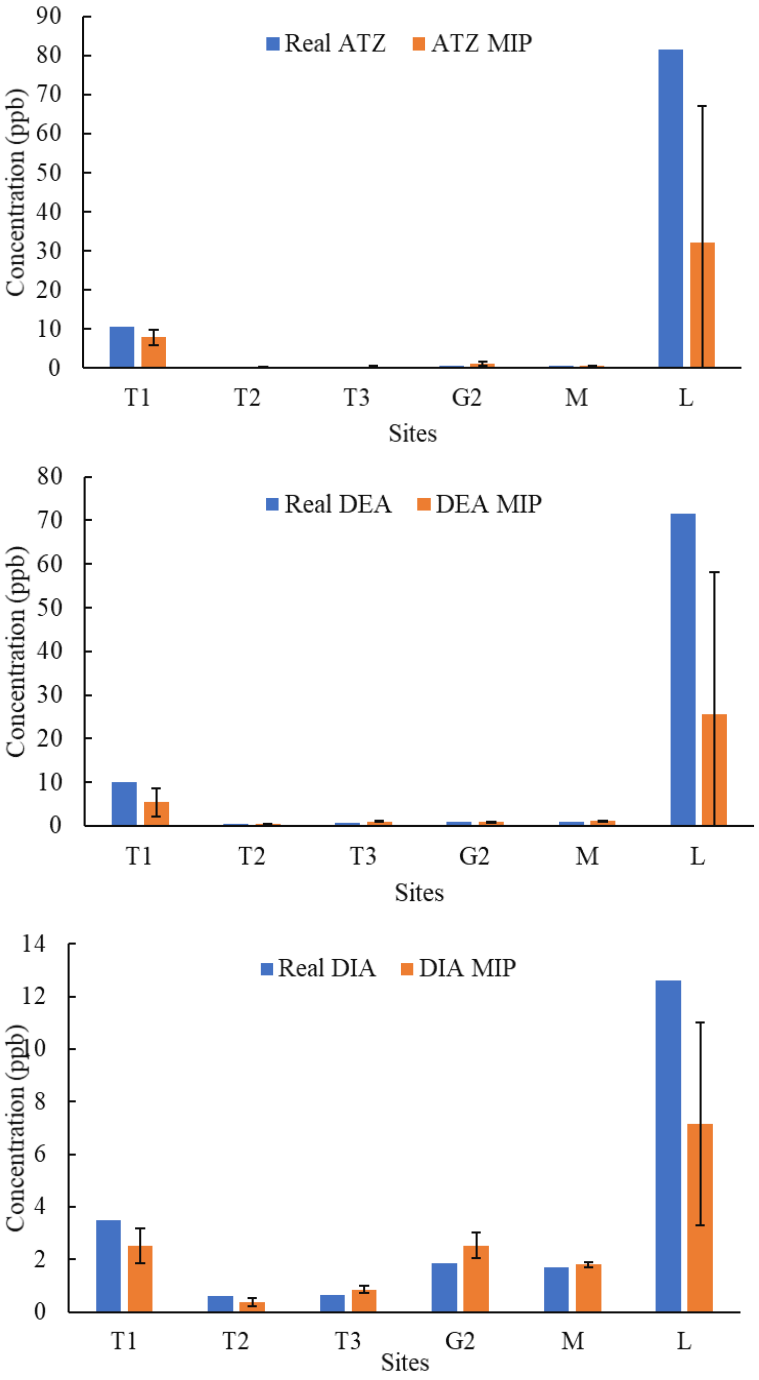

Figure 30. Average response of MIPs to ATZ, DEA, and DIA compared to real concentrations validated by LCMS/MS for samples of August 11th, 2020.

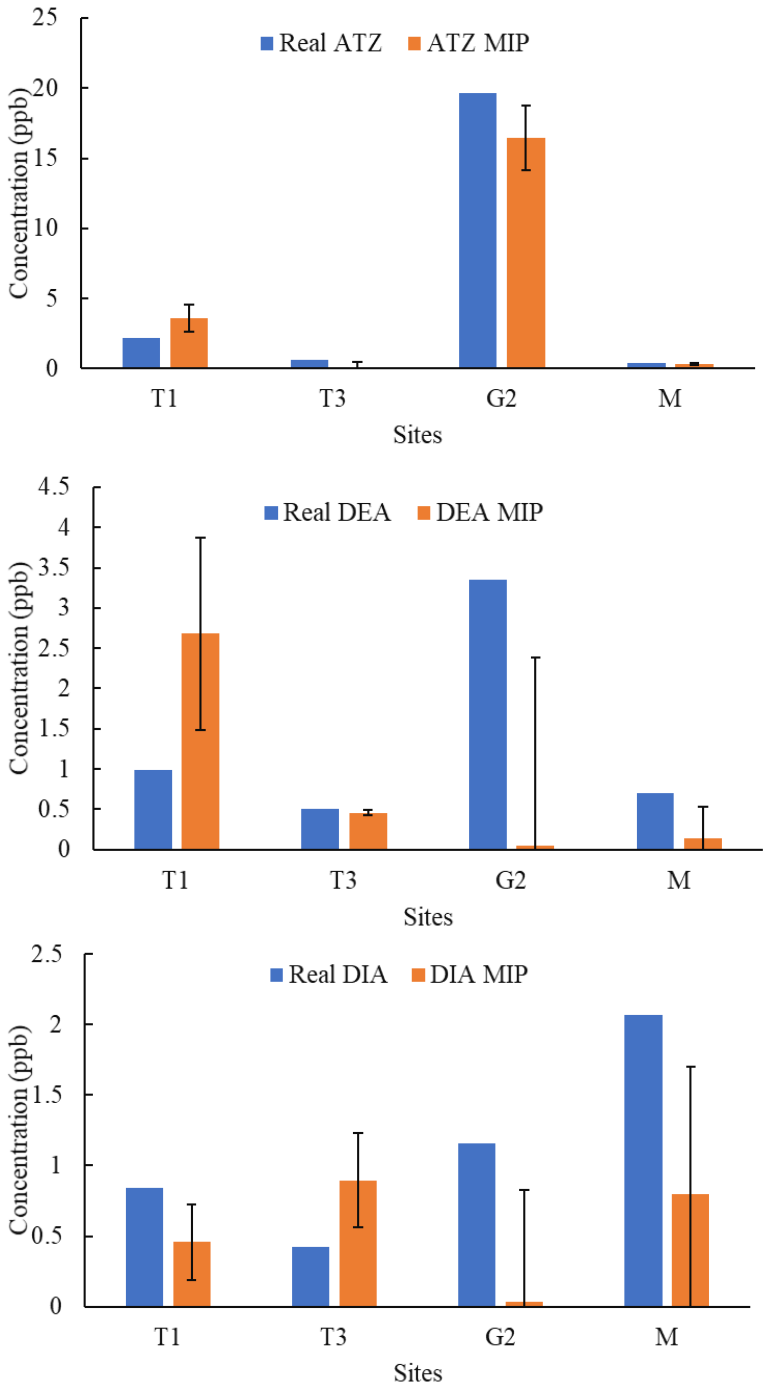

Figure 31. Average response of MIPs to ATZ, DEA, and DIA compared to real concentrations validated by LCMS/MS for samples of October 23rd, 2020.

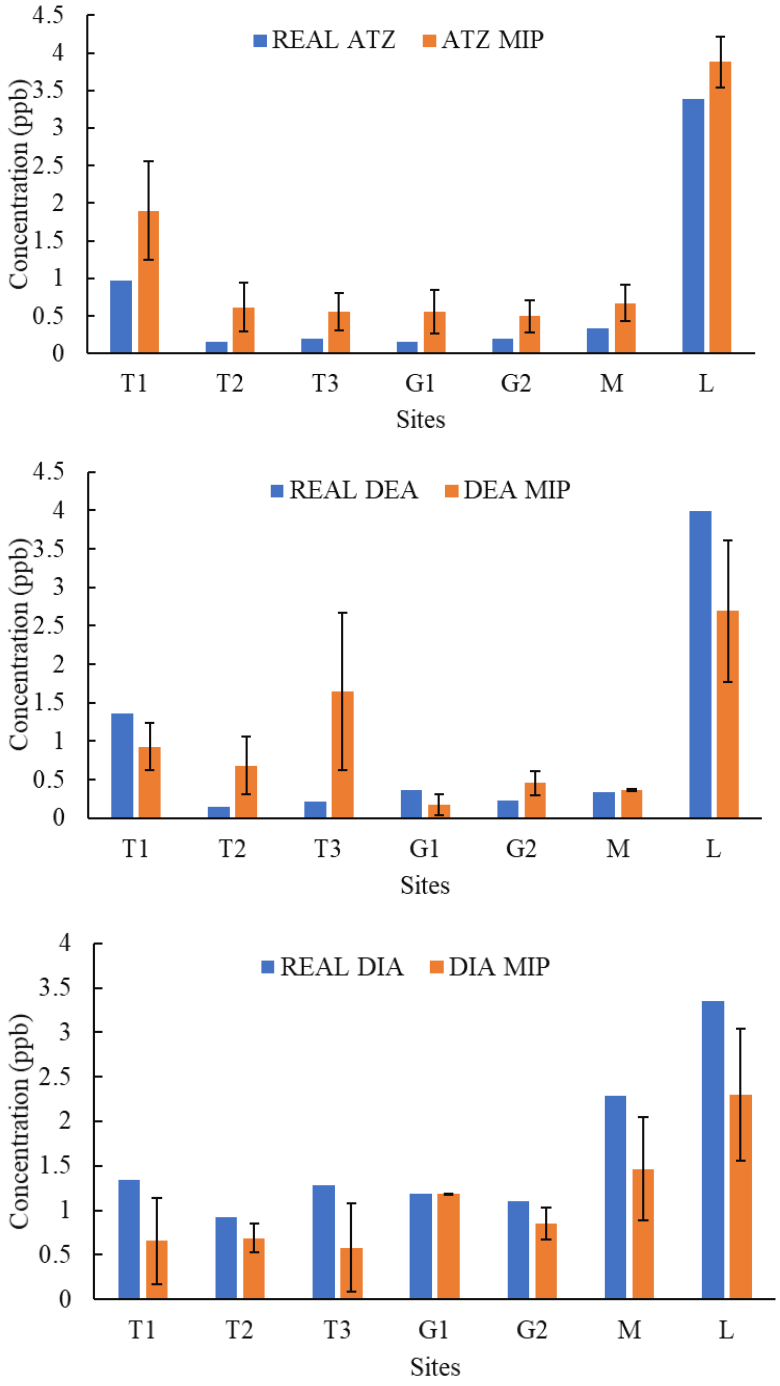

Figure 32. Average response of MIPs to ATZ, DEA, and DIA compared to real concentrations validated by LCMS/MS for samples of March 14th, 2021.

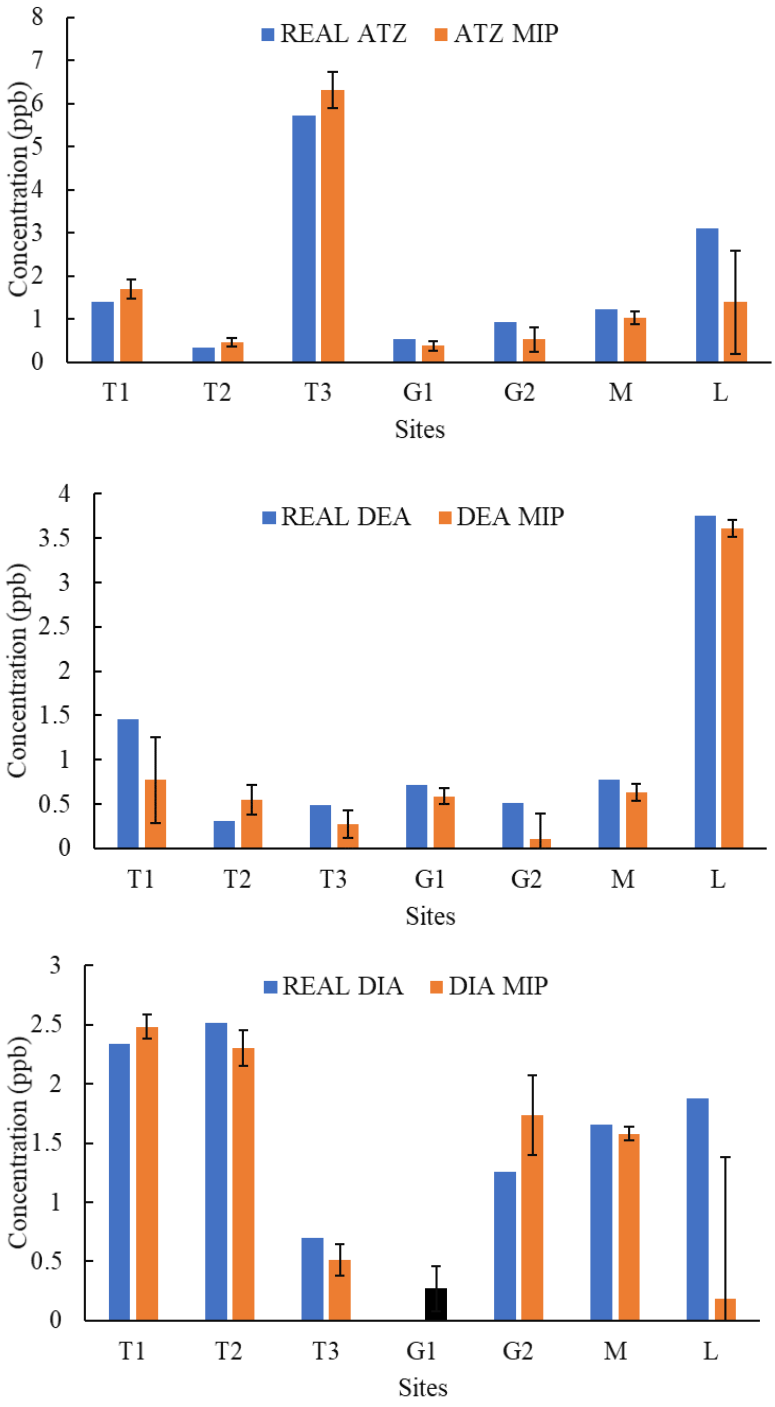

Figure 33. Average response of MIPs to ATZ, DEA, and DIA compared to real concentrations validated by LCMS/MS for samples of April 24th, 2021.

Figure 34 demonstrates degree of agreement, i.e. concordance of MIPs response and real concentrations of analytes measured by LCMS/MS. The X-axis represents LCMS/MS measurements, which is the gold standard, and Y-axis represents MIPs measurements of the analytes in samples. Having points closer to the X=Y line indicates better agreement of MIPs response with gold standard. In order to avoid unclarity in the distance of points from X=Y line, they have been divided into two different ranges: from 0 to 3 ppb, and concentrations above 3 ppb. In most cases, MIPs responses were relatable to real concentrations and showed good relevance with the gold standard. On the other hand, in few cases the MIPs responses were further from real concentration which could be due to a number of reasons such as natural waters characteristics (ionic strength, organic matter, other similar compounds present), or structural differences in the polymer film that leads to differences in MIPs responses. Having multiple steps in procedure of MIP fabrication, causes some variety in MIPs and impedes their reproducibility and this causes variabilities in MIPs responses to samples. However, MIPs provide a useful, simple, and efficient tool for the purpose of screening natural waters for ATZ and its metabolites contamination in comparison with complex analytical methods that need preparation of samples, expert technician, and expensive materials and instruments.

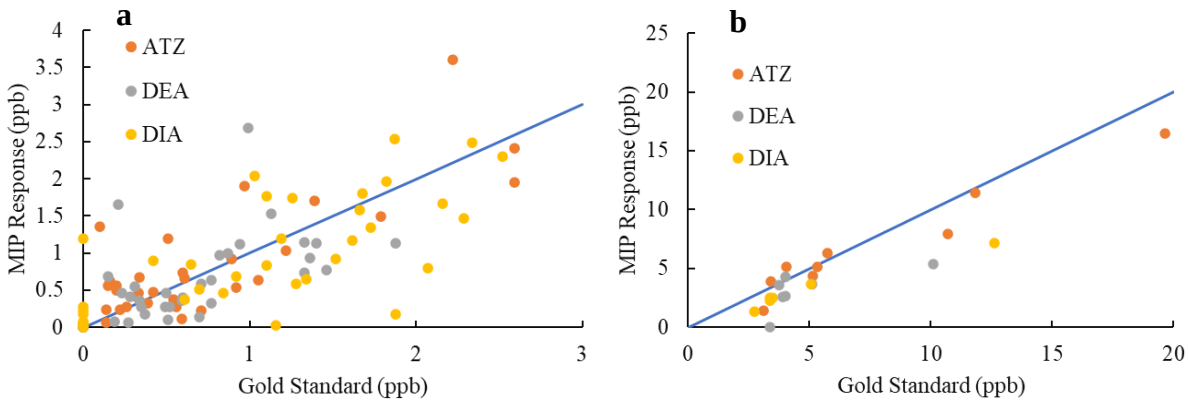

Figure 34. Degree of agreement (concordance) between MIP response and LCMS/MS measurements (gold standard); a) 0 to 3 ppb, b) >3 ppb

6.4. Conclusion

The fabricated molecularly imprinted polymers supported on PMMA slides were used to measure concentrations of ATZ and its metabolites, DEA and DIA, in natural waters collected from rural areas adjacent to farms after precipitation events during different seasons. MIPs measurements error was due to lack of reproducibility that made some structural differences in MIP films that were result of multistep fabrication process in a lab bench and led to variations in the MIPs responses. MIPs responses were compared to LCMS/MS measurements and in general, showed good relevance with the gold standard except for few cases that the difference could be a result of high ionic strength and NOM content along with presence of miscellaneous compounds with similar chemical structure to the targets, as for ionic strength, depending on the cation it could result in swelling suppression or chelation-related increase in swelling, and NOM could absorb light partially and cause error in reading MIP response, or molecules with similar structure to

the targets could have interactions with MIP surface and hence, create positive interference. The fabricated sensor showed good potential to be used as a monitoring tool for detection of its targets in natural waters in environmentally relevant concentrations.

7. Conclusion and Future Study

A photonic molecularly imprinted polymer was developed to detect atrazine and its metabolites, DEA and DIA, in natural waters. The sensor was supported on a PMMA slide and their reflectance spectra was measured by UV-Vis spectrophotometer. It showed good sensitivity to the target and there was minimal cross-reactivity of the sensors to the other analytes. The required time for sensor to reach equilibrium was 20 minutes. The LOD and LOQ of the sensors were 0.1, 0.2, 0.3, and 0.3, 0.6, and 1 ppb for ATZ, DEA, and DIA, respectively.

Ionic strength of the solutions affected the MIPs response and decreased it in presence of monovalent cation (Na^{+}) by 26% and increased it in presence of divalent cation (Ca^{2+}) by 23%. Presence of NOM in the water affected the MIP response by a 35% increase. However, rinsing the MIP before measuring its reflectance spectra could abate this effect.

Natural waters samples were collected from sites in vicinity of farms in rural areas northeast of Columbia Missouri after rain events and they were characterized for their physicochemical properties such as temperature and pH (on-site), conductivity and TOC (in the lab), as well as the content of ATZ, DEA, and DIA using LCMS/MS. pH was very consistent, but other parameters varied extensively depending on different factors including the amount of precipitation, the season of sampling, and ecological features of each site (i.e. vegetation and microorganism population). Levels of pesticides were considerably higher later in spring and in summer and that is because of pesticide application by farmers. Differences in the analytes level on the same day for different sites is a reason of different factors such as site vicinity to ATZ applying point,

geochemical features of each site, and their position in the path of rainfall runoffs along with depth and sedentariness of water bodies.

Finally, the fabricated sensor was used to measure the concentration of analytes in the samples collected without pretreatment and the results were compared to real concentrations obtained from LCMS/MS analysis. In general, the MIP-based sensors showed good agreement with the real concentration of the analytes, although in few cases there was a considerable difference that could be a result of high ionic strength or organic content of the samples. Also, lack of producibility in multistep fabrication process of MIPs led to some structural differences in polymer film and high intrinsic error of MIPs. However, compared to current complex, time-consuming, and expensive analytical methods, the MIP-based sensors are simple, fast, and reliable tools to monitor the level of ATZ and its metabolites in aqueous solutions and natural waters.

For future studies, it is suggested to develop a sensing mechanism made of array of MIPs to monitor different analytes and deliver the effect of varying physicochemical conditions of the natural waters at the same time, as control sensors, to be able to analyze the natural waters with more precise results and monitor them simultaneously in order to sustain the health and safety of wetlands and other natural waters ecology. Also, the different steps of MIPs fabrication could be studied more extensively to optimize the reproducibility of the MIPs in order to get more consistent responses of MIPs.

References

1. Wu Z, Tao CA, Lin C, Shen D, Li G. Label-free colorimetric detection of trace atrazine in aqueous solution by using molecularly imprinted photonic polymers. Chem - A Eur J. 2008;14(36):11358–68.

2. Graziano N, Mcguire MJ, Roberson A, Adams C, Jiang H, Blute N. 2004 National atrazine occurrence monitoring program using the abraxis ELISA method. Environ Sci Technol. 2006;40(4):1163–71.

3. Enoch RR, Stanko JP, Greiner SN, Youngblood GL, Rayner JL, Fenton SE. Mammary gland development as a sensitive end point after acute prenatal exposure to an atrazine metabolite mixture in female long-evans rats. Environ Health Perspect. 2007;115(4):541–7.

4. Giddings J, Anderson T, LW H, Kendall R, RP R, Solomon K, et al. Atrazine in North America Surface Waters: A Probabilistic Aquatic Ecological Risk Assessment. 2005.

5. BelBruno JJ. Molecularly Imprinted Polymers. Chem Rev [Internet]. 2019 Jan 9;119(1):94–119. Available from: https://doi.org/10.1021/acs.chemrev.8b00171

6. Gavrilović I, Mitchell K, Brailsford AD, Cowan DA, Kicman AT, Ansell RJ. A molecularly imprinted receptor for separation of testosterone and epitestosterone, based on a steroidal cross-linker. Steroids. 2011 Apr;76(5):478–83.

7. Alvarez-Lorenzo C, Concheiro A. Molecularly imprinted polymers for drug delivery. J Chromatogr B, Anal Technol Biomed life Sci. 2004 May;804(1):231–

45.

8. Vasapollo G, Sole R Del, Mergola L, Lazzoi MR, Scardino A, Scorrano S, et al. Molecularly imprinted polymers: present and future prospective. Int J Mol Sci. 2011;12(9):5908–45.

9. EPA. Wetland Fact Sheets. Ocean and Watersheds. 1995.

10. Atwood D, Paisley-Jones C. 2008-2012 Market Estimates. Pestic Ind Sales Usage. 2017;

11. Kolosova AY, Park JH, Eremin SA, Kang SJ, Chung DH. Fluorescence polarization immunoassay based on a monoclonal antibody for the detection of the organophosphorus pesticide parathion-methyl. J Agric Food Chem. 2003;51(5):1107–14.

12. Shim WB, Yang ZY, Kim JY, Choi JG, Je JH, Kang SJ, et al. Immunochromatography using colloidal gold-antibody probe for the detection of atrazine in water samples. J Agric Food Chem. 2006;54(26):9728–34.

13. Cooper J, Dobson H. The benefits of pesticides to mankind and the environment. Crop Prot [Internet]. 2007;26(9):1337–48. Available from: https://www.sciencedirect.com/science/article/pii/S026121940700097X

14. Akanmu AO, Babalola OO, Venturi V, Ayilara MS, Adeleke BS, Amoo AE, et al. Plant Disease Management: Leveraging on the Plant-Microbe-Soil Interface in the Biorational Use of Organic Amendments. Front Plant Sci [Internet]. 2021;12. Available from: https://www.frontiersin.org/article/10.3389/fpls.2021.700507

15. Kaufmann BYK. No 主観的健康感を中心とした在宅高齢者における 健康関連指標に関する共分散構造分析Title. 2005;(March):25–7.

16. Casillas Ituarte NN. Atrazine adsorption at the air/silica interface. Ohio State University / OhioLINK; 2005.

17. Al NEHSRC et. Herbicide handbook of the Weed Science Society of America. 6. ed. Champaign (Ill.) : Weed science society of America,; 1989.

18. Howard PH. Handbook of Environmental Fate and Exposure Data for Organic Chemicals, Volume IV. 1993.

19. Kaur J, Singh KV, Boro R, Thampi KR, Raje M, Varshney GC, et al. Immunochromatographic dipstick assay format using gold nanoparticles labeled protein-hapten conjugate for the detection of atrazine. Environ Sci Technol. 2007;41(14):5028–36.

20. Huang S Ben, Stanton JS, Lin Y, Yokley RA. Analytical Method for the Determination of Atrazine and Its Dealkylated Chlorotriazine Metabolites in Water Using SPE Sample Preparation and GC-MSD Analysis. J Agric Food Chem. 2003;51(25):7252–8.

21. Moorhead DL, Barrett JE, Virginia RA, Wall DH, Porazinska D. Organic matter and soil biota of upland wetlands in Taylor Valley, Antarctica. Polar Biol [Internet]. 2003;26(9):567–76. Available from: https://doi.org/10.1007/s00300-003-0524-x

22. Kingsford RT, Basset A, Jackson L. Wetlands: conservation's poor cousins. Aquat

Conserv Mar Freshw Ecosyst [Internet]. 2016 Sep 1;26(5):892–916. Available from: https://doi.org/10.1002/aqc.2709

23. Keddy PA. Wetland ecology: principles and conservation. Cambridge university press; 2010.

24. Rydin H, Jeglum JK. The biology of peatlands, 2nd edn Oxford: Oxford University Press.[Google Scholar]. 2013;

25. United States Environmental Protection Agency. America's Wetlands: Our Vital Link Between Land and Water. 2002;16 pp.

26. Shirdashtzadeh M, Chua LHC, Brau L. Microbial Communities and Nitrogen Transformation in Constructed Wetlands Treating Stormwater Runoff. Front Water [Internet]. 2022;3. Available from: https://www.frontiersin.org/article/10.3389/frwa.2021.751830

27. Ravikumar Y, Yun J, Zhang G, Zabed HM, Qi X. A review on constructed wetlands-based removal of pharmaceutical contaminants derived from non-point source pollution. Environ Technol Innov [Internet]. 2022;102504. Available from: https://www.sciencedirect.com/science/article/pii/S2352186422001201

28. Junk WJ. Freshwater fishes of South America: Their biodiversity, fisheries, and habitats—a synthesis. Aquat Ecosyst Health Manag [Internet]. 2007 Jun 8;10(2):228–42. Available from: https://doi.org/10.1080/14634980701356733

29. Christie J. Wetland Water Quality Standards for States. 2012;

30. Goldsborough LG, Crumpton WG. Distribution and Environmental Fate of

Pesticides in Prairie Wetlands. Gt Plains Res. 1998;8(1):73–95.

31. Muir D, Kenny D, Grift N, Robinson R, Titman R, Murkin H. Fate and acute toxicity of bromoxynil esters in an experimental prairie wetland. Environ Toxicol Chem. 1991;10:395–406.

32. Smith M, Blanchard P, Johnson W, Smith G, Smith MB, Blanchard PE. Atrazine Management and Water Quality.

33. Mosbach K. New Possibilities for Sensor Technology. 1997;(7).

34. Yan M, Ramstrm O. Molecularly imprinted materials : science and technology. New York: Marcel Dekker; 2005.

35. Cormack PAG, Elorza AZ. Molecularly imprinted polymers: synthesis and characterisation. J Chromatogr B, Anal Technol Biomed life Sci. 2004 May;804(1):173–82.

36. Cao S, Chen J, Sheng W, Wu W, Zhao Z, Long F. Chapter 3 - The Fabrication and Development of Molecularly Imprinted Polymer-based Sensors for Environmental Application. In: Li S, Ge Y, Piletsky SA, Lunec JBT-MIS, editors. Amsterdam: Elsevier; 2012. p. 57–72. Available from: https://www.sciencedirect.com/science/article/pii/B9780444563316000037

37. Velev OD, Jede TA, Lobo RF, Lenhoff AM. Microstructured Porous Silica Obtained via Colloidal Crystal Templates. 1998;(13):3597–602.

38. Waterhouse GIN, Waterland MR. Opal and inverse opal photonic crystals: Fabrication and characterization. Polyhedron. 2007;26(2):356–68.

39. Griffete N, Frederich H, Maître A, Ravaine S, Chehimi MM, Mangeney C. Inverse Opals of Molecularly Imprinted Hydrogels for the Detection of Bisphenol A and pH Sensing. Langmuir [Internet]. 2012 Jan 10;28(1):1005–12. Available from: https://doi.org/10.1021/la202840y

40. Dai J, Dong X, Fidalgo de Cortalezzi M. Molecularly imprinted polymers labeled with amino-functionalized carbon dots for fluorescent determination of 2,4-dinitrotoluene. Microchim Acta. 2017;184(5):1369–77.

41. Hu X, An Q, Li G, Tao S, Liu J. Imprinted Photonic Polymers for Chiral Recognition. Angew Chemie Int Ed [Internet]. 2006 Dec 11;45(48):8145–8. Available from: https://doi.org/10.1002/anie.200601849

42. Liu L, Li P, Asher SA. Entropic trapping of macromolecules by mesoscopic periodic voids in a polymer hydrogel. Nature [Internet]. 1999;397(6715):141–4. Available from: https://doi.org/10.1038/16426

43. Sharma AC, Jana T, Kesavamoorthy R, Shi L, Virji MA, Finegold DN, et al. A general photonic crystal sensing motif: creatinine in bodily fluids. J Am Chem Soc. 2004 Mar;126(9):2971–7.

44. Chen W, Meng Z, Xue M, Shea KJ. Molecular imprinted photonic crystal for sensing of biomolecules. Mol Imprinting [Internet]. 2016;4(1):1–12. Available from: https://doi.org/10.1515/molim-2016-0001

45. Iskandar F. Nanoparticle processing for optical applications - A review. Adv Powder Technol. 2009 Jul 1;20:283–92.

46. Xue J-Q, Li D-W, Qu L-L, Long Y-T. Surface-imprinted core–shell Au nanoparticles for selective detection of bisphenol A based on surface-enhanced Raman scattering. Anal Chim Acta [Internet]. 2013;777:57–62. Available from: https://www.sciencedirect.com/science/article/pii/S0003267013003966

47. Duan H, Leilei L, Wang X, Wang Y, Li J, Luo C. CdTe quantum dots@luminol as signal amplification system for chrysoidine with chemiluminescence-chitosan/graphene oxide-magnetite-molecularly imprinting sensor. Spectrochim Acta Part A Mol Biomol Spectrosc. 2015 Sep 1;153.

48. Cacho C, Turiel E, Martin-Esteban A, Pérez-Conde C, Cámara C. Characterisation and quality assessment of binding sites on a propazine-imprinted polymer prepared by precipitation polymerisation. J Chromatogr B, Anal Technol Biomed life Sci. 2004 Apr;802(2):347–53.

49. Shi X, Wu A, Qu G, Li R, Zhang D. Development and characterisation of molecularly imprinted polymers based on methacrylic acid for selective recognition of drugs. Biomaterials. 2007 Sep;28(25):3741–9.

50. Chen CY, Wang CH, Chen AH. Recognition of molecularly imprinted polymers for a quaternary alkaloid of berberine. Talanta [Internet]. 2011;84(4):1038–46. Available from: http://dx.doi.org/10.1016/j.talanta.2011.03.009

51. Karim K, Breton F, Rouillon R, Piletska E V, Guerreiro A, Chianella I, et al. How to find effective functional monomers for effective molecularly imprinted polymers? Adv Drug Deliv Rev. 2005 Dec;57(12):1795–808.

52. Annamma K, Mathew B. Design of 2, 4-Dichlorophenoxyacetic Acid Imprinted

Polymer with High Specificity and Selectivity. Mater Sci Appl. 2011 Jan 1;2.

53. García-Calzón JA, Marta Elena DG. Characterization of binding sites in molecularly imprinted polymers. Sensors and Actuators B: Chemical, 123(2), 1180-1194. Sensors Actuators B Chem. 2007;123:1180–94.

54. Kadhem AJ, Gentile GJ, Fidalgo de Cortalezzi MM. Molecularly Imprinted Polymers (MIPs) in Sensors for Environmental and Biomedical Applications: A Review. Vol. 26, Molecules . 2021.

55. Uzun L, Turner APF. Molecularly-imprinted polymer sensors: realising their potential. Biosens Bioelectron. 2016 Feb;76:131–44.

56. Xu D, Zhu W, Jiang Y, Li X, Li W, Cui J, et al. Rational design of molecularly imprinted photonic films assisted by chemometrics. J Mater Chem [Internet]. 2012;22(32):16572–81. Available from: http://dx.doi.org/10.1039/C2JM32833J

57. Piletsky SA, Turner APF. Chapter 14 - IMPRINTED POLYMERS AND THEIR APPLICATION IN OPTICAL SENSORS. In: Ligler FS, Taitt CRBT-OB (Second E, editors. Amsterdam: Elsevier; 2008. p. 543–81. Available from: https://www.sciencedirect.com/science/article/pii/B9780444531254500164

58. Kanekiyo Y, Naganawa R, Tao H. pH-responsive molecularly imprinted polymers. Angew Chemie - Int Ed. 2003;42(26):3014–6.

59. Henry OYF, Cullen DC, Piletsky SA. Optical interrogation of molecularly imprinted polymers and development of MIP sensors: A review. Anal Bioanal Chem. 2005;382(4):947–56.

60. Moreno-Bondi MC. Songjun Li, Yi Ge, Sergey A. Piletsky, Joseph Lunec (Eds.): Molecularly imprinted sensors: overview and applications. Anal Bioanal Chem [Internet]. 2013;405(20):6385–6. Available from: https://doi.org/10.1007/s00216-013-6990-2

61. Pan G, Guo Q, Cao C, Yang H, Li B. Thermo-responsive molecularly imprinted nanogels for specific recognition and controlled release of proteins. Soft Matter. 2013;9(14):3840–50.

62. Wu HG, Ju XJ, Xie R, Liu YM, Deng JG, Niu CH, et al. A novel ion-imprinted hydrogel for recognition of potassium ions with rapid response. Polym Adv Technol. 2011;22(9):1389–94.

63. Dai J, Fidalgo de Cortalezzi M. Influence of pH, ionic strength and natural organic matter concentration on a MIP-Fluorescent sensor for the quantification of DNT in water. Heliyon [Internet]. 2019;5(6):e01922. Available from: https://doi.org/10.1016/j.heliyon.2019.e01922

64. Davoodi D, Hassanzadeh-Khayyat M, Asgharian Rezaei M, Mohajeri SA. Preparation, evaluation and application of diazinon imprinted polymers as the sorbent in molecularly imprinted solid-phase extraction and liquid chromatography analysis in cucumber and aqueous samples. Food Chem [Internet]. 2014;158:421–8. Available from: http://dx.doi.org/10.1016/j.foodchem.2014.02.144

65. Kueseng P, Noir ML, Mattiasson B, Thavarungkul P, Kanatharana P. Molecularly imprinted polymer for analysis of trace atrazine herbicide in water. J Environ Sci Heal Part B [Internet]. 2009 Oct 19;44(8):772–80. Available from:

https://doi.org/10.1080/03601230903238319

66. Alizadeh T, Zare M, Ganjali MR, Norouzi P, Tavana B. A new molecularly imprinted polymer (MIP)-based electrochemical sensor for monitoring 2,4,6-trinitrotoluene (TNT) in natural waters and soil samples. Biosens Bioelectron [Internet]. 2010;25(5):1166–72. Available from: https://www.sciencedirect.com/science/article/pii/S095656630900534X

67. Hao T, Wei X, Nie Y, Xu Y, Yan Y, Zhou Z. An eco-friendly molecularly imprinted fluorescence composite material based on carbon dots for fluorescent detection of 4-nitrophenol. Microchim Acta [Internet]. 2016;183(7):2197–203. Available from: https://doi.org/10.1007/s00604-016-1851-2

68. Wen Y, Chen L, Li J, Ma Y, Xu S, Zhang Z, et al. Molecularly imprinted matrix solid-phase dispersion coupled to micellar electrokinetic chromatography for simultaneous determination of triazines in soil, fruit, and vegetable samples. Electrophoresis. 2012;33(15):2454–63.

69. Yin Y-M, Chen Y-P, Wang X-F, Liu Y, Liu H-L, Xie M-X. Dummy molecularly imprinted polymers on silica particles for selective solid-phase extraction of tetrabromobisphenol A from water samples. J Chromatogr A [Internet]. 2012;1220:7–13. Available from: https://www.sciencedirect.com/science/article/pii/S002196731101781X

70. Rao TP, Prasad K, Kala R, Gladis JM. Biomimetic Sensors for Toxic Pesticides and Inorganics based on Optoelectronic/Electrochemical Transducers—An Overview. Crit Rev Anal Chem [Internet]. 2007 Aug 7;37(3):191–210. Available

from: https://doi.org/10.1080/10408340701244664

71. Solomon KR, BAKER DB, RICHARDS RP, DIXON KR, KLAINE SJ, POINT TW LA, et al. Ecological Risk Assessment of Atrazine in. Environ Toxicol. 1996;15(1):31–76.

72. Sakamoto S, Putalun W, Vimolmangkang S, Phoolcharoen W, Shoyama Y, Tanaka H, et al. Enzyme-linked immunosorbent assay for the quantitative/qualitative analysis of plant secondary metabolites. J Nat Med [Internet]. 2017/11/21. 2018 Jan;72(1):32–42. Available from: https://pubmed.ncbi.nlm.nih.gov/29164507

73. Katz E, Willner I. Integrated nanoparticle-biomolecule hybrid systems: synthesis, properties, and applications. Angew Chem Int Ed Engl. 2004 Nov;43(45):6042–108.

74. Chen L, Wang X, Lu W, Wu X, Li J. Molecular imprinting: perspectives and applications. Chem Soc Rev [Internet]. 2016;45(8):2137–211. Available from: http://dx.doi.org/10.1039/C6CS00061D

75. Peeters M, Kobben S, Jiménez-Monroy KL, Modesto L, Kraus M, Vandenryt T, et al. Thermal detection of histamine with a graphene oxide based molecularly imprinted polymer platform prepared by reversible addition-fragmentation chain transfer polymerization. Sensors Actuators, B Chem. 2014;203:527–35.

76. Dai J, Vu D, Nagel S, Lin CH, Fidalgo de Cortalezzi M. Colloidal crystal templated molecular imprinted polymer for the detection of 2-butoxyethanol in water contaminated by hydraulic fracturing. Microchim Acta. 2018;185(1):1–8.

77. Kadhem AJ, Xiang S, Nagel S, Lin CH, de Cortalezzi MF. Photonic molecularly imprinted polymer film for the detection of testosterone in aqueous samples. Polymers (Basel). 2018;10(4):1–13.

78. Gao R, Kong X, Su F, He X, Chen L, Zhang Y. Synthesis and evaluation of molecularly imprinted core-shell carbon nanotubes for the determination of triclosan in environmental water samples. J Chromatogr A. 2010 Dec;1217(52):8095–102.

79. Amalric L, Mouvet C, Pichon V, Bristeau S. Molecularly imprinted polymer applied to the determination of the residual mass of atrazine and metabolites within an agricultural catchment (Brévilles, France). J Chromatogr A [Internet]. 2008;1206(2):95–104. Available from: https://www.sciencedirect.com/science/article/pii/S0021967308013034

80. Wang S, She Y, Hong S, Du X, Yan M, Wang Y, et al. Dual-template imprinted polymers for class-selective solid-phase extraction of seventeen triazine herbicides and metabolites in agro-products. J Hazard Mater [Internet]. 2019;367:686–93. Available from: https://www.sciencedirect.com/science/article/pii/S030438941831238X

81. Mavumengwana-khanyile B, Katima Z, Songa EA. extraction of atrazine and its metabolites deisopropylatrazine and International Journal of Environmental Analytical Recent advances in sorbents applications and techniques used for solid-phase extraction of atrazine and its metabolites deisopropylatrazin. Int J Environ Anal Chem [Internet]. 2019;00(00):1–52. Available from:

https://doi.org/10.1080/03067319.2019.1597866

82. Muldoon MT, Stanker LH. Development and Application of Molecular Imprinting Technology for Residue Analysis. ACS Symp Ser. 1996;657:312–30.

83. Xu S, Li J, Chen L. Molecularly imprinted polymers by reversible addition–fragmentation chain transfer precipitation polymerization for preconcentration of atrazine in food matrices. Talanta [Internet]. 2011;85(1):282–9. Available from: https://www.sciencedirect.com/science/article/pii/S0039914011002657

84. Siemann M, Andersson LI, Mosbach K. Selective Recognition of the Herbicide Atrazine by Noncovalent Molecularly Imprinted Polymers. J Agric Food Chem. 1996;44(1):141–5.

85. Xu S, Lu H, Chen L. Double water compatible molecularly imprinted polymers applied as solid-phase extraction sorbent for selective preconcentration and determination of triazines in complicated water samples. J Chromatogr A [Internet]. 2014;1350:23–9. Available from: https://www.sciencedirect.com/science/article/pii/S0021967314007766

86. Valero-Navarro A, Salinas-Castillo A, Fernández-Sánchez JF, Segura-Carretero A, Mallavia R, Fernández-Gutiérrez A. The development of a MIP-optosensor for the detection of monoamine naphthalenes in drinking water. Biosens Bioelectron. 2009 Mar;24(7):2305–11.

87. Yang M, Han A, Duan J, Li Z, Lai Y, Zhan J. Magnetic nanoparticles and quantum dots co-loaded imprinted matrix for pentachlorophenol. J Hazard Mater. 2012 Oct;237–238:63–70.

88. Chiappini A, Pasquardini L, Bossi AM. Molecular imprinted polymers coupled to photonic structures in biosensors: The state of art. Sensors (Switzerland). 2020;20(18):1–23.

89. Ng E, Koh YK, Wong CC. Colloidal Crystals. In: Contemporary Physics - CONTEMP PHYS. 2012.

90. Jiang P, Bertone JF, Hwang KS, Colvin VL. Single-crystal colloidal multilayers of controlled thickness. Chem Mater. 1999;11(8):2132–40.

91. Kibechu RW, Mamo MA, Msagati TAM, Sampath S, Mamba BB. Synthesis and application of reduced graphene oxide and molecularly imprinted polymers composite in chemo sensor for trichloroacetic acid detection in aqueous solution. Phys Chem Earth. 2014;76–78(Complete):49–53.

92. Kempe H, Kempe M. Influence of salt ions on binding to molecularly imprinted polymers. Anal Bioanal Chem. 2010;396(4):1599–606.

93. Changa DM. The binding of free calcium ions in aqueous solution using chelating agents, phosphates and poly(acrylic acid). J Am Oil Chem Soc [Internet]. 1983;60(3):618–22. Available from: https://doi.org/10.1007/BF02679800

94. Wang QG, Wimpenny I, Dey RE, Zhong X, Youle PJ, Downes S, et al. The unique calcium chelation property of poly(vinyl phosphonic acid-co-acrylic acid) and effects on osteogenesis in vitro. J Biomed Mater Res A. 2018 Jan;106(1):168–79.

95. Wulff G. Molecular Imprinting in Cross-Linked Materials with the Aid of Molecular Templates— A Way towards Artificial Antibodies. Angew Chemie Int

Ed English [Internet]. 1995 Sep 15;34(17):1812–32. Available from: https://doi.org/10.1002/anie.199518121

96. Arshady R, Mosbach K. Synthesis of substrate-selective polymers by host-guest polymerization. Die Makromol Chemie [Internet]. 1981 Jan 1;182(2):687–92. Available from: https://doi.org/10.1002/macp.1981.021820240

97. Abu-Alsoud GF, Hawboldt KA, Bottaro CS. Assessment of cross-reactivity in a tailor-made molecularly imprinted polymer for phenolic compounds using four adsorption isotherm models. J Chromatogr A [Internet]. 2020;1629:461463. Available from: https://www.sciencedirect.com/science/article/pii/S0021967320307391

98. Liu Y, Liu Y, Liu Z, Hu X, Xu Z. β-Cyclodextrin molecularly imprinted solid-phase microextraction coatings for selective recognition of polychlorophenols in water samples. Anal Bioanal Chem [Internet]. 2018;410(2):509–19. Available from: https://doi.org/10.1007/s00216-017-0746-3

99. Yang Y-J, Liu X-W, Kong X-J, Qin Z, Jiao Z-H, Li S-H, et al. Preparation and Evaluation of Oseltamivir Molecularly Imprinted Polymer Silica Gel as Liquid Chromatography Stationary Phase. Vol. 23, Molecules . 2018.

100. Yusof NA, Zakaria ND, Maamor NA, Abdullah AH, Haron MJ. Synthesis and Characterization of Molecularly Imprinted Polymer Membrane for the Removal of 2,4-Dinitrophenol. Vol. 14, International Journal of Molecular Sciences . 2013.

101. Han S, Su L, Zhai M, Ma L, Liu S, Teng Y. A molecularly imprinted composite based on graphene oxide for targeted drug delivery to tumor cells. J Mater Sci

[Internet]. 2019;54(4):3331–41. Available from: https://doi.org/10.1007/s10853-018-3023-8

102. Zander Å, Findlay P, Renner T, Sellergren B, Swietlow A. Analysis of Nicotine and Its Oxidation Products in Nicotine Chewing Gum by a Molecularly Imprinted Solid-Phase Extraction. Anal Chem [Internet]. 1998 Aug 1;70(15):3304–14. Available from: https://doi.org/10.1021/ac971272w

103. Turiel E, Martín-Esteban A, Fernández P, Pérez-Conde C, Cámara C. Molecular Recognition in a Propazine-imprinted Polymer and Its Application to the Determination of Triazines in Environmental Samples. Anal Chem [Internet]. 2001 Nov 1;73(21):5133–41. Available from: https://doi.org/10.1021/ac0105538

104. Ferrer I, Lanza F, Tolokan A, Horvath V, Sellergren B, Horvai G, et al. Selective Trace Enrichment of Chlorotriazine Pesticides from Natural Waters and Sediment Samples Using Terbuthylazine Molecularly Imprinted Polymers. Anal Chem [Internet]. 2000 Aug 1;72(16):3934–41. Available from: https://doi.org/10.1021/ac000015f

105. Tomida T, Hamaguchi K, Tunashima S, Katoh M, Masuda S. Binding Properties of a Water-Soluble Chelating Polymer with Divalent Metal Ions Measured by Ultrafiltration. Poly(acrylic acid). Ind Eng Chem Res. 2001 Jul 10;40.

VITA

Zahra Salahshoor was born on August 12, 1991, in Ghorveh, Iran. She received her bachelor's degree in chemical engineering and master's degree in chemical engineering, focusing on environmental engineering, from Sharif University of Technology in Tehran, Iran in 2014 and 2016, respectively. She attended the University of Missouri in August 2017 and received her PhD in environmental engineering in 2022.